東海大学大学院　令和 2 年度博士論文

高分子マイクロ・ナノディスクの創製と面接触相互作用にて発現するユニークな物性評価

Fabrication and Evaluation of Polymer Micro/Nano Discs with Their Unique Properties Induced by Surface-Contact Interactions

指導 岡村 陽介 教授

東海大学大学院総合理工学研究科

総合理工学専攻

ワランユー　タンタナテ―ウイン

WARANYOU TUNTANATEWIN

Contents

List of abbreviations

AR_{dt}	Aspect ratio between the average length of diameter of thickness
AR_{xy}	Aspect ratio between the average length of major and minor axis
ATRP	Atom transfer radical polymerization
BSA	Bovine serum albumin
C/LRP	Controlled/living radical polymerization
cm^{-1}	Kaiser
CSDA	Co-structure direct agent
DAMM	2-dimethylaminoethyl methacrylate
DDSs	Drug delivery systems
$DiOC_2(3)$	3,3'-Diethyloxacarbocyanine iodides
DIP	1,5-diiodopentane
DMAPMA	Dimethylamino propyl methacrylamide
DP	Degree of polymerization
DPPs	Discoidal polymeric particles
DSPs	Disassembling disc-stacked particles
DVB	Divinylbenzene
EDTA	Ethylenediaminetetraacetic acid
EGDM	Ethyleneglycol dimethacrylate
EHMA	2-ethylhexyl methacrylate
E_m	Emission wavelength
E_x	Excitation wavelength
FE-SEM	Field emission scanning electron microscope
FTIR	Fourier-transform infrared spectroscopy
GA	Glutaraldehyde
ICAM	Anti-intercellular adhesion molecule
LCST	Lower critical solution temperature
MEPM	Meropenem
MMA	Methyl methacrylate
M_w	Molecular weight
n	The number of particles per volume (particles/mL)
N	The number of replications
Na-Alg	Sodium alginate
NMP	Nitroxide-mediated polymerization
O/W	Oil-in-water
ODS	Octadecyltrimethoxysilane
PBS	Phosphate buffered saline
PDMS	Polydimethylsiloxane
PEG	Poly (ethylene glycol)
PEN	Polyethylene naphthalate
PET	Polyethylene terephthalate
PFPE	Perfluoropolyether
PI	Polyimide
PLA	Poly (lactic acid)
PLGA	Poly (lactic-co-glycolic acid)
PLGA	Poly (D, L-lactide-co-glycolide)
PLLA	Poly (L-lactic acid)

PRINT	Particle replication in non-wetting templates
PS	Polystyrene
PSP	Paintable pressure-sensitive paint
PU	Polyurethane
PVA	Polyvinyl alcohol
PVP	Polyvinylpyrrolidone
RAFT	Reversible addition fragmentation chain transfer
SD	Standard deviation
SiO_2	Silicon dioxide
SPG	Shirasu Porous Glass
T_g	Glass transition temperature
THF	Tetrahydrofuran
TiO_2	Titanium dioxide
UCST	Upper critical solution temperature
UV	Ultraviolet
VBC	Vinylbenzyl chloride
W/O	Water-in-oil
w/w	weight per weight
wt%	weight-weight percentage
ϕ	The diameter symbol (phi)

Chapter 1
Introduction

1-1 Research background

In the past decades, polymer micro/nano particles have been considered as one of the most attractive research areas among the materials research community since they can be used in a wide range of applications [1-5], via various fabrication methods [6-9]. Depending on the particular application, polymer particles have been created to achieve desired properties by having the fabrication methods as a vital tool. Various fabrication methods for polymer micro/nano-sized particles are shown in Fig.1-1, which could be classified in to two groups namely the fabrication method that derives directly from monomer via classical polymerization such as, emulsion, interfacial, and controlled/living radical etc., and the one that is from preformed polymer such as, solvent evaporation, salting-out, dialysis and supercritical fluid technology, etc [8].

1-2 Fabrication methods of polymer micro/nano particles

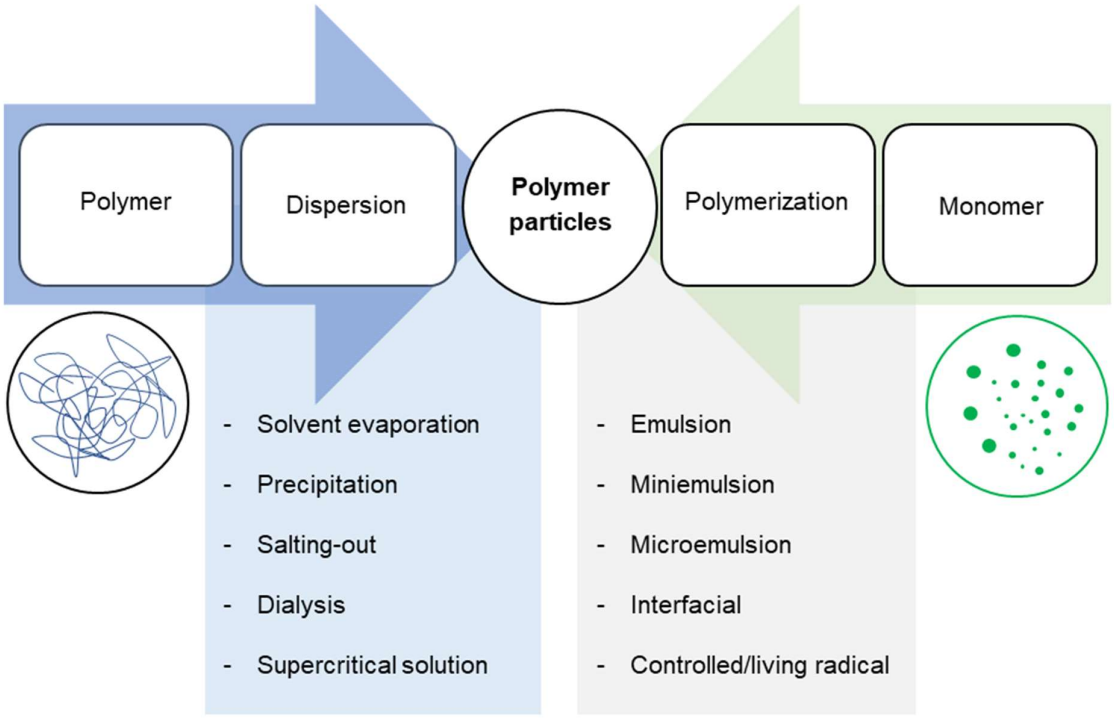

Fig. 1-1 Schematic diagram of various techniques for the preparation of polymer particles (cited and partially modified from ref. 8).

1-2-1 Fabrication methods of polymer particles from monomer

In these fabrication methods, polymer particles are created from monomers via polymerization process. The desired properties for each particular application are desired by the selection of suitable polymer as well as adjusting polymerization operating conditions. The major methods currently in use are discussed as following.

Emulsion polymerization

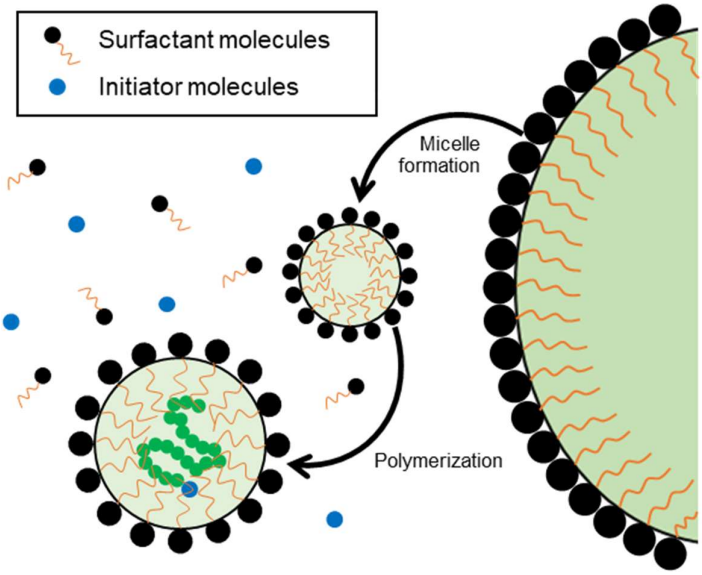

Fig. 1-2 Schematic diagram of emulsion polymerization for the preparation of polymer particles (cited and partially modified from ref. 10).

Emulsion polymerization is one of the most common method, using water as dispersion medium which is considered as environmentally friendly (see Fig. 1-2). This method can be classified to be main two types namely conventional and surfactant-free emulsion polymerization. In conventional emulsion polymerization, a monomer of lower water soluble is polymerized with initiator and surfactant in water. The common polymers used in convention emulsion polymerization method are styrene, methyl methacrylate, etc., by having potassium persulfate and sodium dodecyl sulfate as a general imitator and surfactant, respectively [8], [11]. Since the surfactant used in conventional emulsion polymerization is difficult to completely remove and it is a time-consuming process, surfactant-free

emulsion polymerization has been proposed to fabricate polymer particles without any required surfactant [12]. Common monomers used in this surfactant-free method are vinyl and acryl monomers with potassium persulfate and ammonium persulfate as common initiators [8], [13].

Miniemulsion polymerization

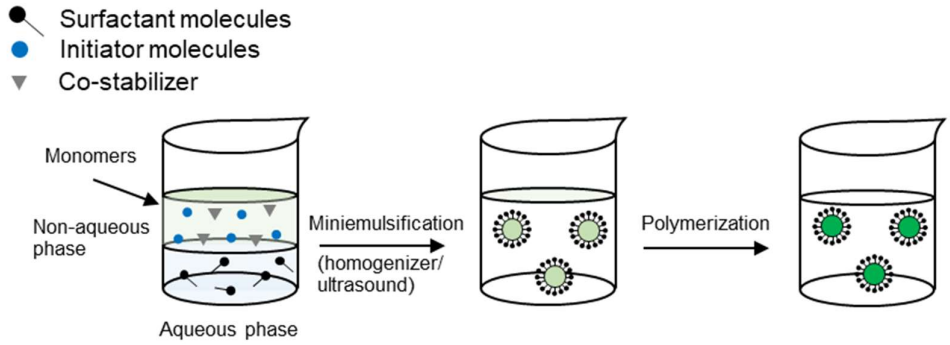

Fig. 1-3 Schematic diagram of miniemulsion polymerization for the preparation of polymer particles (cited and partially modified from ref. 14).

The typical substrates of mini/micro emulsion polymerization are the same with conventional emulsion polymerization, namely water, monomer mixture, surfactant, and initiator. The crucial differences of these two methods are the using a low molecular mass compound as the co-stabilizer and the using of a high-shear in mini/micro emulsion polymerization. Hexadecane and cetyl alcohol are the most common co-stabilizers in publications [15]. In this method (see Fig 1-3), the solution of surfactant in water is mixed with the co-stabilizer which is dissolved in the monomers under stirring. Then, the mixture is homogenized (normally by rotor-stator systems, sonifers or high-pressure homogenizers) to form the miniemulsion. The growing of each polymer droplet dominates through nucleation during polymerization and considered as a mini reactor which is different from the growing of polymer particles driven by the monomer mass transfer between discrete droplets in emulsion polymerization.

Microemulsion polymerization

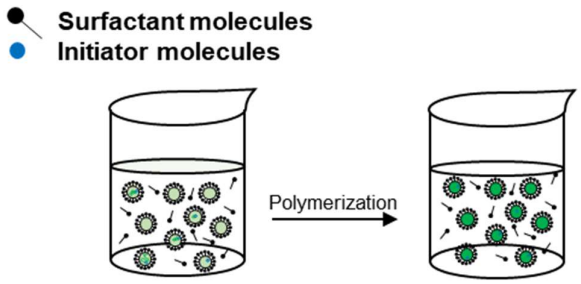

Fig. 1-4 Schematic diagram of microemulsion polymerization for the preparation of polymer particles (cited and partially modified from ref. 8, 16).

Microemulsion and emulsion polymerization seem to be very similar method which both can be fabricated polymer particles of high molar mass. However, particle size and the average number of chains per particle obtained from microemulsion are considerably smaller than emulsion polymerization. [17]. Another key difference between these two processes is the amount of surfactant consumption in microemulsion is significantly larger for the formation of microemulsion droplets with fast nucleation and to stabilize latex particles. However, the remaining of surfactant in polymer particles is the key drawback of microemulsion method, thus, two main approaches have been recently reported to overcome this problem. The first one is the using surfactants that are able to solubilize large amounts of monomer, while, another employs the increase amount of polymer produced for a given amount of surfactant [18]. In this method, an initiator is added to the aqueous phase of a thermodynamically stable microemulsion containing swollen micelles where the polymerization starts from (see Fig.1-4).

Interfacial polymerization

This method involves the polymerization at the interface of two immiscible phases namely continuous- and dispersed-phase (see Fig. 1-5). Generally, two highly reactive monomers dissolved in each phase are polymerized by polycondensation reaction when they come in contact with each other at the interface [19]. Since the polymerization reaction is confined to the interface, higher molecular weights can be achieved at mild reaction conditions because reactants are expected to encounter the growing polymer chain instead of other monomers [20].

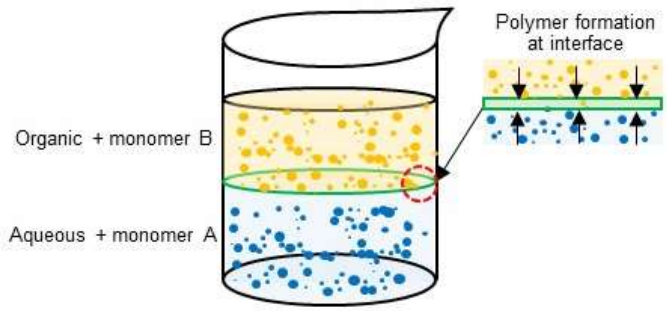

Fig. 1-5 Schematic diagram of interfacial polymerization polymerization for the preparation of polymer particles (cited and partially modified from ref. 19, 21).

Controlled/living radical polymerization (C/LRP)

Fast radical-radical termination reactions seem to be the key limitations of radical polymerization. This results in difficult problems of molar mass and molar mass distribution control in conventional radical polymerization [(19)]. C/LRP method has been proposed to solve this problem via three approaches namely nitroxide-mediated polymerization (NMP), atom transfer radical polymerization (ATRP) and reversible addition and fragmentation transfer chain polymerization (RAFT) [(22)]. By this method, the structure and composition of polymer chains could be controlled which is expected to open a new potential in a wide range of applications. However, the remaining of residual control agents are the drawback of this method raising the concerns about color, odor, stability, and environmental legislative compliance [(8)].

1-2-2 Fabrication methods of polymer particles from preformed polymer

In these fabrication methods, polymer particles are derived from preformed polymer by miscellaneous techniques. However, these methods shared one specific principle in common which is polymer precipitation. This can be obtained by adding poor solvent or decreasing polymer solubility in a solvent [(23)]. The major methods currently in use are discussed as following.

Solvent evaporation

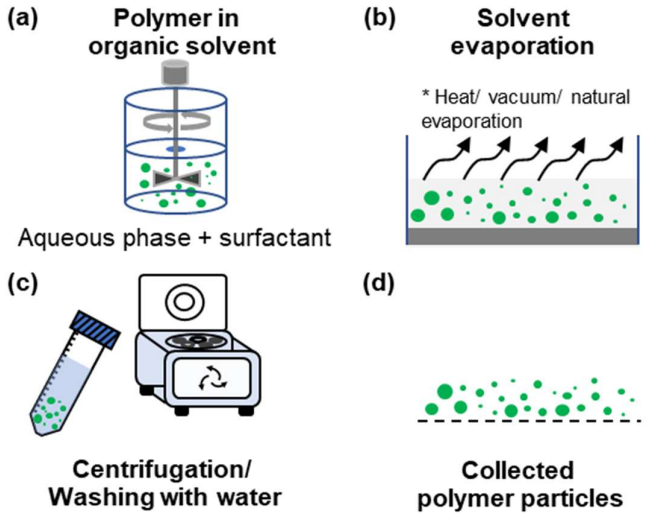

Fig. 1-6 Schematic description of solvent evaporation method for preparation of polymer particles (cited and partially modified from ref. 24).

Solvent evaporation is one of the most common fabrication methods for polymer particles. It has been applied extensively in pharmaceutical application for various purposes such as controlled drug delivery and protection of drug degradation [25]. As can be seen in Fig 1-6, polymer is dissolved and disperses in volatile organic solvent such as dichloromethane, chloroform, and ethyl acetate. Then, emulsions are formulated by adding organic phase to the aqueous phase with the presence of surfactant. The organic phase and the aqueous phase are mixed by high-speed homogenization or ultrasonication, which results in the formation of a stable emulsion [26]. The solvent is then evaporated by continuous magnetic stirring at room temperature, room temperature with vacuum or at high temperature to obtain polymer particle suspension. Afterwards, polymer particles can be collected by centrifugation and washed with distilled water.

Precipitation

Precipitation method is also known as interfacial deposition or solvent displacement method. The basic principal of this technique bases on the decrease of interfacial tension between the two phases, which increases the surface area which induces the forming of small droplets of organic solvent [27]. As

shown in Fig. 1-7, Polymer is initially dissolved in a good solvent (the solvent that has solubility parameter closely matches to polymer) and then mixed with a poor solvent, which is miscible with the good solvent. The solution gradually shifts to the poor solvent since the evaporation of the good solvent, when the polymer precipitates as polymer particles and disperses in the poor solvent [28]. Due to this reason, boiling point of a good solvent should be lower than that of the poor solvent. The solvents that most frequently use as a good solvent in this method are ethanol, acetone, hexane, methylene chloride or dioxane, while the most common poor solvent is water.

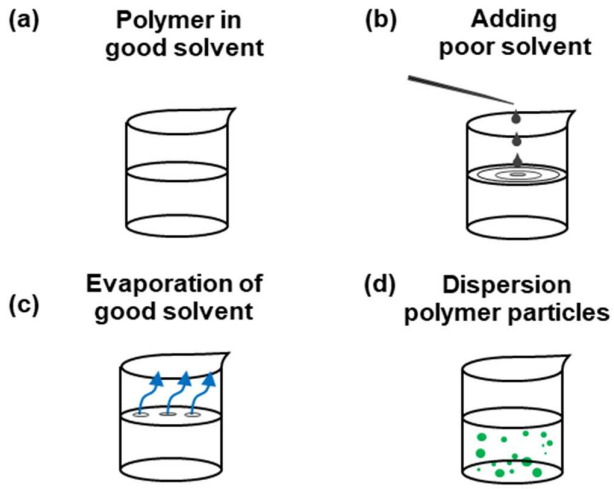

Fig. 1-7 Schematic description of precipitation method for preparation of polymer particles (cited and partially modified from ref. 28).

Salting out

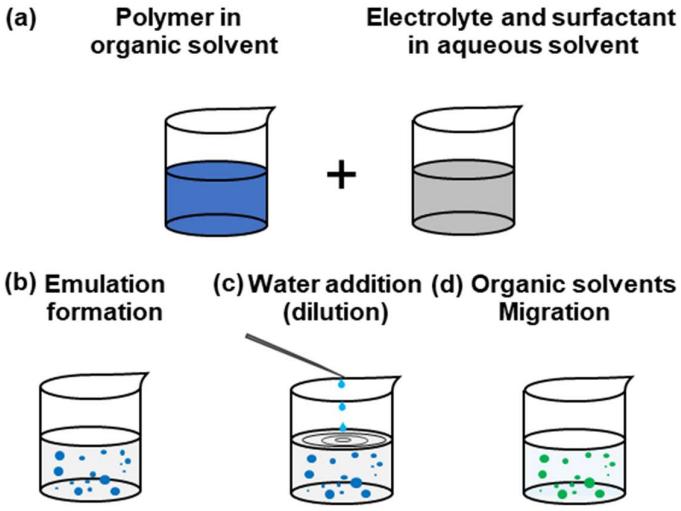

Fig. 1-8 Schematic description of salting out method for preparation of polymer particles (cited and partially modified from ref. 29).

This method modifies from the conventional method which generally requires chlorinated solvent, which is considered as hazardous to the environment as well as human health. As shown in Fig 1-8, polymer is dissolved in the organic solvent which is miscible with water such as tetrahydrofuran (THF) and acetone. Then, this solution is mixed with the aqueous solution containing of surfactant and saturated solution of electrolyte, by continuous stirring. According to the miscibility of the aqueous phase with the organic phase, the formation of an emulsion can be achieved. With excess of water, the diffusion of organic solvent into the aqueous phase by a reverse salting out effect takes place, which leads to the formation of polymer particles. Finally, the polymer particles are purified to remove electrolytes by centrifugation process [29), (30)].

Dialysis

Dialysis is another well-known method for polymer particles fabrication which is quite similar to the precipitation method mentioned previously (see in Fig. 1-9). The only different is that the polymer with dissolved in the water-miscible organic solvent (good solvent) is placed inside a dialysis membrane which is then put into water [(26)]. The organic solvent diffuses to the water phase through the dialysis membrane resulting in a loss of polymer solubility, and subsequent formation of polymer particles [(31)].

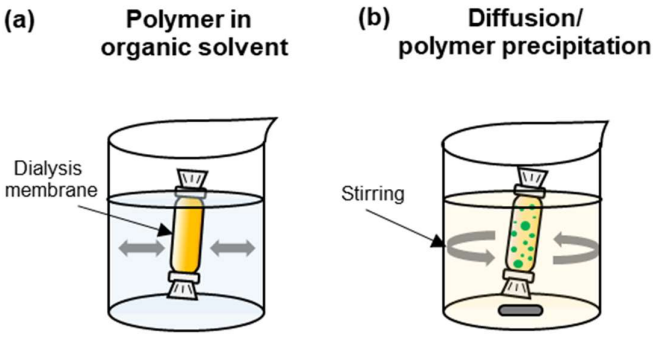

Fig. 1-9 Schematic description of dialysis method for preparation of polymer particles (cited and partially modified from ref. 32).

Supercritical solution

In this method, polymer is dissolved in the supercritical fluid without any organic solvents which is recognized as more environmental friendly method (see Fig. 1-10). Then, this solution is

immediately depressurized through capillary nozzle to the ambient pressure. This leads to the polymer precipitation since the solubility difference of the polymer in supercritical fluids at high and low pressures, respectively [33].

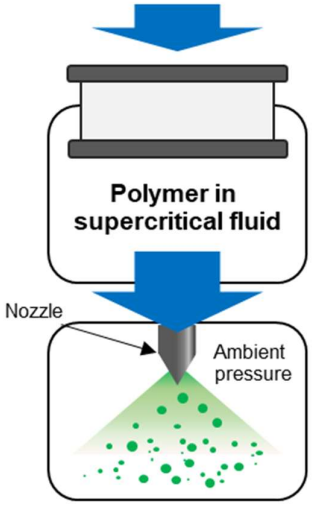

Fig. 1-10 Schematic description of supercritical solution method for preparation of polymer particles (cited and partially modified from ref. 32, 33).

1-3 Current fabrication methods of polymer micro/nano discs

Since their unique properties, there are a significant number of researches that have addressed the fabrication method of polymer discs. These methods can be broadly classified into two main categories namely bottom-up methods and top-down methods (see Fig. 1-11).

1-3-1 Bottom-up methods

Bottom-up method generally refers to the process that starts from smaller building blocks such as monomer or block copolymer to be polymer discs. The key bottom-up methods include of seeded dispersion polymerization [34], electrosprayed synthesis [35], and phase inversion in emulsions [36], disassembling of stacked block copolymer particles [37], [38].

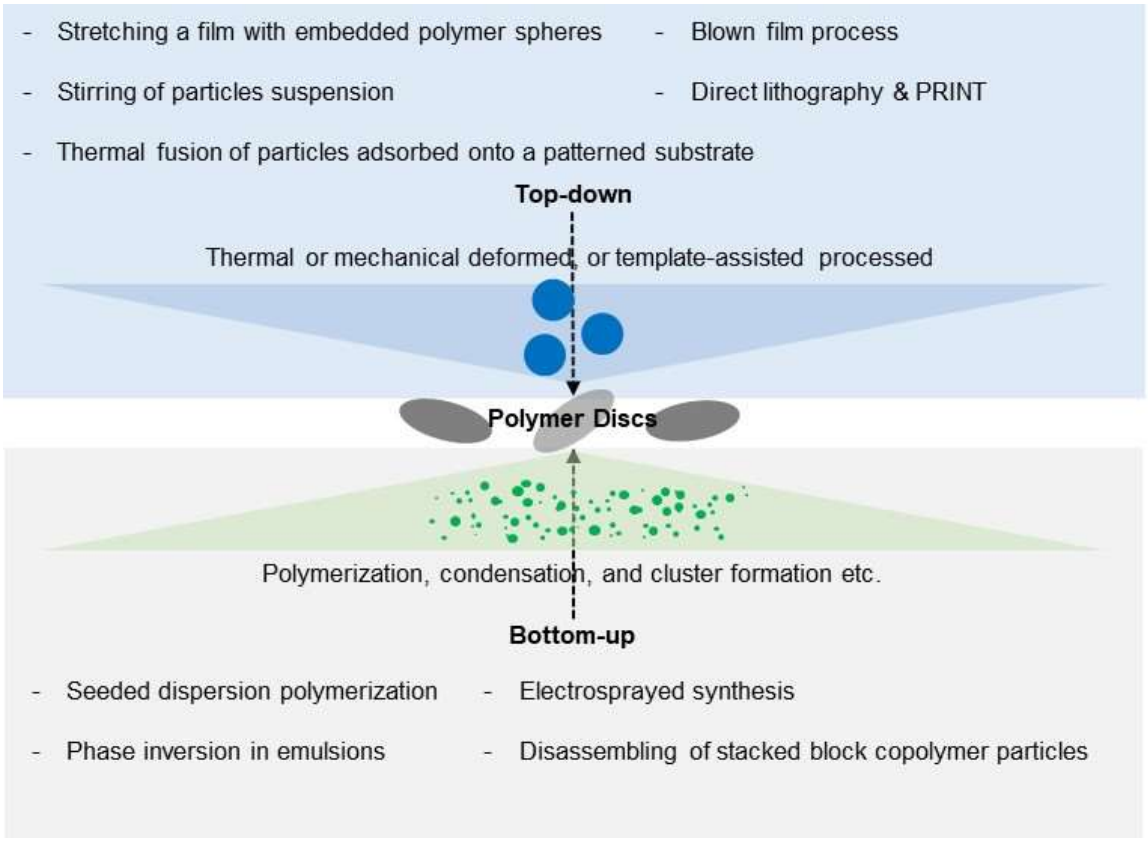

Fig. 1-11 Schematic diagram of fabrication methods of polymer micro/nano discs.

Seeded dispersion polymerization

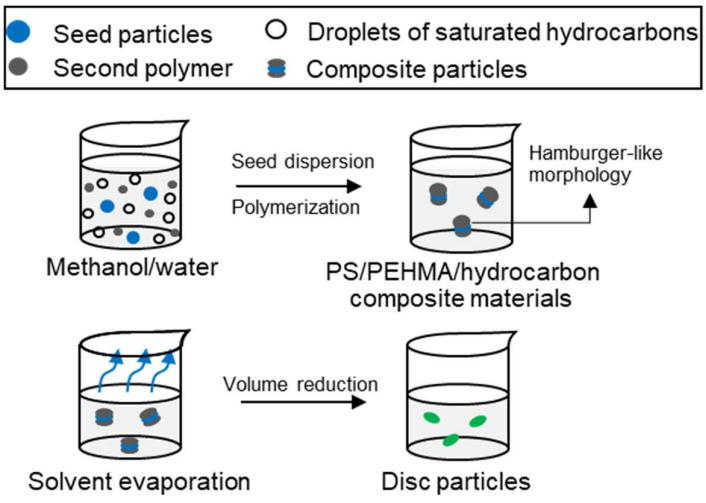

Fig. 1-12 Schematic description of seeded dispersion polymerization for preparation of polymer discs (cited and partially modified from ref. 34).

In this method, polystyrene (PS) seed particles in methanol/water was used as a media with the presence of droplets of various saturated hydrocarbon (see Fig. 1-12). These hydrocarbons are selected to be predominantly absorbed by the domain comprising the second polymer, 2-ethylhexyl methacrylate (EHMA). The evaporation of the solvent after polymerization encourages the significant volume reduction of the phase comprising the second polymer and the solvent. Hamburger-like morphology was observed to as metastable before evaporation of the hydrocarbon before converting to be disc-like shapes [34].

Electrosprayed synthesis

Electrospraying based on electrospinning (see Fig. 1–13), generally using for fabrication polymer fiber, has potential for the fabrication of disc like particles. A polymer solution is forced to pass through a small nozzle under the electric field. The formation of an electrified jet induces by the electrostatic charge on the surface of a liquid droplet. In cellulose derivatives, the crystal structure of the cellulose results in the formation of the sheet structure. This sheet structure might become discoid and dent in its center because of electrostatic repulsions between the surface charge and the resistance undergone during the moving from needle to collector [34].

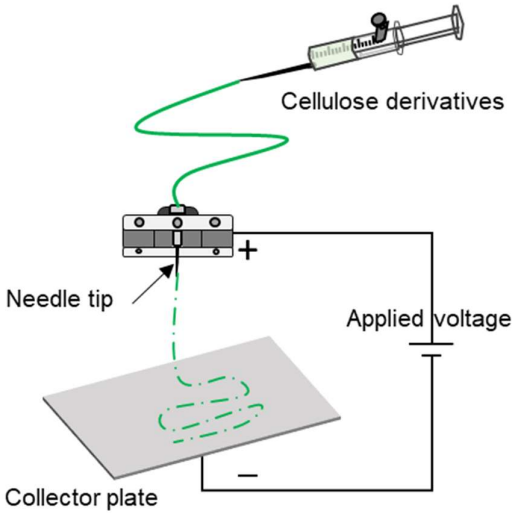

Fig. 1-13 Schematic description of electrosprayed synthesis for preparation of polymer discs (cited and partially modified from ref. 35).

Disassembling of stacked block copolymer particles

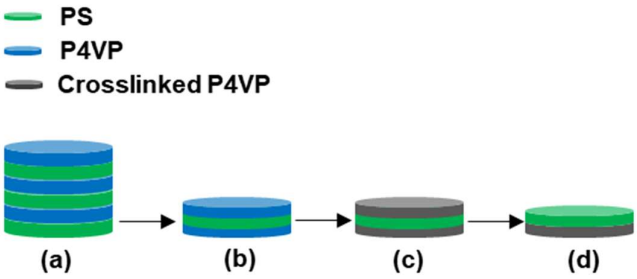

Fig. 1-14 Schematic description of disassembling disc-stacked particles (DSPs) of a deblock copolymer for preparation of polymer discs; a) disc-stacked particles of PS- b -P4VP diblock copolymer; (b) P4VP/PS/P4VP sandwiched nanodiscs; (c) crosslinking both the top and bottom P4VP layers; (d) Janus nanodiscs (cited and partially modified from ref. 38).

In this method, disc-stacked particles (DSPs) of PS- *b* -P4VP diblock copolymer is dissembled by emulsion droplet confined self-assembly (see Fig. 1–14a). By using selective solvent of poly(4-vinyl pyridine) (P4VP), the DSPs are partially disassembled into P4VP/PS/P4VP sandwiched nanodiscs (see Fig. 1-14b). Then, both top and bottom layers of these sandwiched nanodiscs are crosslinked with 1, 5-diiodopentane (DIP), turning to be positive charged (see Fig. 1–14c). Finally, chloroform is used to disassemble the crosslinked sandwiched nanodiscs into two isolated nanodiscs eventually (see Fig. 1-14d) [38].

Phase inversion in emulsions

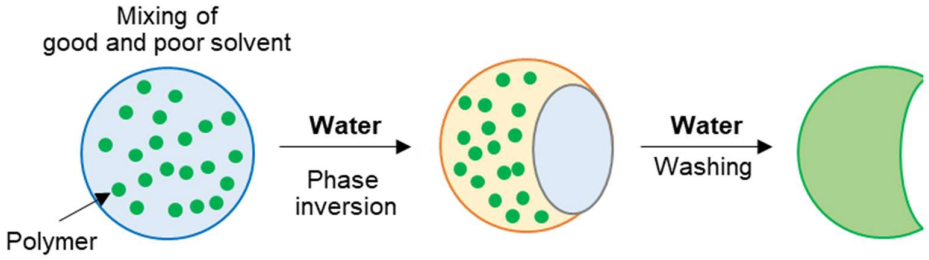

Fig. 1-15 Schematic description of phase inversion in emulsions for preparation of polymer discs (cited and partially modified from ref. 36).

In this method, phase inversion from water-in-oil (W/O) to oil-in-water (O/W) emulsions is utilized to fabricate non-spherical particles (*e.g.*, disc-like particles) by generating inhomogeneous distribution of polymers within the oil droplets (see Fig. 1-15). To achieve such an inhomogeneous distribution, a mixed solvent comprising good and poor solvents as the oil phase of the O/W emulsion for the polymer is used. The addition of water induces phase separation which is required for the phase inversion from W/O to O/W emulsions [(36)].

1-3-2 Top-down methods

On the other hand, top-down methods generally refers to the process that polymer is thermal or mechanical deformed, or template-assisted processed, such as stretching a film with embedded polymer spheres [(39)], blown film process [(40)], stirring of particles suspension [(41)], direct lithography [(42)], and particle replication in non-wetting templates (PRINT) [(43)] and thermal fusion of particles adsorbed onto a patterned substrate [(44), (45)].

Stretching a film with embedded polymer spheres

This method is considered as the well-known method for fabrication various shapes of particles including polymer discs since its simplicity. First, spherical polymer particles are put in polymer mixture which is normally polyvinyl alcohol (PVA) with small amount of plasticizer such as glycerol. This polymer mixture is casted as film by drying and then stretched with heat (see Fig. 1–16) [(39)].

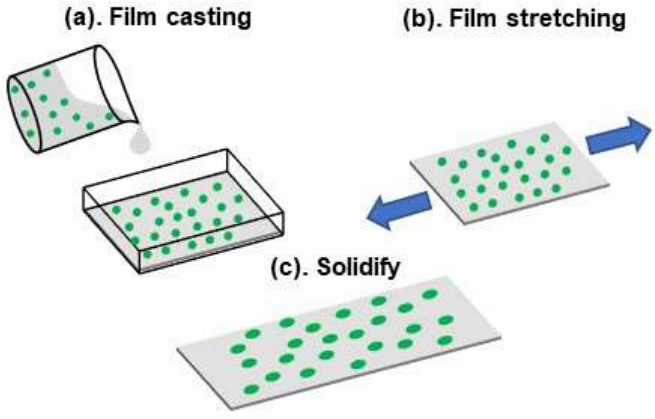

Fig. 1–16 Schematic description of stretching a film with embedded polymer spheres for preparation of polymer discs (cited and partially modified from ref. 39).

Blown film process

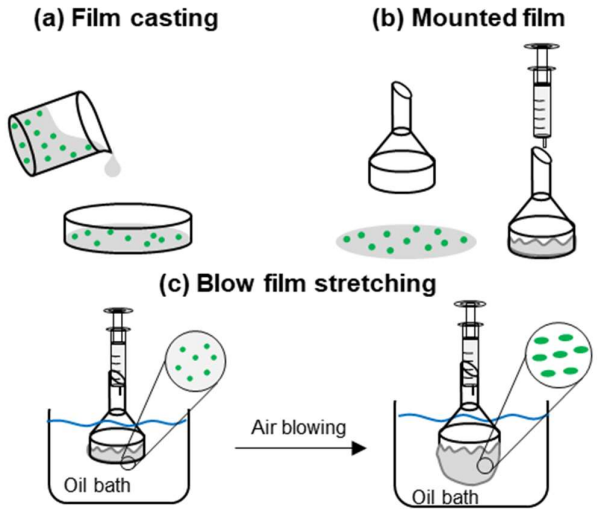

Fig. 1-17 Schematic description of blown film process for preparation of polymer discs (cited and partially modified from ref. 40).

This method is utilized the same principal with film stretching method mentioned in previous section. The key difference of these two methods is that in blown film process air is used to stretch cast film with embedded polymers instead of using stretcher (see Fig. 1-17). Similar to film stretching method, a thin composite polymer/PVA film is initially prepared by slowly evaporating the solvent. Then, embedded film is mounted to on top of the wide opening of a ceramic filtering funnel, and tightly sealed. This mounted film is then immersed into a hot silicon oil bath to soften the film. Air is then injected into the system to blow the film into a dome-like shape. Finally, the film is cooled in air with the pressure maintained and dissolved in isopropanol/water to collect polymer discs [(40)].

Stirring of particles suspension

In this method, the high-throughput production of colloidal discs can be achieved via magnetic stirring of sulfate-stabilized PS spheres in aqueous solution in the presence of a good organic solvent (see Fig. 1-18). This solvent could be whether water-miscible or water-immiscible. In the case of water-immiscible organic solvents, the aqueous solution with the presence of sulfate-stabilized PS particle is mixed with the solvent. Morphology of PS discs could be controlled by magnetic stirring time and speed, the stirring bar weight, and the amount of organic solvent [(41)].

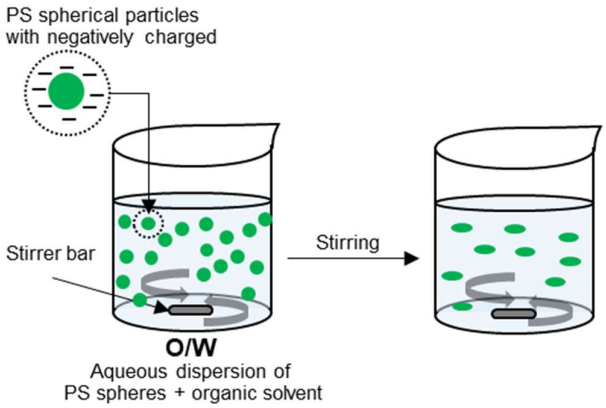

Fig. 1-18 Schematic description of stirring of particles suspension for preparation of polymer discs (cited and partially modified from ref. 41).

Direct lithography

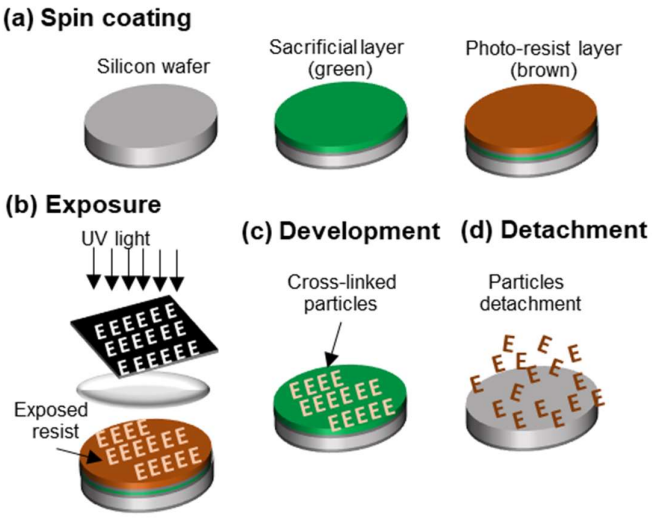

Fig. 1-19 Schematic description of direct lithography for preparation of polymer discs (cited and partially modified from ref. 42).

Lithography is unique model systems that uses for mass-producing exotic colloids (LithoParticles). As can be seen in Fig.1-19, this method starts with the spin-coating of polished wafers with sacrificial layer of water-soluble polymer. Then, these wafers are then coated with one more layer by UV-sensitive photoresist. The thickness of the resist layer can be controlled from about 100 nm to many microns with excellent uniformity. Next, lithographic projection exposure system, or “stepper”, is used to rapidly expose the photoresist. The mask patterns of letters or other shapes on a photomask

is exposed to the coated wafer which causes cross-linking of the polymer resist. Finally, the unexposed area is removed followed by the sacrificial layer by water where the particles are lifted completely off of the surface into aqueous solution [42].

Particle replication in non-wetting templates (PRINT)

Particle replication in non-wetting templates (PRINT) is the method that develop based on a soft lithography technique. As can be seen in Fig. 1-20, PRINT mold is initially prepared by perfluoropolyether (PFPE) elastomers on silicone master to create patterns. Then, a liquid pre-particle material is filled into the cavities of PRINT mold using a roll-to-roll process. These pre-particles are solidified through a number of different processes and removed from the mold by bringing the mold in contact with an adhesive layer for detachment [43].

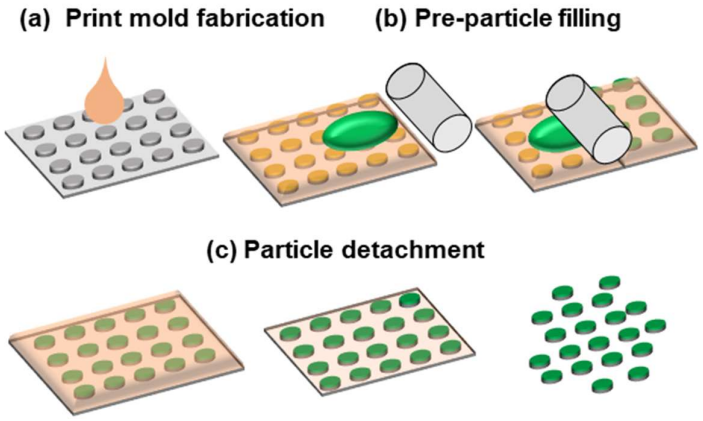

Fig. 1-20 Schematic description of Particle replication in non-wetting templates for preparation of polymer discs (cited and partially modified from ref. 44).

Thermal fusion of particles adsorbed onto a patterned substrate

In this method, disc-shaped nanosheets is fabricated using patterning process. First, SiO_2 is patterned with 3 μm disc shaped hydrophobic regions of octadecyltrimethoxysilane/mPEO-SAM (ODS/mPEO-SAM) which is immersed into a suspension of the poly(D,L-lactide-co-glycolide) (PLGA) nanoparticles (see Fig. 1-21). After withdrawing from the suspension, the substrate slowly blown off with a horizontal N_2 and washed with distilled water. This process is repeated for ten times to obtain packed pattern of PLGA nanoparticles. Then, the substrate is dried and heated to initiate thermal fusion

of the adsorbed PLGA nanoparticles. To obtain freestanding disc-shaped nanosheets, PVA is used to detach disc-shaped nanosheets from SiO_2 substrate [45], [46].

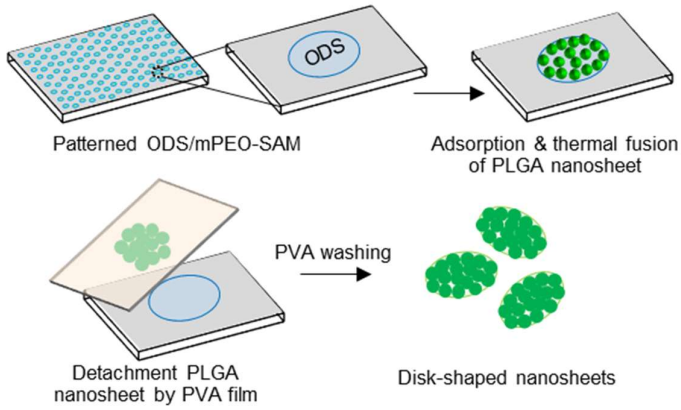

Fig. 1–21 Schematic description of thermal fusion of particles adsorbed onto a patterned substrate for preparation of polymer discs (cited and partially modified from ref. 46).

1-4 Applications of polymer micro/nano particles and discs

As mentioned previously, polymer micro/nano particles, which will be further referred as polymer particles, have been used in many applications and in various fields; for example, ***Painting***: the using of polymer particles instead of TiO_2 particles to prevent the reduction in the luminescent intensity in pressure-sensitive paint [47], ***Printing***: the using of polymer particles as a binder for textile inkjet printing of cotton fabrics [48], ***Paper manufacturing***: the using of hydrophobic particles with different charge for paper surface hydrophobation (frequently referred to as surface sizing) [49], ***Electronics***: the using of conducting magnetic nano composite polymer particles for potential applications such as energy storage devices, electron field emitters, chemical and biological sensors, actuators, etc [50], [51]. ***Energy***: the using of microporous polymer particles as a hydrogen storage [52]. ***Construction***: the using of polymer particles for improvement of various properties, such as impermeability, durability, adhesive and mechanical strength, toughness in cementitious materials [53]. ***Cosmetic***: the using of polymer particles with encapsulated ultraviolet (UV) absorbent, fluorescent agent, and blue pigment for cosmetic [54], ***Biomedical***: the using of polymer magnetic particles for drug vectoring and antitumoral therapy, etc. and the using of polymer particles for drug delivery systems (DDSs) [55], [56] (see more details in Table 1-1).

The most general shape of polymer particles is sphere since the tendency to form the minimum surface energy. However, many studies have been shifted to fabricate non-spherical polymer particles in these past several years to utilize their unique and fascinating properties [57]-[62]. Among them, a polymer disc is one of the promising shapes that can improve the surface adhesion to an interface owing to their larger surface area for contact and interaction. Both computational and experimental studies have demonstrated a stronger interfacial adhesion and margination to the wall under flow for polymer discs [63]-[65], which is, for example, the key feature for use as a drug carrier in a drug delivery system [66]-[68]. In addition, a seminal work reported that the shape at the contact point between particles and cells is crucial for phagocytosis, and polymer discs may have longer lifetime due to the inhibited macrophagic uptake compared to that of the spherical particles [69]. Such unique and fascinating properties obtained from polymer discs provide competitive advantages to overcome the problems that spherical particles may unable to solve [66].

Accordingly, polymer discs have intensively used in biomedical applications to improve or overcome conventional limitations which spherical particles cannot serve. For example, the using polymer discs as a drug carrier for bone repair to overcome the problem of non-localised high oral doses [70], the using disc prototype of anti-intercellular adhesion molecule (ICAM) carriers to prolong half-life in the circulation in blood [71], the using polymer discs to maximize accumulation in the target organ while reducing sequestration by the liver [72], improving cellular uptake by intestinal cells of oral drug [1-62], and improving cellular uptake by mammalian cells [60] *etc*.

Table 1-1 The application of polymer particles in various fields

Applications	Fields	Details of study	Polymer particles	References
Pressure-sensitive paint with high photostability	Painting	A novel fast-responding and paintable pressure-sensitive paint (PSP) based on polymer particles	PS of ~1 μm	(47)
Latex nanoparticles using nanoemulsions for textile printing	Printing	Nanoparticles by the polymerization in miniemulsion templates using as a binder for textile inkjet printing	Styrene, butyl acrylate and methyl methacrylate /nonionic surfactant of 30–110 nm	(48)
Hydrophobic particles for paper surface hydrophobation (surface sizing)	Paper manufacturing	Hydrophobic particles with different charge for paper surface hydrophobation	The monomer mixture of styrene, dimethylamino propyl methacrylamide (DMAPMA), and 2-dimethylaminoethyl methacrylate (DAMM).	(49)
Conducting magnetic nano composite polymer particles for various electronic devices	Electronics	Conducting magnetic composite polymer particles by seeded emulsion polymerization and seeded chemical oxidative polymerization	Methyl methacrylate (MMA) in presence of nano-sized Fe_3O_4 core (Fe_3O_4/PMMA) of 1–3 μm	(50)
Uniform microporous polymer nanoparticles for hydrogen storage	Energy	Synthesis of polymer nanoparticles by emulsion polymerization with higher hydrogen adsorption capacity	Vinylbenzyl chloride (VBC)/divinylbenzene (DVB) copolymers of 36 to 131 nm	(52)
Polymer particles to increase the fluidity of fresh cement pastes	Construction	The effect of colloidal polymers with different surface properties on the rheological properties and meso-structure development of cement pastes	PS latexes with varied surface properties in a range of 170–320 nm	(53)

Table 1-1 The application of polymer particles in various fields (Cont'd)

Applications	Fields	Details of study	Polymer particles	References
Micrometer-sized polymer particles for cosmetic	Cosmetic	Capsule particles of UV absorbent, fluorescent moiety, and blue pigment by microsuspension polymerization	Ethyleneglycol dimethacrylate (EGDM) and MMA particles of 1–2 μm	(54)
Magnetic polymer particles as an intelligent drug	Biomedical	Magnetic particles with biodegradable and biocompatible synthetic polymers for various applications, such as drug vectoring and antitumoral therapy.	Various polymer such as of poly (lactic acid) (PLA), PVA, chitosan of a wide range from 5 nm –3,000 μm	(55)
Micro-sized discoidal polymeric particles for lung-targeted delivery system	Biomedical	Biological properties of micro-sized discoidal polymeric particles (DPPs) as lung-targeted drug delivery carriers	PLGA of ~2.8 μm	(56)

1-5 Purpose of this thesis

Although a significant number of studies have been proposed for the fabrication of polymer discs as mentioned in previous section, there are still limitations of these current methods in term of high production cost, low yield, process complexity, and/or shape polydispersity. In addition, most of these processes consume a huge amount of organic solvent which is realized as non-environmentally friendly. Therefore, to develop a facile, versatile, and environmental friendly method for fabrication disc-shaped polymer particles remains an imperative for their applications.

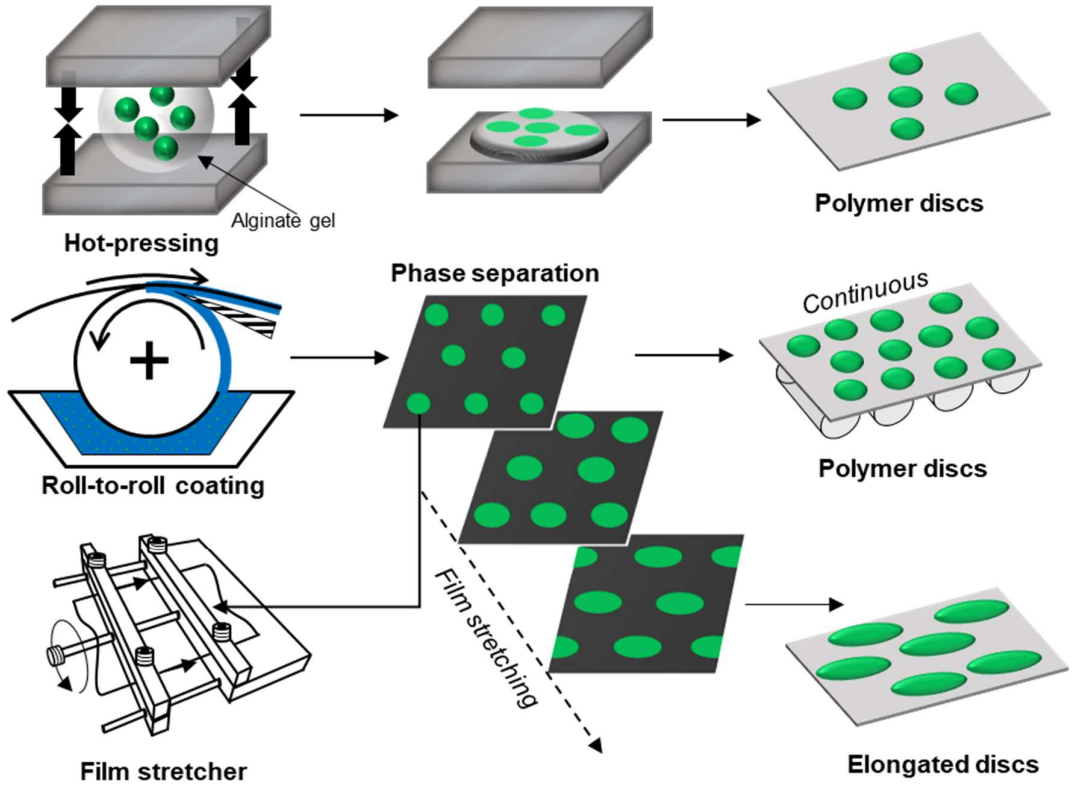

Fig. 1-22 Schematic description purpose of this study

First, we aimed to propose a novel method to fabricate polymer discs by hot-press process combined with a sacrificial matrix technique. By this method, only aqueous solution and suspension are employed which is less toxic for the human health and environmental pollution. The simplified pressing process was utilized to fabricate individual polymer discs in a controllable manner from PS and poly(L-lactic acid) (PLLA) microspheres with a wide range of size in a controllable manner.

Furthermore, the unique high interfacial adhesion of the prepared discs was verified, including the adhesiveness of polymer discs to surface of cover glass under airflow, as well as the enhancement of aggregation for bovine serum albumin (BSA)-coated polymer discs in the presence of glutaraldehyde (GA). However, complication is still likely to be encountered when scaling up this process by having the size of pressing equipment as a bottleneck.

Second, to overcome the difficulties of both hot-press, we aimed to propose a novel, straightforward, and time-saving method to continuously fabricate micro/nano-discs via phase separation and a roll-to-roll coating process. By combining phase separation with roll-to-roll coating process on PVA film, large amounts of polymer micro/nano-discs can be continuously produced in a one-pot manner. Polyvinylpyrrolidone (PVP) and PS, as model discs components, are chosen as the major and minor components in the polymer blend. Since PVA and PVP are water-soluble, the micro/nano-discs composed of PS could be continuously obtained in large amounts by washing with water in a one-pot manner. Since PVA substrate film used for the roll-to-roll coating shows a good extensibility and heat resistance, which implies a high likelihood of combining this method with a stretching method for fabrication of polymer particles with further peculiar shapes.

Finally, we aimed to propose a facile method to fabricate disc micro/nano particles with high aspect ratio by combining our previously proposed method of phase separation and a roll-to-roll coating process with film stretching. Biodegradable PLGA is herein selected as a minor component by having PVP as a major component in the polymer blend. The surface adhesiveness of elongated PLGA discs is compared with three distinct shapes, namely discs before stretching, spheres and elongated spheres by water-dropping test.

1-6 Organization of this thesis

This paper consists of the following five chapters:

Chapter 1 is an introduction which describes the applications and the fabrication methods of polymer particles. In addition, the advantages and fabrication method of polymer micro/nano discs were also discussed. Finally, the purpose and the organization of this thesis have been described.

In Chapter 2, a hot-press process combined with a sacrificial matrix technique was proposed and discussed. PS and PLLA microspheres with a wide range of size was used as model polymer. The choice of sacrificial matrix and the optimal condition for hot-press is also discussed. Moreover, the adhesiveness of polymer discs to surface of cover glass under airflow, as well as the enhancement of aggregation for BSA-coated polymer discs in the presence of GA were investigated.

In Chapter 3, a continuously fabricate micro/nano-discs via phase separation and a roll-to-roll coating process was proposed and discussed. The effect of operating conditions of roll-to-roll machine on phase separation morphology was studied having PVP and PS, as model discs components. The effect of polymer mixture blend ratio and the percentage of total concentration on morphology of PS discs before and after collection was investigated. Then, how to control aspect ratios of polymer discs by these parameters was established. Finally, the versatility of this method was also evaluated with various polymers.

In Chapter 4, a facile method combining the phase separation and a roll-to-roll coating process with film stretching was proposed. The effect of film stretching and stretching temperature on polymer elongated discs was discussed having PLGA and PVP as minor and major components, respectively. The effect of film stretching and stretching temperature were studied. Finally, the surface adhesiveness of PLGA elongated discs comparing with other distinct shapes of polymer particles were evaluated and discussed by water-dropping test.

Chapter 5 summarizes the results obtained in Chapters 2-4 and the future works.

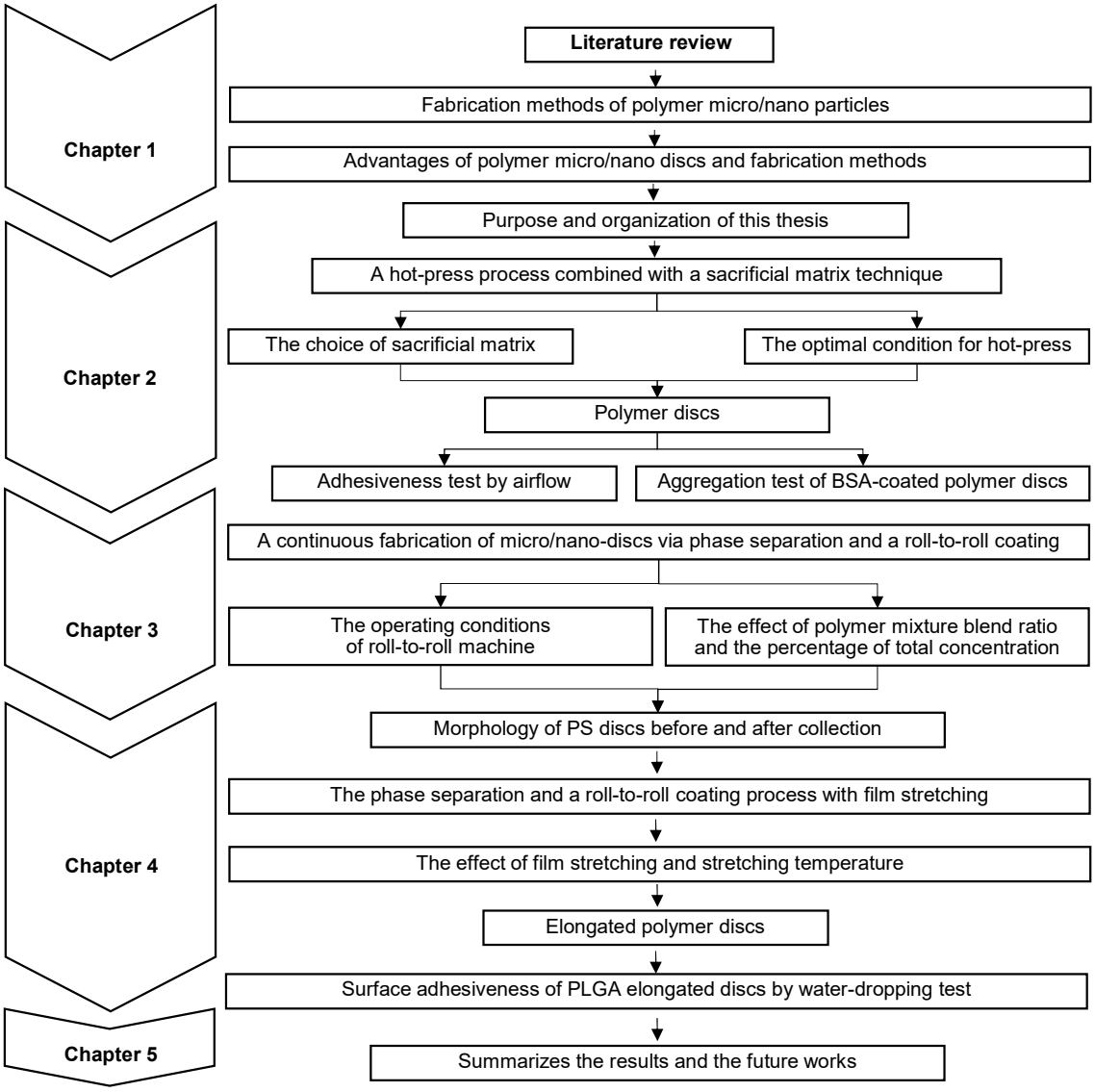

Fig. 1-23 Organization of this thesis

References

[1] J. W. Hickey, J. L. Santos, J. M. Williford, H. Q. Mao, Control of polymeric nanoparticle size to improve therapeutic delivery, J. Control. Release 219 (2015) 536–547.

[2] A. Kowalczuk, R. Trzcinska, B. Trzebicka, A. H. E. Müller, A. Dworak, C. B. Tsvetanov, Loading of polymer nanocarriers: factors, mechanisms and applications, Prog. Polym. Sci. 39 (2014) 43–86.

[3] M. Xiong, Y. Bao, X. Yang, Y. Zhu, J. Wang, Delivery of antibiotics with polymeric particles, Adv. Drug Deliv. Rev. 78 (2014) 63–76.

[4] Z. Tang, C. He, H. Tian, J. Ding, B. S. Hsiao, B. Chu, X. Chen, Polymeric nanostructured materials for biomedical applications, Prog. Polym. Sci. 60 (2016) 86–128.

[5] A. George, P. A. Shah, P. S. Shrivastav, Natural biodegradable polymers based nano-formulations for drug delivery: a review, Int. J. Pharm. 561 (2019) 244–264.

[6] A. Sosnik, K. P. Seremeta, Advantages and challenges of the spray-drying technology for the production of pure drug particles and drug-loaded polymeric carriers, Adv. Colloid Interface Sci. 223 (2015) 40–54.

[7] H. Tian, Z. Tang, X. Zhuang, X. Chen, X. Jing, Biodegradable synthetic polymers: preparation, functionalization and biomedical application, Prog. Polym. Sci. 37 (2012) 237–280.

[8] J. P. Rao, K. E. Geckeler, Polymer nanoparticles: preparation techniques and size-control parameters, Prog. Polym. Sci. 36 (2011) 887–913.

[9] D. Qi, Z. Cao, U. Ziener, Recent advances in the preparation of hybrid nanoparticles in miniemulsions, Adv. Colloid Interface Sci. 211 (2014) 47–62.

[10] A. N. M. B. El-hoshoudy, Emulsion Polymerization Mechanism, Recent Research in Polymerization, N. Cankaya Eds., IntechOpen: UK, 2018, Chapter 1, 3–14.

[11] A. Gharieh, S. Khoee, A. R. Mahdavian, Emulsion and miniemulsion techniques in preparation of polymer nanoparticles with versatile characteristics, Adv. Colloid Interface Sci 269 (2019) 152–186.

[12] D. Nagao, T. Sakamoto, H. Konno, S. Gu, M. Konno, Preparation of micrometer-sized polymer particles with control of initiator dissociation during soap-free emulsion polymerization, Langmuir 22 (2006) 10958–10962.

[13] C.S. Chern, Emulsion polymerization mechanisms and kinetics, Prog. Polym. Sci. 31 (2006) 443–486.

[14] M. Antonietti, K. Landfester, Polyreactions in miniemulsions, Prog. Polym. Sci. 27 (2002) 689–757.

[15] J. M. Asua, Miniemulsion polymerization, Prog. Polym. Sci. 27 (2002) 1283–1346.

[16] G. Haifeng, A personal journey on using polymerization in aqueous dispersed media to synthesize polymers with branched structures, Chin. Chem. Lett. 30 (2019) 1996–2002.

[17] F. M. Pavel, Microemulsion polymerization, J Dispers Sci Technol 25 (2004) 1–6.

[18] X.-J. Xu, L. M. Gan, Recent advances in the synthesis of nanoparticles of polymer latexes with high polymer-to-surfactant ratios by microemulsion polymerization, Curr. Opin. Colloid Interface Sci. 10 (2005) 239–244.

[19] Y. Song, J.-B. Fan, S. Wang, Recent progress in interfacial polymerization, Mater. Chem. Front. 1 (2017) 1028–1040.

[20] P. W. Morgan, Interfacial polymerization, In: Encyclopedia of polymer science and technology, Wiley: NY, 2002, 18.

[21] M. J. T. Raaijmakers, N. E. Benes, Current trends in interfacial polymerization chemistry, Prog. Polym. Sci 63 (2016) 86–142.

[22] K.S.V. K. Rao, K. M. Rao, A review on radical polymerization used for design and development of biomaterials, Radical Polymerization: New Developments, Nova Science Publishers: NY, Chapter 5 (2012) 175–198.

[23] K. Miladi, D. Ibraheem, M. Iqbal, S. Sfar, H. Fessi, A. Elaissari, Particles from preformed polymers as carriers for drug delivery, Excli J. 13 (2014) 28– 57.

[24] Neeta, M. Mehta, S. Satija, P. Pandey, M. Dahiya, Solvent evaporation technique: An innovative approach to increase gastric retention, Int. J. Adv. Sci. Res. 1 (2016) 60–67.

[25] S. Freitas, H. P. Merkle, B. Gander, Microencapsulation by solvent extraction/evaporation: reviewing the state of the art of microsphere preparation process technology, J Control Release. 102 (2005) 313–332.

[26] S. Sur, A. Rathore, V. Dave, K. R. Reddy, R. S. Chouhan, V. Sadhu, Recent developments in functionalized polymer nanoparticles for efficient drug delivery system, Nano-Structures & Nano-Objects 20 (2019) 100397.

[27] H. Fessi, F. Puisieux, J.Ph. Devissaguet, N. Ammoury, S. Benita, Nanocapsule formation by interfacial polymer deposition following solvent displacement, Int. J. Pharm. 55 (1989) R1–R4.

[28] H. Yabu, Self-organized precipitation: an emerging method for preparation of unique polymer particles, Polym. J. 45 (2013) 261–268.

[29] M. Tarhinia, H. Greige-Gergesb, A. Elaissari, Protein-based nanoparticles: from preparation to encapsulation of active molecules, Int. J. Pharm. 522 (2017) 172–197.

[30] Y. Wang, P. Li, T. T.-D. Tran, J. Zhang, L. Kong, Manufacturing techniques and surface engineering of polymer based nanoparticles for targeted drug delivery to cancer, Nanomaterials 6 (2016) 26.

[31] M. Liu, Z. Zhou, X. Wang, J. Xu, K. Yang, Q. Cui, X. Chen, M. Cao, J. Weng, Q. Zhang, Formation of poly(L,D-lactide) spheres with controlled size by direct dialysis, Polymer 48 (2007) 5767–5779.

[32] B. K. Lee, Y. Yun, K. Park, PLA micro- and nano-particles, Adv. Drug Deliv. Rev. 107 (2016) 176–191.

[33] S.-D. Yeob, E. Kiran, Formation of polymer particles with supercritical fluids: a review, J. Supercrit. Fluids 34 (2005) 287–308.

[34] T. Fujibayashi, M. Okubo, Preparation and thermodynamic stability of micron-sized, monodisperse composite polymer particles of disc-like shapes by seeded dispersion polymerization, Langmuir 23 (2007) 7958–7962.

[35] K. Hayashi, K. Ono, H. Suzuki, M. Sawada, M. Moriya, W. Sakamoto, T. Yogo, Electrosprayed synthesis of red-blood-cell-like particles with dual modality for magnetic resonance and fluorescence imaging, Small 6 (2010) 2384–2391.

[36] S. Ichikawa, T. Kawai, One-pot fabrication of multiporous polymer particles by phase inversion in emulsions, Colloids Surf. A 532 (2017) 570–577.

[37] R. Deng, F. Liang, P. Zhou, C. Zhang, X. Qu, Q. Wang, J. Li, J. Zhu, J. Z. Yang, Janus nanodiscs: Janus nanodisc of diblock copolymers, Adv. Mater. 26 (2014) 4402–4402.

[38] R. Deng, F. Liang, P. Zhou, C. Zhang, X. Qu, Q. Wang, J. Li, J. Zhu, Z. Yang, Janus nanodisc of diblock copolymers. Adv. Mater. 26 (2014) 4469−4472.

[39] J.A. Champion, Y.K. Katare, S. Mitragotri, Making polymeric micro- and nanoparticles of complex shapes, Proc. Natl. Acad. Sci. U.S.A. 104 (2007) 11901–11904.

[40] B.Y. Hu, J. Ge, T. Zhang, Y. Yin, A blown film process to disk-shaped polymer ellipsoids, Adv. Mater. 20 (2008) 4599–4602.

[41] B. Liu, D. Wang, High-throughput transformation of colloidal polymer spheres to discs simply via magnetic stirring of their dispersions, Langmuir 28 (2012) 6436–6440.

[42] C.J. Hernandez, T.G. Mason, Colloidal alphabet soup: monodisperse dispersions of shape-designed lithoparticles, J. Phys. Chem. C 111 (2007) 4477–4480.

[43] J. P. Rolland, B. W. Maynor, L. E. Euliss, A. E. Exner, G. M. Denison, J. M. DeSimone, Direct fabrication and harvesting of monodisperse, shape-specific nanobiomaterials. J. Am. Chem. Soc. 127 (2005) 10096−10100.

[44] J. Xu, Future of the particle replication in nonwetting templates (PRINT) technology, Angew Chem Int Ed Engl. 52 (2013) 6580–6589.

[45] Y. Okamura, S. Utsunomiya, H. Suzuki, D. Niwa, T. Osaka, S. Takeoka, Fabrication of free-standing nanoparticle-fused nanosheets and their hetero-modification using sacrificial film, Colloids Surf. A 318 (2008) 184−190.

[46] Y. Okamura, Y. Fukui, K. Kabata, H. Suzuki, M. Handa, Y. Ikeda, S. Takeoka, Novel platelet substitutes: disk-shaped biodegradable nanosheets and their enhanced effects on platelet aggregation. Bioconjug. Chem. 20 (2009)1958–1965.

[47] Y. Matsuda, K. Uchida, Y. Egami, H. Yamaguchi, T. Niimi, Polymer-particle pressure-sensitive paint with high photostability, Sensors 16 (2016) 550.

[48] M. Elgammal, R. Schneider, M. Gradzielski, Preparation of latex nanoparticles using nanoemulsions obtained by the phase inversion composition (PIC) method and their application in textile printing, Colloids Surf. A 470 (215) 70–79.

[49] F. Iselau, P. Restorp, M. Andersson, R. Bordes, Role of the aggregation behavior of hydrophobic particles in paper surface hydrophobation, Colloids Surf. A 483 (2015) 264–270.

[50] H. Ahmad, K. Kumar, M. A. Rahman, M. M. Rahman, M. A. J. Miah, H. Minami, M. A. Nuri, Preparation and characterization of conducting polyaniline layered magnetic nano composite polymer particles, Polym. Adv. Technol. 24 (2013) 740–746.

[51] R. Gensler, P. Gröppel, V. Muhrer, N. Müller, Application of nanoparticles in polymers for electronics and electrical engineering, Part. Part. Syst. Charact. 19 (2002) 293–299.

[52] B. Li, X. Huang, L. Liang, B. Tan, Synthesis of uniform microporous polymer nanoparticles and their applications for hydrogen storage, J. Mater. Chem. 20 (2010) 7444–7450.

[53] Z. Lu, X. Kong, C. Zhang, F. Xing, Y. Zhang, Effect of colloidal polymers with different surface properties on the rheological property of fresh cement pastes, Colloids Surf. A 520 (2017) 154–165.

[54] S. Nakai, M. Akiyoshi, M. Okubo, Preparation of Micrometer-Sized, Multifunctional capsule particles for cosmetic by microsuspension polymerization utilizing the self-assembling of phase separated polymer method, J. Appl. Polym. Sci 127 (2013) 2407–2413.

[55] L. Bălăită, M. Popa, Polymer magnetic particles in biomedical applications, Revue Roumaine de Chimie, 54 (2009) 185–199.

[56] J. Y, Park, S. Park, T. S. Lee, Y. H. Hwang, J. Y. Kim, W. J. Kang, J. Key, Biodegradable micro-sized discoidal polymeric particles for lung-targeted delivery system, Biomaterials 218 (2019) 119331.

[57] B. Yu, H. Cong, Q. Peng, C. Gu, X. Xu, C. Tian, F. Zhai, Current status and future developments in preparation and application of nonspherical polymer particles, Adv. Colloid Interface Sci. 256 (2018) 126–151.

[58] J. Chen, N. Clay, H. Kong, Non-spherical particles for targeted drug delivery, Chem. Eng. Sci. 125 (2015) 20–24.

[59] L.K. Koegel, T. Vernon, R.L. Koegel, B.L. Koegel, A.W. Paullin, Particle shape: a new design parameter for micro- and nanoscale drug delivery carriers, J Control Release. 121 (2007) 3–9.

[60] A.B. Jindal, The effect of particle shape on cellular interaction and drug delivery applications of micro- and nanoparticles, Int. J. Pharm. 532 (2007) 450–465.

[61] S. Venkataraman, J.L. Hedrick, Z.Y. Ong, C. Yang, P.L.R. Ee, P.T. Hammond, Y.Y. Tanf, The effects of polymeric nanostructure shape on drug delivery, Adv. Drug Deliv. Rev. 63 (2011) 1228–1246.

[62] A. Banerjee, J. Qi, R. Gogoi, J. Wong, S. Mitragotri, Role of nanoparticle size, shape and surface chemistry in oral drug delivery, J. Control. Release 238 (2016) 176–185.

[63] P. Decuzzi, M. Ferrari, The adhesive strength of non-spherical particles mediated by specific interactions, Biomaterials 27 (2006) 5307–5314.

[64] N. Doshi, B. Prabhakarpandian, A. Rea-Ramsey, K. Pant, S. Sundaram, S. Mitragotri, Flow and adhesion of drug carriers in blood vessels depend on their shape: A study using model synthetic microvascular networks, J Control Release. 146 (2010) 196–200.

[65] J. W. Myerson, A. C. Anselmo, Y. Liu, S. Mitragotri, D. M. Eckmann, V. R. Muzykantov, Non-affinity factors modulating vascular targeting of nano- and microcarriers, Adv. Drug Deliv. Rev. 99 (2016) 97−112.

[66] X. Zhu, C. Vo, M. Taylor1, B.R. Smith, Non-spherical micro- and nanoparticles in nanomedicine, Mater. Horizons 6 (2019) 1094–1121.

[67] O. Mhatre, S. Sodha, Pharmaceutical feasibility and flow characteristics of polymeric non-spherical particles, Nanomedicine 18 (2019) 243–258.

[68] G. Sharma, D.T. Valenta, Y. Altman, S. Harvey, H. Xie, S. Mitragotri, J.W. Smith, Polymer particle shape independently in fluences binding and internalization by macrophages, J. Control. Release 147 (2010) 408–412.

[69] J. A. Champion, S. Mitragotri, Role of target geometry in phagocytosis. Proc. Natl. Acad. Sci. U.S.A. 103 (2006) 4930−4934.

[70] A. M. Young, S. M. Ho, Drug release from injectable biodegradable polymeric adhesives for bone repair, J Control Release. 127 (2008) 162–172.

[71] S. Muro, C. Garnacho, J. A. Champion, J. Leferovich, C. Gajewski, E. H. Schuchman, S. Mitragotri, V. R. Muzykantov, Control of endothelial targeting and intracellular delivery of therapeutic enzymes by modulating the size and shape of ICAM-1-targeted carriers, Mol. Ther. 16 (2008)1450–1458.

[72] P. Decuzzi, B. Godin, T. Tanaka, S.-Y. Lee, C. Chiappini, X. Liu, M. Ferrari, Size and shape effects in the biodistribution of intravascularly injected particles, J Control Release. 141 (2010) 320–327.

Chapter 2
Hot-pressing fabrication method of polymer discs and their adhesiveness

2-1 Background

Polymer micro/nano particles have shown great potentials in various industrials especially in biomedical applications, which seems to be a permanent topic in the field of polymer materials. In general, such particles can be synthesized by various fabrication methods as mentioned in Chapter 1. In order to minimalize the surface energy during the formation process, the shape of prepared particles is always spherical. Recently, the particle shape effect has been intensely studied, and the non-spherical polymer particles, especially disc shaped particles or oblate particles have been emphasized. There are a number of studies showing that disc shaped particles provide better interfacial adhesion than other shape of particles in both computational and experimental studies [1-4]. In addition, the shape at the contact point between particles and cells was reported to be crucial for phagocytosis. Polymer discs showed ability to inhibit macrophagic uptake compared to that of the spherical particles and thus may have longer lifetime [5]. Encouraging by its unique and fascinating properties of polymer discs, competitive advantages to improve their performances and address the problems that spherical particles may unable to solve could be expected.

As mentioned previously, there are a significant number of studies that have been proposed the fabrication method of polymer discs, which could be divided into two main groups namely bottom-up method and top-down method. The key advantage of top-down method is the simplicity of the process utilizing the deformation of original spherical particles to become discs. Among these, hot-pressing is one of the top-down method applying the combination between thermal and mechanical force to deform sperical particles to be discs. Based on the fact that polymer will obviously deform at temperatures higher than T_g for sufficient time [6], however fusion between spherical polymer particles during hot-pressing could be expected leading to a film of particles instead of monodisperse discs. Accordingly, to develop a facile and versatile method to fabricate disc-shaped polymer particles remains an imperative for their applications.

2-2 Purpose

In this chapter, we propose a facile method to fabricate polymer discs by hot-press process combined with a sacrificial matrix technique. By this technique, it allows to employ only aqueous solution and suspension to achieve discs without any organic solvent. PS and PLLA and PLGA microspheres with various in size as a model polymer were mechanical pressed into individual polymer discs in a controllable manner. The choice of sacrificial matrix and the optimal condition for hot-press is also discussed. In addition, to improve the idea of the unique high interfacial adhesion of the prepared discs, adhesiveness of polymer discs to surface of cover glass and the enhancement of aggregation for BSA-coated polymer discs in the presence of GA were used to evaluated.

2-3 Material and methods

2-3-1 Materials

PS microspheres (Polybead®, *ca*. 0.2, 1.0 or 10 μm in diameter, Polysciences Inc., Warrington, PA) and fluorescent-labeled PS microspheres with or without carboxyl groups (Fluoresbrite® YG, *ca*. 1.0 μm in diameter, Ex: 441 nm, Em: 486 nm, Polysciences Inc.) were employed as a model of the spherical polymer particles. While, PLLA (M_w: 80–100 kDa, Polysciences Inc.) were used to prepare microspheres. Na-Alg (M_w: 106 kDa, Kanto Chemical Co., Inc., Tokyo, Japan) used as a sacrificial matrix by having $CaCl_2$ (Kanto Chemical Co., Inc.) as a gelation agent. An aqueous solution of 0.1 M ethylenediaminetetraacetic acid (EDTA, Kanto Chemical Co., Inc.) was used to dissolve gel. Without a sacrificial matrix test, a silicon wafer (KST World Co., Fukui, Japan, size: 10×10 mm^2) was used as a substrate. Moreover, PVA (M_w: 22 kDa, 89% hydrolyzed, Kanto Chemical Co., Inc.) was used to evaluate as an alternative sacrificial matrixes and used as aqueous solution in Shirasu Porous Glass (SPG) emulsification process. An aqueous solution of poly(ethylene glycol) (PEG, M_w: 100 kDa, final concentration 25 mg/mL, FUJIFILM Wako Pure Chemical Co., Osaka, Japan) was used to evaluate the concentration of the PLLA microspheres.

To evaluate the adhesiveness of the PS particles to the surfaces, cover glasses (diameter: 25 mm, thickness: 0.13–0.16 mm, Model No.: 0111650, AS ONE Co.) were used as a substrate. PLL (M_w:

150–300 kDa, Sigma-Aldrich Co., St. Louis, MO) was applied to the surface of the cover glass to achieve positively charged surfaces. To evaluate the enhancement of aggregation for BSA-coated polymer discs in the presence of GA, BSA (Product No.: A7906, SigmaAldrich Co.) and GA aqueous solution (FUJIFILM Wako Pure Chemical Co.) were used.

2-3-2 Fabrication of PS disc-shaped particles

To prepare PS disc-shaped particles, PS microspheres and fluorescent-labeled PS microspheres with or without carboxyl groups were used as model polymer. First, sodium alginate used as a sacrificial matrix was dissolved in 10 mL of distilled water at a concentration of 20 mg/mL. Then, 0.5 mL of the microspheres (*ca.* 1 μm, 0.25% (w/v), corresponding to 5×10^9 particles/mL) were added in and stirred at room temperature (RT) for 5 min. To allow gelation, 20 mL of $CaCl_2$ aqueous solution (20 mg/mL) was gently added to the suspension, slowly centrifuged to be gel-ball in shape and further incubated at RT overnight. Next, the alginate gel-ball was washed with distilled water to remove all the non-gelation part out and pressed under conditions of varying temperatures and pressures (AH-2003, AS ONE Co., Osaka, Japan). The pressed gels were dissolved in an aqueous solution of ethylenediaminetetraacetic acid (25 mL, 0.1 M) at RT for 3 h. The pressed particles were collected with distilled water by centrifugation (13,000*g*, 5 min, RT, 5 times). According to the same procedure, the disc shaped particles with different diameters were fabricated as well. The concentrations for 0.5 mL of *ca.* 0.2 μm and *ca.* 10 μm microspheres are corresponding to 5×10^9 particles/mL and 5×10^7 particles/mL, respectively.

We also tested whether the PS microspheres without a sacrificial matrix can be deformed. In this case, 0.1 mL of microspheres at the concentration of 5×10^9 particles/mL (*ca.* 1.0 μm in diameter) were deposited on a silicon wafer and dried in a desiccator. Then, the samples were incubated at 110°C for 2 min on a hot-plate (ND-2A, AS ONE Co.). In addition, PVA was also considered the possibility to be an alternative of sacrificial matrixes instead of alginate gel. To this end, PVA was dissolved in 5 mL of distilled water to obtain the final concentration of 100 mg/mL, to which 0.5 mL of PS microspheres with the concentration of 5×10^9 particles/mL (*ca*. 1.0 μm in diameter) were added and the mixture and stirred at RT for 5 min. The suspension was gently casted into petri dishes (40 mmϕ) and dried at 50°C overnight in an oven (EO-600B, AS ONE Co.). The obtained cast films were hot-pressed

at 110°C for 10 min and dissolved in distilled water (25 mL) at RT for 3 h. The particles were collected by centrifugation with the same process as mentioned above. The size of alginate gel and the thickness of PVA cast film were measured with a digimatic micrometer (QuantuMike, Mitutoyo Co., Kanagawa, Japan).

2-3-3 Fabrication of biodegradable PLLA microspheres and discs

PLLA microspheres were fabricated by a membrane emulsification technique according to a procedure reported previously [7, 8]. First, PLLA was dissolved in methylene chloride (10 mg/mL) and the solution was then added to the oil tank on the membrane emulsification apparatus as shown in Fig. 2-1 (MN-20, SPG Technology Co. Ltd., Miyazaki, Japan) with the SPG membrane with a pore size of 1.1 μm. The PLLA solution was pressed through the SPG membrane by nitrogen gas and emulsified into an aqueous solution of PVA (*ca.* 190 mL,10 mg/mL). The suspension was stirred at 800 rpm at RT for 4 h in order to evaporate the solvent. The PLLA microspheres were collected with distilled water by centrifugation (13,000*g*, 5 min, RT, 5 times) to remove PVA. To determine the concentration of PLLA particles, the volume ratio of the microspheres in the suspension according to a procedure reported previously was used [9]. In summary, the suspension was mixed with an aqueous solution of PEG and incubated at 37°C for 1 h to enhance aggregation. The suspension was filled into a hematocrit capillary tube and precipitated by the centrifugation (15,000*g*, 10 min, RT). The number of particles per volume (*n*, particles/mL) was calculated by the following equation,

$$n = 3b/(a - b) \times 4\pi r^3 \times 10^3 \quad (1)$$

where a (m), b (m) and r (m) were the height of the water surface from the bottom of the capillary tube, the height of the precipitate of the microspheres, and the average radius of the microspheres, respectively.

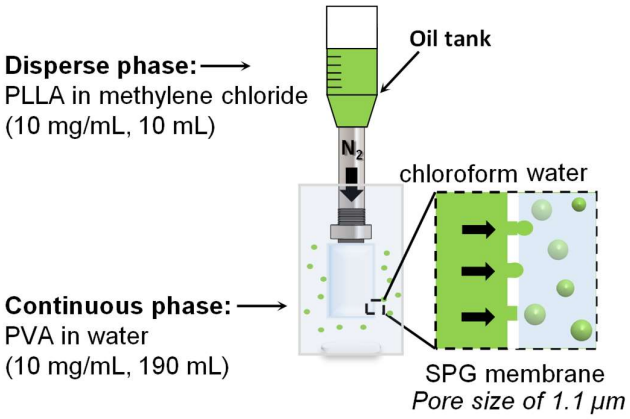

Fig. 2-1 Schematic diagram of SPG emulsification method (permitted reuse reproduction for doctor thesis from the publisher, cited and partially modified from ref. 1).

The PLLA discs were prepared by hot-press process as well. In short, 0.5 mL PLLA microspheres (3×10^9 particles/mL, 0.5 mL) were added to the solution of Na-Alg of 10 mL at the concentration of 20 mg/mL, followed by gelation process to create the alginate containing the microspheres. The gel-balls were then hot-pressed at 10 MPa for 10 MPa which the temperature was set at 70 ºC (near the glass transition temperature (T_g) of PLLA (65°C). After pressing, the gels were dissolved with an EDTA solution of 25 mL (0.1 M). Finally, the discs were collected by the centrifugation (13,000*g*, 5 min, RT, 5 times).

2-3-4 Morphology, rheology and composition of polymer particles

Morphology of particles both before and after hot-press process was evaluated with a field emission scanning electron microscope (FE-SEM S-4800, Hitachi High-Technologies Co., Tokyo, Japan) at an accelerating voltage of 3 kV. Briefly, particles were filtrated on a Whatman® membrane filter (Anodisc™ (for cross-sectional view) or Nuclepore™ (for other conditions) with a pore size of 0.1 μm, GE healthcare, Chicago, IL) and dried at RT overnight in a desiccator. The filters were fixed on the stage with a carbon tape, to which gold was sputtered at an ionic current of 3 mA for 60 s by using a SC-701 Quick coater (Sanyu Electron Co., Ltd., Tokyo, Japan) prior to observation. The dimensions of the particles were manually measured from the SEM images. The obtained values of long axis (more than 50 particles taken from 5–18 top view images) and short axis (more than 10 particles

taken from three cross-sectional view images) of the particles were averaged for each condition. The long axis diameter was plotted against the pressure, time, and temperature used in the hot-press process. Values were given as mean ± standard deviation (SD). The calibration curve between fluorescent intensity and concentration of the microspheres using a microplate reader (SH-9000Lab, Corona Electronic Co., Ltd., Ibaraki, Japan) set in the fluorescent mode (E_x: 441 nm, E_m: 486 nm) was used to determine the concentration of fluorescent-labeled particles both discs and microspheres. Their concentrations were also measured by a Burker-Turk counting chamber (Sunlead Glass Co., Saitama, Japan). For fluorescent-labeled PS discs and microspheres (*ca*. 1.0 μm in diameter), the concentration of 1.0 wt% particles equal to 1.8×10^{10} particles/mL in suspension. The rheological measurements were evaluated by a rotational rheometer (Physica MCR 101, Anton Paar GmbH, Graz, Austria), equipped with a cone-plate CP50-0.5 (50 mm diameter, 0.5° cone angle). The suspension of PS discs and microspheres (*ca*. 1.0 μm in diameter) in water, varying concentrations from 0.75 to 6.0 wt% of 380 μL was injected into the rheometer. The measurements were performed at 25°C at the shear rate from 1 to 10,000 s^{-1}. The shear viscosity at 237 s^{-1} was extracted and plotted versus the concentration of particles (N = 3–4). Values were given as the mean ± SD.

To confirm whether alginate used as a sacrificial matrix remains on the surface of the discs or not, Fourier-transform infrared spectroscopy (FTIR-8400, Shimadzu Co., Kyoto, Japan) was used to evaluate PS discs (non-fluorescent-labeled, *ca*. 1.0 μm in diameter). The freeze-dried powder of disc sample was mixed and ground with potassium bromide. The obtained pellets were dried overnight in a vacuum dryer (ETTAS AVO-250NB, AS ONE Co.) just before measurement. As controls, FTIR spectra of the microspheres (non-fluorescent-labeled) and the only Na-Alg were measured as well.

2-3-5 Loading and release behavior of PLGA particles

The PLGA microspheres (lactide:glycolide = 50:50 (mol%), intrinsic viscosity: 0.6 dL/g, T_g: 50°C, Polysciences Inc.) were fabricated by membrane emulsification technique with SPG membrane with a pore size of 10.1 μm. Other parameters were the same as mentioned in the fabrication and collection PLLA microspheres. 3,3'-Diethyloxacarbocyanine iodide ($DiOC_2(3)$, Sigma-Aldrich Co.) was used as model of a hydrophobic drug to be loaded into the PLGA particles. Specifically, $DiOC_2(3)$

was dissolved in 10 mg/mL PLGA methylene chloride solution at a concentration of 24 μg/mL, and thus the amount of encapsulated drug in PLGA particles was 0.24 wt%. The PLGA discs were prepared by embedding microspheres in alginate gel and hot-pressing with the conditions of 30 s, 10 MPa, and 55°C. Both top view and cross-sectional view of PLGA microspheres and discs were investigated by SEM. The drug release test was performed by incubating 2×10^5 $DiOC_2(3)$ loaded PLGA particles suspended in 1 mL of phosphate buffered saline (PBS) buffer (pH: 7.4) containing 0.05% Triton™ X-100 (Sigma-Aldrich Co.) at 37°C. At certain time intervals, the suspension was centrifuged (13,000*g*, 5 min, RT), and the concentration of $DiOC_2(3)$ in the supernatant was determined by the microplate reader (SH-9000Lab). The cumulative release percentage, namely of the ratio of the total released amount of $DiOC_2(3)$ to the original encapsulated amount, was calculated and plotted versus time for both PLGA microspheres and discs ($N = 3$). Values were given as the mean ± SD.

2-3-6 Adhesiveness of the PS particles to the surfaces

To evaluate adhesiveness of the PS particles to the surfaces, cover glasses were cleaned with piranha solution, followed by rinsing with distilled water. Then, an aqueous solution of PLL (300 μL, 1 mg/mL) was applied to the surface of the cover glass set into a 6-well plate and incubated at RT overnight. After that, these PLL-coated glasses were gently rinsed with distilled to remove all the uncoated reagent out. The fluorescent-labeled PS discs and microspheres with carboxyl groups (*ca*. 1.0 μm in diameter, 1×10^8 particles/mL, 0.2 mL) were deposited on the PLL-coated glass and the glass were incubated at RT for 1h, followed by washing with distilled water. The glass was placed in a custom-made circulating chamber mounted with a syringe pump (SPS-1, ASONE Co.) established previously [10-12]. The chamber was mounted on an Olympus IX71 fluorescence microscope with a 20×0.45 NA objective lens (LUCPlanFLN, Olympus Co., Tokyo, Japan) and a cooled digital color camera (DP72, Olympus Co.). Air was injected into the chamber using the pump at flow rates ranging from 0.5 to 3 mL/min. To evaluate the detachment of the discs and microspheres on the PLL-coated glass, the filter set U-MWIB3 (Olympus Co.) was utilized in combination with a 200 W metal halide-lamp integrated into a microscope illumination system (ScopeLite 200, Optical Building Blocks, Birmingham, NJ). Images were taken at an exposure time of 50 ms. The number of particles adhered to

the PLL-coated glass was counted using ImageJ software (NIH, Bethesda, MD). The adhesion number prior to air flow was defined as 100% and the corrected values were averaged for each condition (N = 3–4), and plotted against the flow rate. Values were given as the mean ± SD.

2-3-7 Aggregation assay with BSA-coated PS particles

To investigate the aggregation assay with BSA-coated PS particles, the fluorescent-labeled PS discs and microspheres with carboxyl groups (*ca*. 1.0 μm in diameter) were mixed with 1 mL of BSA dissolved in PBS buffer (pH: 7.4) at a concentration of 20 mg/mL (corresponding to 5×10^9 particles/mL) and stirred at RT for 2 h. The BSA-coated PS particles were collected by centrifugation (13,000*g*, 10 min, 4°C) and washed with 10 mM PBS buffer (pH: 7.4). The amount of BSA adsorbed on the surface of PS particles was quantified using Micro BCA™ protein assay kit (Thermo Fisher Scientific Inc., Waltham, MA). The aggregation test was performed by adding 100 μL of 25% GA aqueous solution into 200 μL of BSA-coated PS microspheres or discs (1×10^9 particles/mL) on a slide glass, and gently stirring pipette tip in the droplet for 1 min. The photos and videos during aggregation test were recorded using a digital camera G7 X Mark II (Canon Inc., Tokyo, Japan). Besides the visual inspection, the morphology of particle aggregations was observed on an inverted confocal microscope (A1R+, Nikon Instruments Inc., Tokyo, Japan) mounted with a 60× water-immersion objective (CFI Plan Apo VC60×WI, 1.20 NA, WD: 0.27 mm). Laser line at 488 nm was used, and fluorescence signals in the wavelength range of 500–550 nm was investigated. After the test, a drop of suspension was deposited on a rectangle cover glass (thickness: 0.12–0.17 mm, Matsunami Glass Ind., Ltd., Osaka, Japan). 3D image stacking was acquired with a 200 nm z-step from the surface of cover glass to a depth of 15 μm through NIS-Elements C software (ver. 4.51, Nikon Instruments Inc.).

2-4 Results and discussion

2-4-1 Deformation from microspheres to discs

PS microspheres with a diameter of *ca*. 1.0 μm were used as model particles to perform the preliminary test on the deformation. The T_g of the microspheres was 109.9°C as measured previously [13]. Hence, the water-suspended microspheres were dropped on a silicon wafer and heated at 110°C on

a hotplate. PS microspheres started to deform and fused with each other (Fig. 2-2b), while their spherical shape before heat almost maintained in shape as can be seen in Fig. 2-2a.

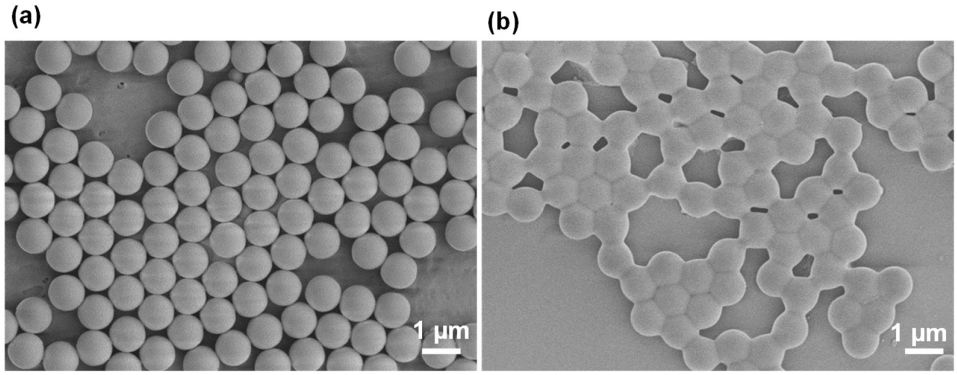

Fig. 2-2 SEM images for PS microspheres (*ca*. 1.0 μm in diameter) without sacrificial matrix (a) before and (b) after heated at 110°C on a hot plate (permitted reuse reproduction for doctor thesis from the publisher, cited and partially modified from ref. 2).

This result confirmed that the T_g of the component polymer is an important parameter for the particle deformation. However, the microspheres were welded and fused with each other by a capillary force during evaporation of water which is difficult to obtain disperse pressed particles by direct hot-press process. To solve this problem, hydrogel as a sacrificial matrix was used to create sufficient space between each microsphere during hot-press process. In this study, Na-Alg which is a natural polysaccharide with some favorable such as it can be converted into a hydrogel instantly by adding divalent cations such as Ca^{2+}, and it can be re-dissolved by adding chelating reagents such as EDTA [14, 15]. In addition, it showed excellent thermal stability up to 200°C [16]. As can be seem in Fig. 2-3, the microspheres (2.5×10^9 particles) were homogenously suspended into the solution of Na-Alg (200 mg), followed by a gelation with Ca^{2+}. When the gel was hot-pressed at 110°C at 10 MPa for 30 s (the optimal condition as discussed below), the gel was broken into pieces and spread out on the plate of the hot-presser. The gels were then dissolved with EDTA, followed by a centrifugation to collect the pressed particles.

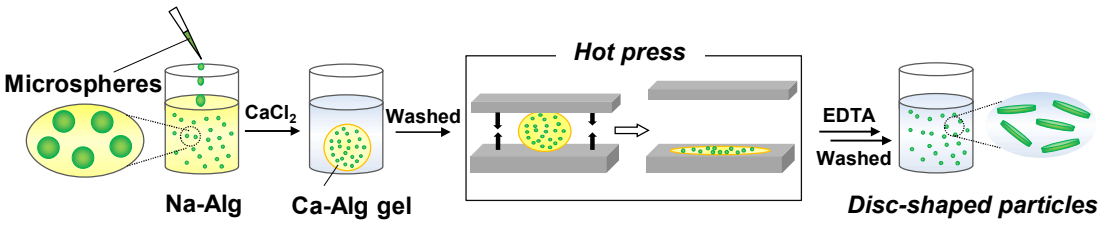

Fig. 2-3 Schematic of fabrication process, including microspheres embedded in alginate gel, hot-press, and washing with EDTA (permitted reuse reproduction for doctor thesis from the publisher, cited and partially modified from ref. 2).

It should be noted here that the obtained suspension solution of discs represented a swirling motion when they were shaken unlike the microspheres. This motion is a well-known unique behavior of disc-shaped platelets suspension [17] which implies that the microspheres have already deformed to be disc-shaped particles. The results by SEM revealed that the long axis diameter of the obtained particles was significantly increased in a spread-out configuration compared to the microspheres prior to the hot-press process which is repeatedly confirmed by cross-sectional observations (as can be seen in Fig. 2-4). It is also noteworthy that our fabrication process is a waterborne technology, which is no organic solvent is required thus it is considered as an environmentally friendly process.

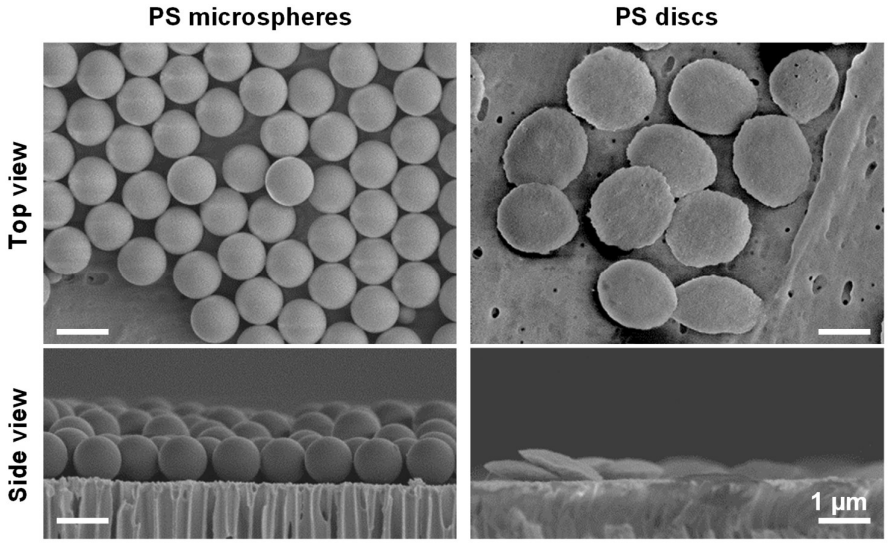

Fig. 2-4 SEM images (top view and cross-sectional view) for PS microspheres (*ca.* 1.0 μm in diameter) before and after hot-press (permitted reuse reproduction for doctor thesis from the publisher, cited and partially modified from ref. 2).

Then, the optimal conditions of the hot-press process to fabricate the discs were evaluated. In this case, PS microspheres with a diameter of 1,015 ± 3 nm were hot-pressed at varying pressures at the constant temperature and time (110°C, 30 s). They were not deformed by applying only heating without pressing. The results showed that the diameter of the microspheres was significantly increased with the pressure of 5 MPa (1,501 ± 103 nm) and reached a plateau of 1,664 ± 39 nm above 10 MPa. The diameter tended to slightly decrease to 1,473 ± 82 nm when hot-pressing at 20 MPa. We assumed that the pressed PS discs under a larger strain level tend to return to their original shape to some extent after the pressure is released (Fig. 2-5a). Then, temperature and pressure were kept constant (110°C, 10 MPa) and varying time, resulting 30 s of hot-press time was sufficient for deformation of the microspheres (10 s: 1,405 ± 135 nm, 30 s: 1,664 ± 39 nm, 60 s: 1,558 ± 62 nm, and 120 s: 1,612 ± 87 nm; Fig. 2-5b). In addition, at the constant pressure and time (10 MPa, 30 s), the diameter of the discs was drastically increased at a temperature higher than 110°C, corresponding to the T_g of the microspheres (25°C: 1,028 ± 14 nm, 50°C: 1,091 ± 45 nm, 70°C: 1,105 ± 23 nm, 100°C: 1,212 ± 105 nm, 110°C: 1,664 ± 39 nm, and 120°C: 1,623 ± 91 nm; Fig. 2-5C).

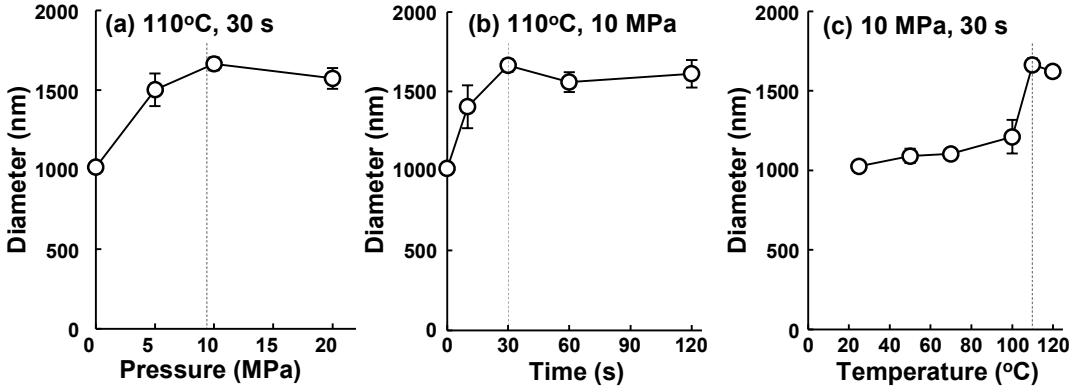

Fig. 2-5 Diameter of prepared PS discs versus the hot-press conditions of (a) pressure, (b) time, and (c) temperature (permitted reuse reproduction for doctor thesis from the publisher, cited and partially modified from ref. 2).

Therefore, it can be concluded that deformation of the microspheres was triggered by a combination between pressing and heating at the T_g of the microspheres. Especially, the hot press at 10 MPa at 110°C for 30 s was sufficient for fabricating the PS discs. In this case, the short axis of the discs

was 358 ± 25 nm, corresponding to a size-aspect ratio of *ca*. 4.6. Due to their anisotropic shapes, the obtained discs were intriguingly filtrated onto the membrane by a surface contact manner (Figure 2-4). Moreover, the band at 3,350 cm^{-1} which is corresponding to the O–H stretching vibration of alginate was not detected in the prepared PS discs in a FTIR analysis (Figure 2-6). This observation suggested that most of alginate used as the sacrificial matrix has been washed out by EDTA. However, there may exist a trace amount of residual alginate on the surface of discs, which cannot be detected by FTIR.

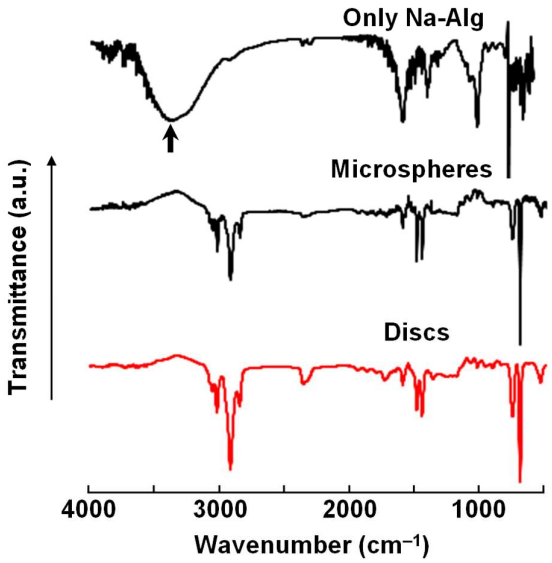

Fig. 2-6 FTIR spectra for only Na-Alg, microspheres and the prepared discs after washing. Arrow indicates the O–H stretching vibration at 3,350 cm^{-1} of alginate (permitted reuse reproduction for doctor thesis from the publisher, cited and partially modified from ref. 2).

The rheological properties of PS particle suspensions were studied as well. It is known that when the moving of spherical particles in fluid (Stokes regime) is isotropic by drag force and governed by Stokes' law. For non-spherical particles, on the other hand, drag force becomes anisotropic with respect to the direction. The drag force parallel to the surface of a disc-shaped particle is much smaller than that of the perpendicular direction [(18)], which results in the spontaneous alignment of discs in fluid, namely the swirling phenomenon. Here, the apparent viscosity of PS discs suspension was measured at various particle concentrations and shear rates. In contrast to the rheological behavior of PS microspheres suspension, the viscosity of PS discs suspension was decreased with increasing of the shear rate, indicating a typical non-Newtonian pseudoplastic behavior. Moreover, the degree of shear

thinning is increased with a higher particle concentration (see Fig. 2-7a). The viscosity at the shear rate of 237 s^{-1} from both microspheres and discs were investigated for comparison (see Fig. 2-7b). The results showed that discs suspension viscosity was significantly increased with the particle concentration, while no such correlation was found for microspheres suspension in the concentration range from 0.75 to 6.0 wt%. It is reasonable to expect the increasing of apparent viscosity with discs concentration since when the alignment of discs increases, there is possibility of their intermittent contact with the large surface area in fluid. These results provide the different rheological properties of disc-shaped particles compared to that of microspheres, which may be closely related to their applications in physiological environment.

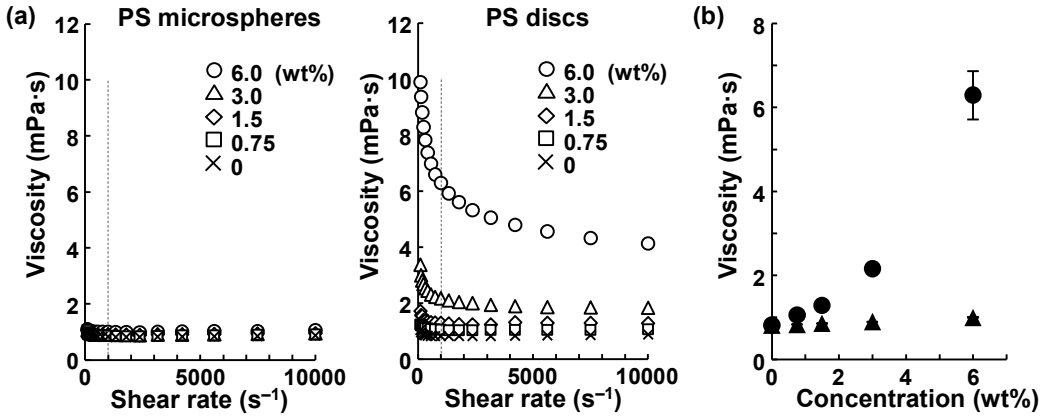

Fig. 2-7 (a) Viscosity of PS microspheres and PS discs (*ca*. 1.0 μm in diameter) suspension at various particle concentrations and shear rates. (b) Viscosity at the shear rate of 237 s^{-1} from both microspheres (triangle) and discs (circle) versus the particle concentration in suspension (N = 3–4, data given as mean ± SD) (permitted reuse reproduction for doctor thesis from the publisher, cited and partially modified from ref. 2).

2-4-2 Operational applicability of the method

This process was also employed to fabricate PS disc with varying original size, and polymers. PS microspheres with diameters of 172 ± 2 nm and 10.7 ± 0.1 μm were embedded in alginate gel, hot-pressed, and collected using the same method as described above. The diameters of particles increased to 249 ± 28 nm and 15.9 ± 1.0 μm, respectively after the hot-press process (Fig. 2-8a and 2-8b).

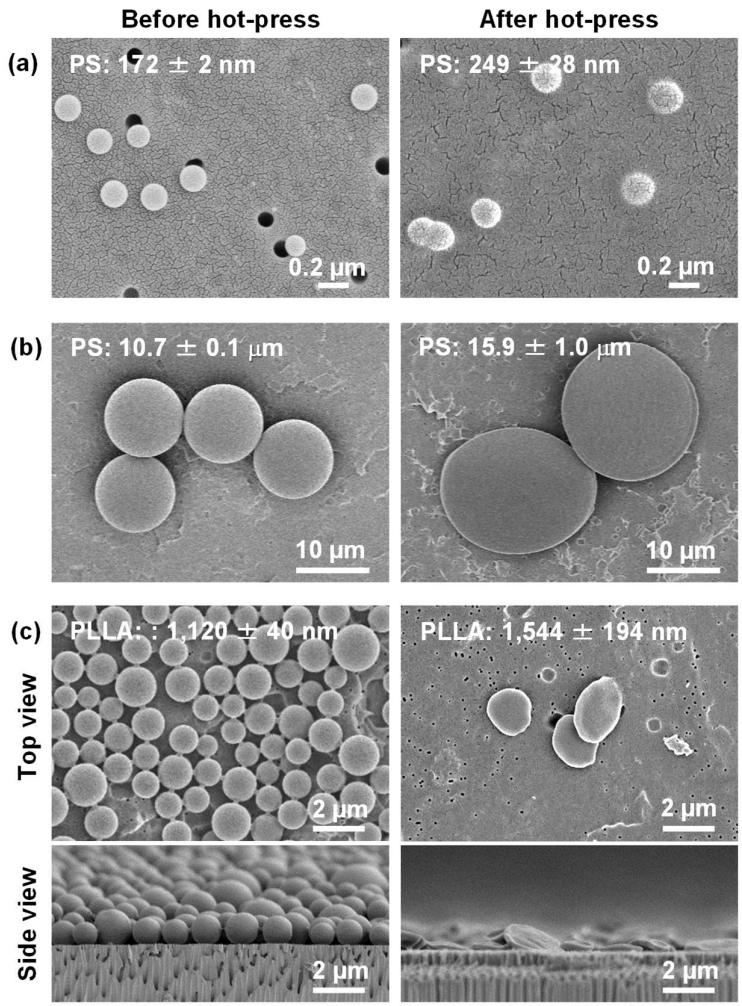

Fig. 2-8 Representative SEM images showing the versatility of the proposed method. (a) PS microspheres (*ca*. 0.2 μm in diameter) and (b) PS microspheres (*ca*. 10 μm in diameter) before and after hot-press. (c) SEM images (top view and cross-sectional view) for the fabricated PLLA microspheres (*ca*. 1.0 μm in diameter) before and after hot-press (permitted reuse reproduction for doctor thesis from the publisher, cited and partially modified from ref. 2).

Including with the results from PS microspheres with a diameter of *ca*. 1.0 μm, the increase of diameter in all the cases is *ca.* 1.5-fold. This increasing is not related to the original size of microspheres. However, the size distribution of discs deteriorated compared to that of the corresponding microspheres. While in general, microspheres with a smaller size is expected to deform more difficult, our proposed method is applicable for a wide range of PS particle size at least with the particles larger than 170 nm

in diameter. In addition, as our method is indeed a mechanical deformation of polymer microspheres at elevated temperature and pressure, it could be anticipated that any other polymers with appropriate T_g and elastic modulus can apply this method. In this study, a commonly used biocompatible and biodegradable polymer PLLA was tested as well. Difference from commercially obtained PS microspheres reported previously, PLLA microspheres were fabricated by SPG membrane emulsification technique with SPG membrane of 1.1 μm in pore size. As can be seen Fig. 2-8c, the diameter of the prepared PLLA microspheres was 1,120 ± 40 nm with a monodisperse particle size distribution. PLLA microspheres were deformed to disc-shaped configuration with a diameter of 1,544 ± 194 nm, after embedded in hydrogel and hot-pressed for 30 s at 10 MPa and 70°C a size-aspect ratio of *ca*. 2.6 which is 5°C above the T_g of PLLA, which further demonstrated the feasibility of our method. Taken together, our method provides a straightforward and versatile way to fabricate disc-shaped polymer particles with a wide range of diameters. Here, the hot-pressing method is valid for both amorphous polymer (PS) and crystalline polymer (PLLA). Our previous studies have demonstrated that the crystallization occurs, and consequently, the elastic modulus increases when a thermal process is performed on PLLA thin films [19, 20]. Accordingly, PLLA discs could be assumed to follow a similar behavior after hot-press process, and their enhanced elastic modulus needs to be characterized with a specific measurement, such as an atomic force microscopy-based nanoscale indentation method [21].

It should be mentioned and discussed here that PS discs looked somewhat more olivary in shape (see Fig. 2-4), comparing with PLLA discs which have very flat surfaces (see Fig. 2-8c). This is a strong evident that the polymer properties are the important parameter in determining the final shape of the particles. This can be explained as following, after hot-press at a certain temperature above T_g of polymer, the system was cooled down. Obviously, for a higher operational temperature, the time spend to cool down the system below the T_g of polymer is shorter. In such a rapid vitrification process, the time may not sufficient for polymer chains to rearrange themselves. Therefore, elastic energy may still store in the discs, which induces the shape recovery. The T_g of PLLA, as mentioned previously, is lower than that of PS, thus the time for PLLA chains in rubber state is longer, which results in a less magnitude of shape recovery, namely disc-shape with very flat surfaces. For PS discs, however, the deformation

recovers to some extent, giving an olivary shape. The observation on PLGA discs also supports this statement, which will be shown later. The performance of PVA which is also water-soluble polymer which is widely used as a sacrificial film in the deforming of polymer microspheres under stretching [22, 23] were also tested in comparison with alginate hydrogel. PS microspheres (*ca*. 1.0 μm in diameter) were embedded in PVA cast film and hot-pressed at 10 MPa and 110°C. After dissolving PVA sacrificial film, PS particles were obtained by centrifugation. Interestingly, PS microspheres became somewhat disc-like shape with a diameter of 1,249 ± 137 nm (see. Fig.2-9a, and 2-9b). The size-aspect ratio was increased to a limit of *ca*. 1.9, even though the hot-press was conducted for a long time of 10 min. According to this result, it is reasonable to conclude that the relative elastic moduli of polymer microspheres and sacrificial matrix play a significant role in determining the final shape of particles.

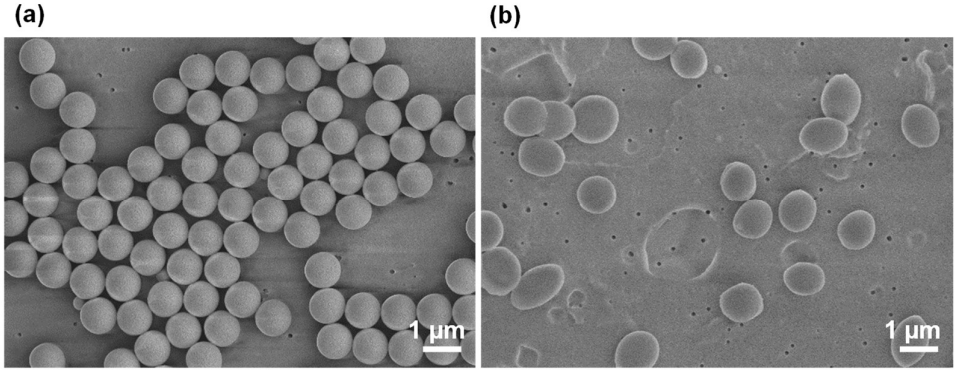

Fig. 2-9 SEM images for PS microspheres (*ca.* 1.0 μm in diameter) embedded in PVA sacrificial film instead of alginate gel (a) before and (b) after hot-press (permitted reuse reproduction for doctor thesis from the publisher, cited and partially modified from ref. 2).

Compared to PS or PLLA used in this study (modulus: *ca*. 3.0 GPa) [24, 25] both alginate gel and PVA are soft. As the T_g of PVA is *ca*. 85°C, the PVA cast film for hot-press at 110°C is in the rubbery state, where its elastic modulus is *ca.* 1.0 GPa [26]. The elastic modulus of alginate gel is extremely low, with a magnitude of *ca*. 7 kPa [27]. Obviously, when using matrix with a less stiffness to encapsulate polymer microspheres upon hot-press, more compressive stress would concentrate at the microspheres, resulting in a deformation of particles to a large size-aspect ratio. In addition, alginate gel (unlike other water-soluble polymers) is humidity insensitive, by this reason, hot-press process with alginate gel is not affected by the environment, and the fabrication reproducibility is expected to be better. While other

candidates may find their fulfilment in our method, we believe that alginate hydrogel provides an ideal sacrificial matrix for its low elastic modulus and unique solubility.

Another concern may come from the productivity of this method, which is the number of microspheres that can be embedded into the hydrogel for fabricating discs under hot-press. In this study, the average diameter of the prepared hydrogel ball was *ca.* 24 mm. In control case, the hydrogel was pressed at 10 MPa at room temperature, and the thickness of the pressed gel in a wet state was measured to be *ca*. 108 μm. Based on the conservation of gel volume, the lateral area of the gel after press was calculated to be *ca.* 6.7×10^4 mm^2. Taken *ca*. 1 μm microspheres as an example, the projected area of an individual particle was *ca*. 7.9×10^{-7} mm^2. And thus, the threshold number for microspheres without contacting each other after hot-press would less than 8.5×10^{10} particles. Here, the total number of embedded microspheres was chosen to be 2.5×10^9 particles, which is less than one thirty of the threshold values as estimated above. In fact, the decrease of threshold capacity could be expected since the particles at the center region would be more concentrated than at the peripheral region. However, the embedding density used in this study satisfied the requirement to provide sufficient space between the microspheres for the deformation of microspheres. With a higher embedding density above 2.5×10^9 particles, the microspheres may fuse with each other after hot-press.

Film stretching of polymer microspheres embedded in matrix film is one of the well-known methods to fabricate polymer discs since the simplicity of their design [22, 23]. The stretching and hot-pressing methods share many things in common namely both are classified into top-down methods utilizing mechanical deformation of polymer. Moreover, matrix (alginate gel in the case of hot-pressing and PVA film for stretching) are used in both processes to create appropriate space between microspheres during deformation. However, some differences of these two methods. First, the most significant difference is the shape of the obtained particles should be discussed for comparison. For hot-pressing, spherical particles were pressed from top to down by the moving of heating plate. Accordingly, the microspheres are squashed into circular discs in a two-dimensional manner. While in the case of stretching of spherical particles in film, the deformation of embedded microspheres is induced by film stretching along with the stretching direction. Elongated disc-shaped with a high aspect ratio is obtained

by varying the film stretching ratio. A two-direction stretching is needed to obtain symmetrical discs-shaped particles, which is considered to be troublesome. While stretching of spherical particles in film is capable of fabricating a variety of shapes, hot-pressing is believed to be a facile and straightforward method to fabricate disc-shaped particles. Moreover, interaction between particles and film is considered as a key parameter to determine the final particle shape in the case of film stretching. This is based on the fact that the deformation of embedded spherical particles in film stretching occurs when the stretching force is transferred from the stretching holder at the edge of the film throughout the film. The strong adhesion between particles and film will facilitate the transferring of stretching force to the entire film. However, the void between particles and matrix film could be observed after stretching if in the case of the adhesion between embedded particles and matrix film [28, 29]. Also, the maximum stretching ratio is highly depended on the stretchability of the matrix film. In contrast, the pressing force in hot-press can be evenly applied throughout the sample, and the adhesion between particles and alginate gel could be neglected in this case. Therefore, hot-pressing method is more versatile and can be used with a wide range of polymers without the concerning of stretchability of the matrix and the adhesion between the matrix and the microspheres.

2-4-3 Enhanced interfacial adhesiveness from polymer discs

The interfacial adhesiveness of polymer particles to a surface substrate and the enhancement of aggregation for polymer particles themselves are directly associated with the contact surface area that participates in adhesion. For a fixed particle volume, the contact surface area of disc particles is significantly larger than that of microspheres. Accordingly, it is assumed that the interfacial adhesiveness of polymer discs prepared in this study can be much enhanced. To prove this assumption, the adhesion strength of PS particles to the surface of cover glass under the airflow using a microchamber were evaluated. The fluorescent-labeled PS microspheres (*ca*. 1 μm in diameter) with carboxyl groups was employed. Surface of cover glasses were coated with PLL, which is a general polycationic substate for facilitating cell adhesion [30]. By this the electrostatic interaction between the carboxyl groups on surface of PS particles and the amino groups of PLL, both PS microspheres and PS discs were firmly adhered to the surface of the PLL-coated cover glass.

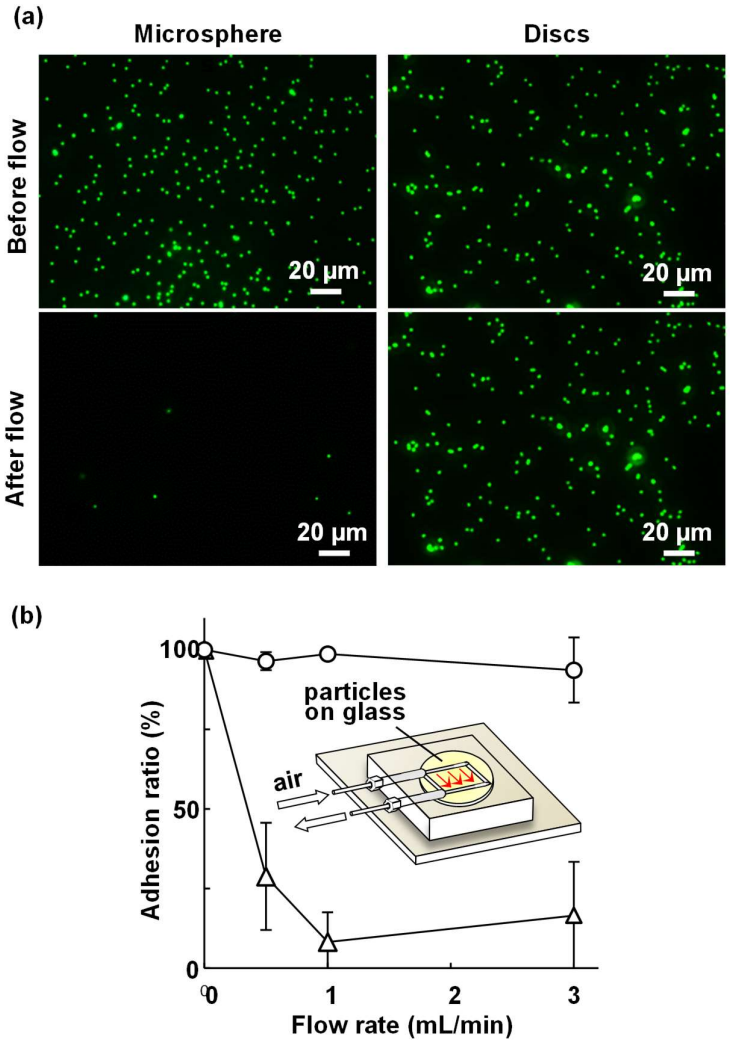

Fig. 2-10 Interfacial adhesiveness test for PS particles to the surface of cover glass under airflow. (a) Fluorescent microscopic images at the same location for PS microspheres and discs before and after airflow at a flow rate of 1 mL/min. (b) Adhesion ratio of PS particles on cover glass versus the flow rate of air (experimental setup schematically shown as inset), triangle: PS microspheres, circle: PS discs (N = 3–4, data given as mean ± SD) (permitted reuse reproduction for doctor thesis from the publisher, cited and partially modified from ref. 2).

The number of particles adhered to the cover glass was counted before and after the injection of airflow and an adhesion ratio was shown in Fig.2-10a. The initial adhesion densities for both microspheres and discs were adjusted to be (1.5 ± 0.5) $\times 10^4$ particles/mm^2, and the flow rate varied from 0.5 to 3 mL/min. By assuming the particles to be sufficiently rigid, the adhesion between

microspheres and a flat surface can be deemed as a point contact. The adhesiveness of a conventional microsphere is always very limited. The result showed that more than 87.6% of particles were blown away, when the flow rate reached 1 mL/min in the case of PS microspheres. On the other hand, for PS discs, almost all the particles were remained on the surface of cover glass, and the adhesion ratio kept at *ca.* 96.2%. While with the increasing of flow rate, the adhesion strength slightly declined as shown in Fig.2-10b.

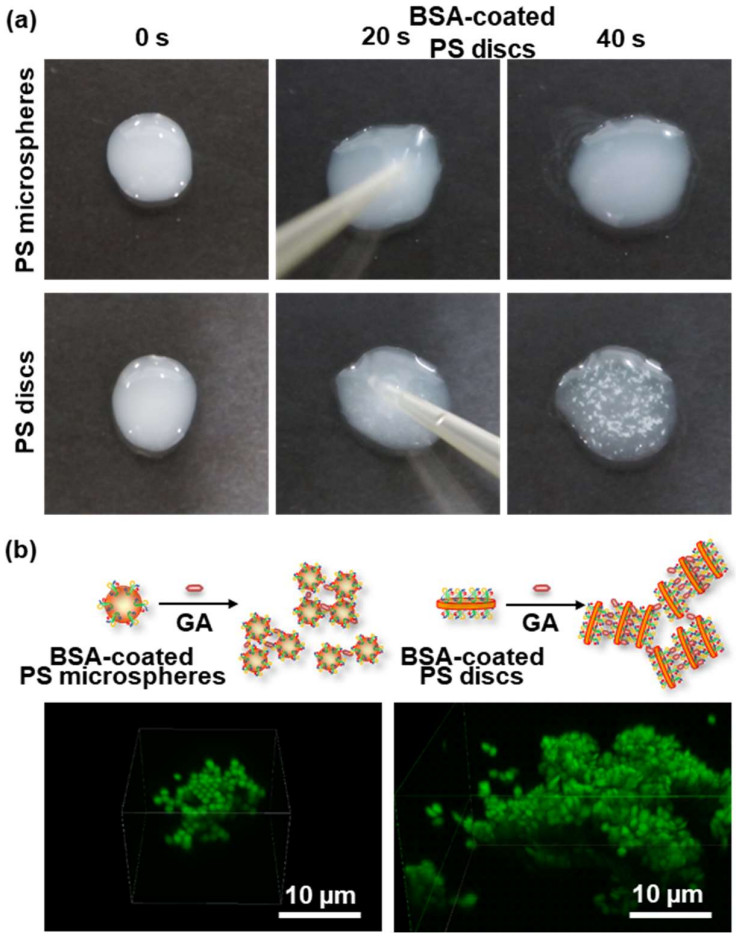

Fig. 2-11 Aggregation assay for BSA-coated PS particles mixed and stirred with GA. (a) Photos of the mixing suspension from PS microspheres and discs during the test at 0, 20, and 40 s. (b) Confocal microscope 3D images for particle aggregations from PS microspheres and discs, respectively (reaction between BSA-coated particles and GA schematically shown above each image) (permitted reuse reproduction for doctor thesis from the publisher, cited and partially modified from ref. 2).

This result agreed well with the previous studies which demonstrated that polymer discs can exhibit an enhanced interfacial adhesion and a higher resistance to the lift-off induced by the drag force exerted on the particles by the fluids. When used as a drug delivery carrier, polymer discs are expected to have a stronger extent of adhesion to target tissues in a physiological environment which will improve their diagnostic and therapeutic ability. It is reasonable to expect that polymer discs are more likely to adhere to each other by the ligand interactions within the contact area, and the aggregation status of polymer discs is different from that of polymer microspheres. GA which is a commonly used dialdehyde cross-linker in biochemistry, can predominantly react with the ε-amino groups of lysine residue in protein to form intermolecular cross-linkages [31]. Here, the surfaces of fluorescent-labeled microspheres and discs were coated with BSA, and the aggregation behaviors triggered by GA were observed. The absorbed amount of BSA on both microspheres and discs were constant to be *ca*. 6.0×10^4 molecules/μm^2, which implies that the particle surface was fully coated with BSA if we assumed BSA is an equilateral triangular molecule with *ca.* 8 nm length on each side [32].

After adding GA into the homogeneous suspension during the stirring process, agglutination of particles can be observed by naked-eye in both cases, which indicates that BSA-coated particles were cross-linked by GA. As shown in Fig.2-11a, the aggregation of PS discs was instant appearance within 20 s, and the size of aggregation was obviously larger than PS microspheres. The morphology of particle aggregations was further observed with a confocal microscope and the result showed that the monodisperse microspheres in an aggregation cluster formed a near close-packed arrangement. The size of aggregation was no larger than *ca*. 10 μm, and the arrangement of in the case of discs looked much random and incompact. Although the numbers of discs and microspheres were adjusted constant before test, the size of an individual aggregation cluster of PS discs was much increased, approaching *ca*. 50 μm Fig.2-11b. In addition of the point contact in the microspheres, discs provide a larger contact area, which leads to a stronger interaction from larger contact area, showing a rapider and larger aggregation. In fact, the above test mimicked the process of a latex turbidimetric assay, where PS discs can be coated with antibodies that react with a specific antigen to trigger the particle aggregation. Our results implied

that polymer discs with an enhanced adhesiveness can provide a fast and high-sensitive detection in latex turbidimetric assay.

2-5 Summary

A novel method to fabricate polymer discs by hot-press process combined with a sacrificial matrix technique was proposed. By embedding polymer microspheres in alginate gel, space between the microspheres is created, and the microspheres are deformed to disc-shaped particles in a separate manner after hot-press near the T_g of the polymer. The feasibility of this method in fabricating polymer discs from different kinds of polymer microspheres with a wide range of size were also demonstrated. Regarding the potential applications of polymer discs, both the interfacial adhesiveness of discs to a foreign surface, and the strength of discs aggregation are verified. The results exhibited that polymer discs enhanced interfacial adhesion compared to that of the microspheres, owing to their larger contact surface area in geometry. This is expected to improve their performances in both particle-based targeted drug delivery and latex turbidimetric immunoassay. We anticipate the method and the findings proposed here will be of practical value in fabrication of desired polymer particles for a number of applications.

References

[1] W. Tuntanatewin, P. Mekwatanakarn, H. Zhang, Y. Okamura, Facile fabrication of elongated polymer micro/nano discs and their surface adhesiveness, J Appl Polym Sci. (2020) 49798.

[2] H. Zhang, W. Tuntanatewin, K. Ishikura, D. Sogabe, K. Sugawara, A. Tokui, A. Nakagawa, Y. Okamura, Polymer discs with high interfacial adhesion fabricated from hot-pressing of microspheres, ACS Appl. Polym. Mater. 2 (2020) 3355−3364.

[3] P. Decuzzi, M. Ferrari, The adhesive strength of non-spherical particles mediated by specific interactions, Biomaterials 27 (2006) 5307–5314.

[4] N. Doshi, B. Prabhakarpandian, A. Rea-Ramsey, K. Pant, S. Sundaram, S. Mitragotri, Flow and adhesion of drug carriers in blood vessels depend on their shape: A study using model synthetic microvascular networks, J Control Release. 146 (2010) 196–200.

[5] J. W. Myerson, A. C. Anselmo, Y. Liu, S. Mitragotri, D. M. Eckmann, V. R. Muzykantov, Non-affinity factors modulating vascular targeting of nano- and microcarriers, Adv. Drug Deliv. Rev. 99 (2016) 97−112.

[6] J. A. Champion, S. Mitragotri, Role of target geometry in phagocytosis, Proc. Natl. Acad. Sci. U.S.A. 2006, 103, 4930–4934.

[7] Z. Q. Sun, X. Chen, J. H. Zhang, Z. M. Chen, K. Zhang, X. Yan, Y. F. Wang, W. Z. Yu, B. Yang, Nonspherical Colloidal crystals fabricated by the thermal pressing of colloidal crystal chips, Langmuir 21 (2005) 8987–8991.

[8] S. Omi, A. Matsuda, K. Imamura, M. Nagai, G.-H. Ma, Synthesis of monodisperse polymeric microspheres including polyimide prepolymer by using SPG emulsification technique, Colloids Surf. A 153 (1999) 373−381.

[9] G.-H. Ma, M. Nagai, S. Omi, Preparation of uniform poly lactide microspheres by employing the shirasu porous glass SPG emulsification technique, Colloids Surf. A 153 (1999) 383−394.

[10] Y. Okamura, Y. Fukui, K. Kabata, H. Suzuki, M. Handa, Y. Ikeda, S. Takeoka, Novel platelet substitutes: disk-shaped biodegradable nanosheets and their enhanced effects on platelet aggregation, Bioconjug. Chem. 20 (2009) 1958–1965.

[11] Y. Okamura, I. Maekawa, Y. Teramura, H. Maruyama, M. Handa, Y. Ikeda, S. Takeoka, Hemostatic effects of phospholipid vesicles carrying fibrinogen γ chain dodecapeptide in vitro and in vivo, Bioconjug. Chem. 16 (2005) 1589−1596.

[12] Y. Okamura, M. Handa, H. Suzuki, Y. Ikeda, S. Takeoka, New strategy of platelet substitutes for enhancing platelet aggregation at high shear rates: cooperative effects of a mixed system of fibrinogen γ-chain dodecapeptide- or glycoprotein Ib α-conjugated latex beads under flow conditions, J. Artif. Organs 9 (2006) 251−258.

[13] H. Zhang, T. Aoki, K. Hatano, K. Kabayama, M. Nakagawa, K. Fukase, Y. Okamura, Porous nanosheet wrapping for live imaging of suspension cells, J. Mater. Chem. B 6 (2018) 6622−6628.

[14] Y. Okamura, S. Utsunomiya, H. Suzuki, D. Niwa, T. Osaka, S. Takeoka, Fabrication of free-standing nanoparticle-fused nanosheets and their hetero-modification using sacrificial film, Colloids Surf. A 318 (2008) 184−190.

[15] K. Y. Lee, D.J. Mooney, Alginate: Properties and biomedical applications, Prog. Polym. Sci. 37 (2012) 106−126.

[16] T. Komachi, H. Sumiyoshi, Y. Inagaki, S. Takeoka, Y. Nagase, Y. Okamura, Adhesive and robust multilayered poly(lactic acid) nanosheets for hemostatic dressing in liver injury model, J. Biomed. Mater. Res. B 105 (2017) 1747−1757.

[17] A. R. Fajardo, M. B. Silva, L. C. Lopes, J. F. Piai, A. F. Rubira, E. C. Muniz, Hydrogel based on an alginate–Ca^{2+}/Chondroitin sulfate matrix as a potential colon-specific drug delivery system, RSC Adv. 2 (2012) 11095−11103.

[18] E. M.-Spurej, K. Chipperfield, Past and future approaches to assess the quality of platelets for transfusion, Transfus. Med. Rev. 21 (2007) 295−306.

[19] E. Loth, Drag of non-spherical solid particles of regular and irregular shape, Powder Technol. 182 (2008) 342–353.

[20] T. Fujie, Y. Kawamoto, H. Haniuda, A. Saito, K. Kabata, Y. Honda, E. Ohmori, T. Asahi, S. Takeoka, Selective molecular permeability induced by glass transition dynamics of semicrystalline polymer ultrathin films, Macromolecules 46 (2013) 395−402.

[21] A. Udagawa, T. Fujie, Y. Kawamoto, A. Saito, S. Takeoka, T. Asahi, Interfacial effects on the crystallization and surface properties of poly(l-lactic acid) ultrathin films, Polym. J. 48 (2016) 157−161.

[22] S. Armini, I. U. Vakarelski, C. M. Whelan, K. Maex, K. Higashitani, Nanoscale indentation of polymer and composite polymer−silica core−shell submicrometer particles by atomic force microscopy, Langmuir 23 (2007) 2007−2014.

[23] J.A. Champion, Y.K. Katare, S. Mitragotri, Making polymeric micro- and nanoparticles of complex shapes, Proc. Natl. Acad. Sci. U.S.A. 104 (2007) 11901–11904.

[24] C. C. Ho, A. Keller, A, J. A. Odell, R. H. Ottewill, Preparation of monodisperse ellipsoidal polystyrene particles, Colloid Polym. Sci. 271 (1993) 469−1479.

[25] R. Hiorns, Polymer Handbook, 4th Edition, J. Brandrup, E. H. Immergut, E. A. Grulke, Eds.; Wiley: NY, 2003; Chapter V/91.

[26] Polylactic Acid, 2nd Edition; T.S. Lee, S.T. Bee, Eds.; Elsevier: MA, 2019; Chapter 5.

[27] L. Jiang, C. Nath, J. Samuel, S. G. Kapoor, An enhanced microstructure-level finite element machining model for carbon nanotube-polymer composites, J. Manuf. Sci. Eng. 137 (2015) 021009.

[28] I. Donati, S. Holtan, Y. A. Mørch, M. Borgogna, M. Dentini, G. Skjåk-Bræk, G. New hypothesis on the role of alternating sequences in calcium–alginate gels, Biomacromolecules 6 (2005) 1031−1040.

[29] G. M. Kim, G. H. Michler, Micromechanical deformation processes in toughened and particle-filled semicrystalline polymers: Part 1. characterization of deformation processes in dependence on phase morphology, Polymer 39 (1998) 5689−5697.

[30] G. M. Kim, G. H. Michler, Micromechanical deformation processes in toughened and particle-filled semicrystalline polymers: Part 2. Model representation for micromechanical deformation processes, Polymer 39 (1998) 5699−5703.

[31] D. Mazia, G. Schatten, W. Sale, Adhesion of cells to surfaces coated with polylysine. applications to electron microscopy, J. Cell Biol. 66 (1975) 198−200.

[32] I. Migneault, C. Dartiguenave, M. J. Bertrand, K. C. Waldron, Glutaraldehyde: Behavior in aqueous solution, reaction with proteins, and application to enzyme crosslinking, Biotechniques 37 (2004) 790−802.

[32] D. C. Carter, J. X. Ho, Structure of serum albumin, Adv. Protein Chem. 45 (1994) 153−203.

Chapter 3
Phase separation and a roll-to-roll coating for polymer disc fabrication

3-1 Background

3-1-1 Basic of roll-to-roll coating process and gravure coating method

Roll-to-roll coating process is a fabrication method which involves the transferring material continuously from one onto another moving roller. This process is also referred as web processing or reel-to-reel processing. This process is considered as a rational solution for high volume production since the ability of continuous fabrication. Generally, thin and flexible web materials such as polyethylene terephthalate (PET), polyethylene naphthalate (PEN), polyimide (PI), metal, paper, and

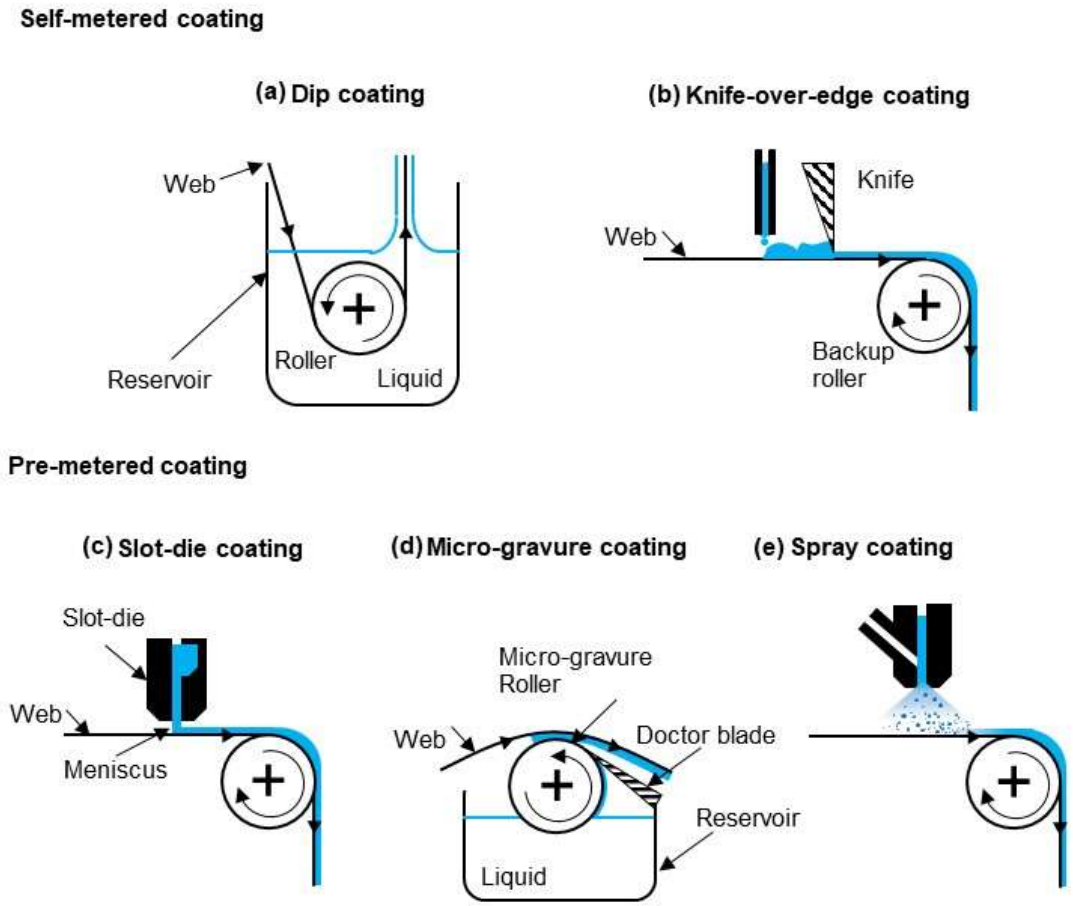

Fig. 3-1 Roll-to-roll coating process of self-metered coating. (a) dip coating; (b) knife-over-edge coating and pre-metered coating. (c) slot-die coating; (d) micro-gravure coating; and (e) spray coating (cited and partially modified from ref 1-4).

textiles have been used as substrates [1]. Roll-to-roll coating process can be divided into two main categories namely self-metered and pre-metered as shown in Fig. 3-1 [4]. The difference between these two methods is that self-metered coating determines the coating thickness (weight) through combined effects of coating parameters such as liquid properties, web velocity, and geometry of coater shapes. While, coating thickness (weight) of pre-metered is independent of coating solution properties such as viscosity but can be controlled by the volumetric flow rate of coating solution per unit width and the web speed. The well-known methods of self-metered coating are dip and knife-over-edge, whereas, the important methods of pre-metered coating are slot-die, direct gravure, micro-gravure, and spray coating techniques.

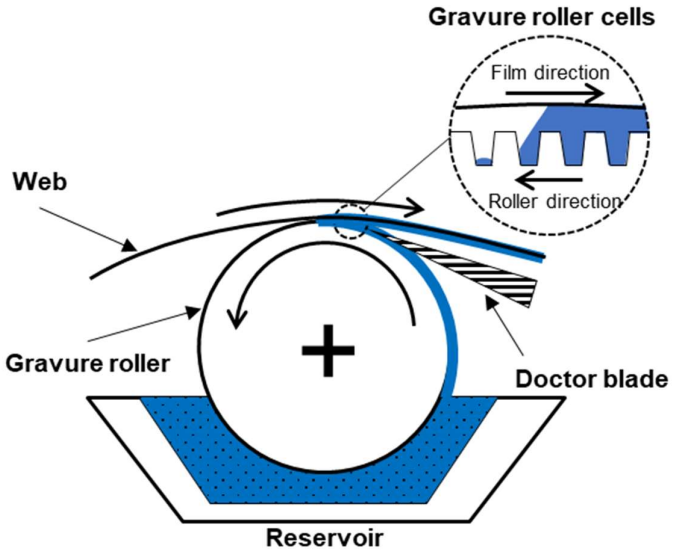

Fig. 3-2 Cross-sectional image of gravure roller and illustrate of fluid transfer process from gravure roller to substrate in reverse gravure coating (cited and partially modified from ref 2).

Gravure coating, one of the most well-known pre-metered coating, is a high-throughput industrial coating method which can be used with fluids of a wide range of viscosity [5] onto substrates at speeds of up to 900 m/min [6]. Gravure coating includes various a number of distinct gravure coating arrangements which can be simply classified according to the operating direction of gravure roller as in the same direction of substrate and in opposite directions. This opposite direction setting called reverse gravure coating, is considered as the most commonly configuration setting because it is considerably more stable than the corresponding forward mode of operation [7]. In gravure coating, the process of

transferring fluid to the substrate can be classified into two consecutive steps. First, a rotating gravure roll picks up fluid from the feed reservoir by having doctor blade positioned against the roll for removing excess fluid. Then, a proportion of fluid is transferred to the coating substrate when it continuously sweeps over the gravure roll surface and create a thin liquid film layer on the substrate (see in Fig. 3-2) [5, 8].

3-1-2 Introduction of phase separation in polymer blend

Polymer blends can either form homogenous mixtures or they can undergo phase separation which is usually based on the concepts of solution thermodynamics [9]. Phase separation, in general, is a de-mixing process, in which is usually induced by a change in temperature or molecular weight. This mechanism takes place when the system enters either the metastable (binodal) or two phase region (spinodal) by slow nucleation followed by growth of the phase separated domain. In the case of temperature, as can be seen in Fig. 3-3, the diagram shows two critical solution temperatures namely lower critical solution temperature (LCST) and upper critical solution temperature (UCST). These temperatures (at specific pressure) are the critical point showing the degree of miscibility of the mixture components. At above UCST, the components of a mixture are miscible in all proportions, while, the components of a mixture are miscible for all compositions at below LCST. In the phase diagram, the LCST and UCST is the shared maximum and minimum of the concave with spinodal and binodal curves which divided area into three regions of different degree of miscibility namely one phase (miscible region between the two binodals), metastable region (regions between binodals and spinodals) and two phase region (regions of immiscibility, bordered by the spinodals) [9, 10].

3-1-3 A simple model of phase separation mechanism in thin polymer films

There is a ton of study about phase separation mechanism of bulk polymers, however, the situation in thin polymer films is complicated by the presence of the substrate/film and film/air interfaces [11]. During this thin film formation process, the solvent simultaneously evaporates and the polymer concentration start to increase rapidly.

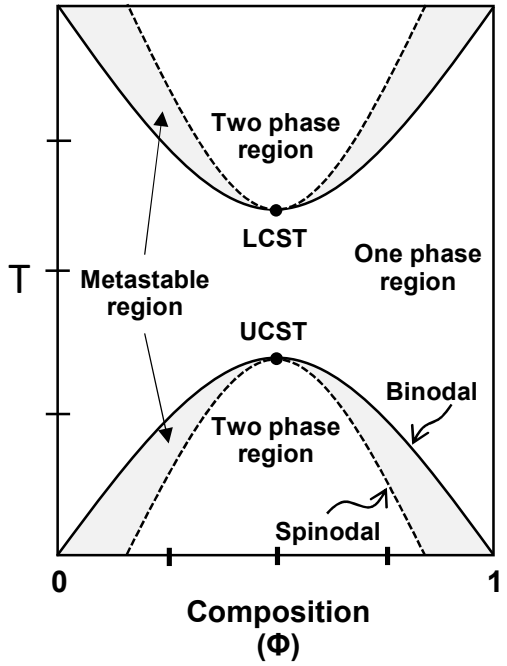

Fig. 3-3 General phase diagram of the mixture components (cited and partially modified from ref 10).

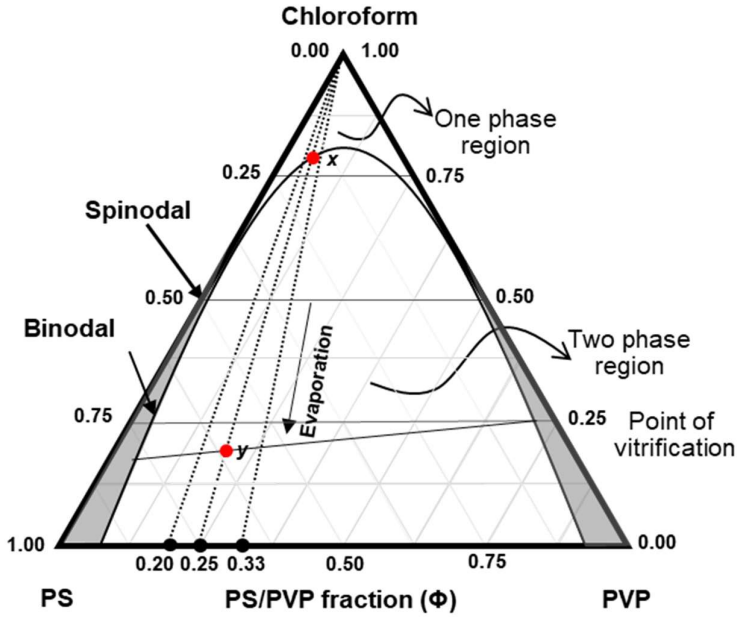

Fig. 3-4 Schematic ternary phase diagram of PS and PVP in chloroform showing the moving from one phase to two phase region along the dotted line induced by evaporation process (cited and partially modified from ref 12).

In the system of PS/PVP in chloroform, as an example, a typical phase diagram of the ternary systems is shown in Fig. 3-4. The system composition changes along the dotted line inducing by solvent evaporation, starting the phase separation and structure formation when the system intersected the binodal points (point *x* in Fig. 3-4) and moving from one phase to two phase region (moving from point *x* to *y* in Fig. 3-4) depending on the initial PS/PVP ratio. The phase separation takes place until the system meet the vitrification point (point *y* in Fig. 3-4). Although the solvent will keep on evaporating, all structures will be frozen until the end of coating process [(12)].

When the system moving to two phase region, a bicontinuous morphology generated by spinodal decomposition could be expected since the concentration fluctuation between two phase increases. In the case that minority component in the blend is sufficient to maintain a continuous morphology, the ribbon-like domains are deemed to be a frozen structure (see in Fig. 3-5a). On the other hand, bicontinuous morphology is going to break up into numerous irregular structures when the system has insufficient amount of minority component. Then, the phase separation continues to form spherical domains by diffusion and coarsening mechanism in order to minimize the interfacial area with surrounding matrix (see in Fig. 3-5b–3-5d) [(13)].

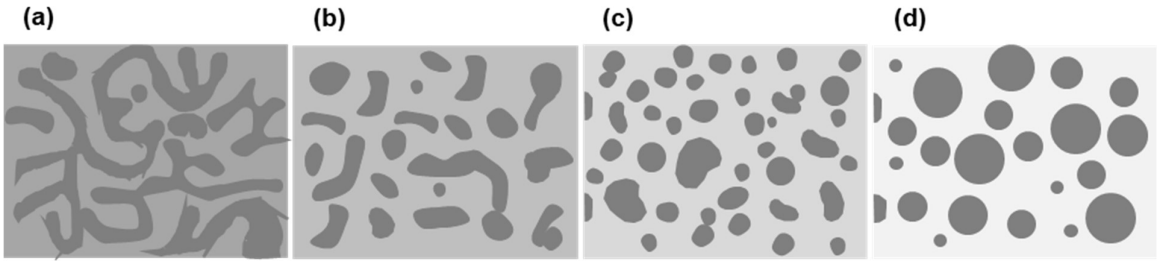

Fig. 3-5 Model for the phase separation mechanism within polymer thin film; (a) bicontinuous morphology when the system moving to two phase region; (b) irregular structure after breaking up of bicontinuous morphology; (c) more spherical domains to reduce surface tension; (d) spherical domain after frozen (cited and partially modified from ref 13).

3-2 Purpose

In this chapter, we would like to propose a novel method combining polymer blend phase separation and a roll-to-roll coating process to able to continuously produce large amounts of polymer

micro/nano-discs in a one-pot manner. To this end, a commercial PVA film is chosen as the coating substrate for the roll-to-roll process, a commonly used choice for large-scale production of thin films [1, 2]. PVP and PS (as model discs) are chosen as the major and minor components in the polymer blend. Among them, as PVA and PVP are water-soluble, the micro/nano-discs composed of PS could be continuously obtained in large amounts by washing with water in a one-pot manner. Herein, the effects of fabrication conditions, such as the blend ratio of the PS/PVP pair and the total polymer concentration on the diameter and thickness of PS discs are systematically investigated.

3-3 Material and methods

3-3-1 Materials

PS (DP: 1,500–1,800; Wako Pure Chemical, Osaka, Japan) were used as a minor component in this study whereas PVP (M_w: 40,000; Sigma-Aldrich) was used as a major component. To test the versatility of proposed process with other polymers, PLGA (L/G: 50:50; IV: 0.6 dL/g, M_w: 35,000; Polysciences, PA, USA), Poly(butyl methacrylate) (PBMA, IV: 0.47–0.56 dL/g, Sigma-Aldrich, MO, USA), and Polycaprolactone (PCL, M_w: 43,000–100,000; Polysciences) were used as a minor component. Chloroform (Wako Pure Chemical) was used as a cosolvent, and all chemicals were used without further purification. The roll-to-roll coating substrate used in this study was PVA film (S-type, commercial called Hi-Selon), purchased from Nippon Gohsei, Tokyo, Japan. This film is completely dissolved in water even at a low temperature of 2–5°C, and it is resistant to most organic solvents and chemicals. The width of the purchased PVA film is 20 cm, and the film thickness is ~60 μm.

3-3-2 Fabrication of micro/nano discs by a roll-to-roll process

The coating process of a polymer mixture on a PVA film is shown in Fig. 3-6. First, the polymer mixture of PS and PVP were dissolved in chloroform by having PS as a minor component. The blend ratio between minor and major component were varied as 1:3, 1:4 and 1:5 (w/w). The total polymer concentration (total amount of both minor and major components) was varied as 1 wt%, 2 wt% and 4 wt%. The polymer mixtures were stirred overnight to obtain complete dissolution and was then coated on a PVA film using a roll-to-roll coating machine (reverse gravure coating, μCoater 350, Yasui Seiki,

Kanagawa, Japan). The line speed of coated substrate (also called web speed) was set at 1.0 m/min with micro gravure roll speed at 16 rpm, and a furnace temperature of 60°C. All of these coating processes were operated at room temperature (25°C) with a normal humidity in a clean environment.

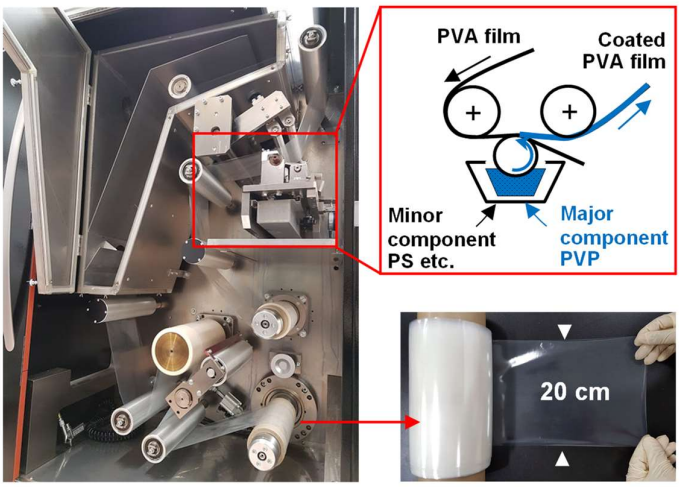

Fig. 3-6 Coating process for a polymer mixture solution on a water-soluble PVA film using a roll-to-roll coating machine (permitted reuse reproduction for doctor thesis from the publisher, cited and partially modified from ref. 14).

3-3-3 Morphology of micro/nano discs

To observe the phase separation morphology of PS/PVP on a PVA film, coated film samples were cut and investigate by FE-SEM (Hitachi S-4800, Hitachi, Tokyo, Japan) at an accelerating voltage of 3.0 kV. To evaluate the number of particles and to investigate the morphology of the discs obtained after collection, coated film samples were cut into three 4×4 cm^2 pieces, put in 40 ml of distilled water and kept overnight. The dissolved solutions were then centrifuged for five times at 21,500*g*, 4°C, for 15 min (Himac CT15RE, Hitachi, Tokyo, Japan). After centrifugation, the sample were adjusted to a final volume of 1 mL and counted under a microscope (20×, Nikon Eclipse TS100, Nikon Corporation, Tokyo, Japan) using a hemacytometer (SLGC A113, Sunleadglass, Saitama, Japan) to evaluate the particle numbers. For top view images, the centrifuged samples were filtered through a 0.1 μm track-etched PC filter membrane (Whatman Nuclepore, GE Healthcare Life Sciences, Maidstone, UK).

To evaluate composition of PS discs after collection process, dried sample of PS discs as well as pure PS, PVP and PVA were examined by FTIR (FTIR-8400, Shimadzu, Japan). For top view images, the centrifuged samples were filtered through a 0.1 μm track-etched PC filter membrane (Whatman Nuclepore, GE Healthcare Life Sciences, Maidstone, UK). The filtered sample with membrane were then dried in a desiccator and observed by FE-SEM. For cross-sectional view images, the samples were dropped on a 0.1 μm inorganic filter membrane (Whatman Anodisc, GE Healthcare Life Sciences, Maidstone, UK), dried in desiccator and examined by FE-SEM. All of SEM samples were pre-treated by sputter-coating with platinum before investigation. By using ImageJ software (NIH), the average diameter of both PS domains before collection and PS discs after collection was from the top view images, while the cross-sectional images were used to evaluate the thickness of the PS discs. With the same process as mentioned above, the solution mixtures of PLGA, PBMA, and PCL with PVP were prepared in chloroform at a predetermined polymer weight fraction as a minor component at the blend ratio of 1:4 (w/w) with a total polymer concentration of 4 wt%. The polymer phase separation morphology as well as the polymer discs were evaluated by FE-SEM.

3-4 Results and discussion

3-4-1 The effect of roll-to-roll operating condition on phase separation morphology

To find the optimum condition of roll-to-roll coating process, polymer mixture of PS/PVP at a total concentration of 4 wt% with blend ratio of 1:4 was used as a model to evaluate the phase separation on coated PVA film. The effect of furnace temperature, gravure roll speed, film line speed as well as speed ratio on the phase separation morphology were studied. First, the effect of furnace temperature was studied by varying at 40°C, 60°C and 80°C.

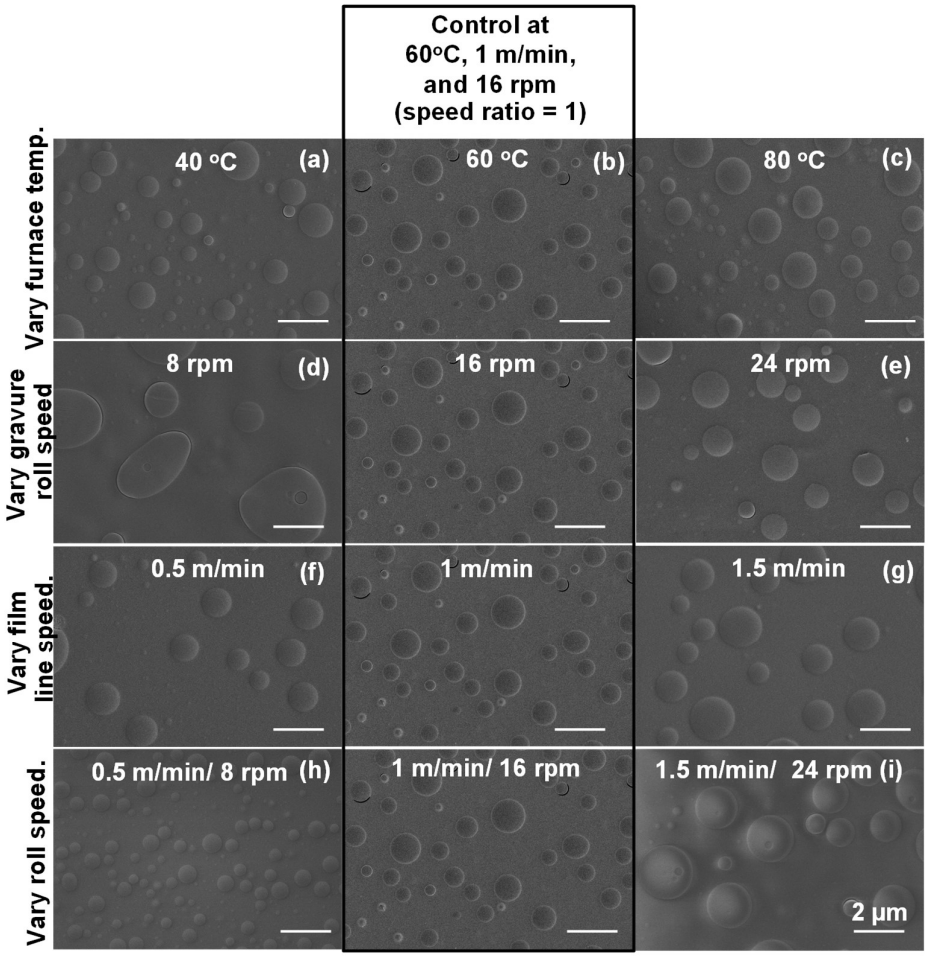

Fig. 3-7 SEM images of PS/PVP blend phase separation with the blend ratio of 1:4 at a total concentration of 4%. By varying furnace temperature at (a) 40 ºC, and (c) 80 ºC. By varying gravure roll speed at (d) 8 rpm, and (e) 24 rpm. By varying film line speed at (f) 0.5 m/min and (g) 1.5 m/min and. By varying roll speed of constant speed ratio 1.0 at (h) 0.5 m/min/ 8 rpm, (i). 1.5 m/min/ 24 rpm. The identical image of control condition (b) furnace temperature 60 ºC, gravure roll speed at 16 rpm, film line speed at 1 m/min (speed ratio = 1.0) was put in the middle in each row for easy comparison. All images shared scale bar of 2 µm as shown in Fig. 3-6i (permitted reuse reproduction for doctor thesis from the publisher, cited and partially modified from ref. 14).

The results show that phase separation of all conditions was about the same demonstrated clearly phase separation providing symmetry circle in shape of PS domains (Fig. 3-7a-7c). This implied that the evaporation of solvent until the polymer mixture reaching to the frozen morphology of phase

separation completed within very short residence time. Based on the film line speed of 1 m/min, the evaporation time through frozen morphology is at least less than ~30 seconds, which is before coated film was conveyed into the furnace chamber. However, it should be noted here that surface of film sample at furnace temperature of 40°C is still remained slightly wet which is the evidence of the remaining solvent residual on coated substrate. On the other hand, coated PVA film was observed to loss their flexibility at furnace temperature of 80°C which is expected to be the effect of too high temperature.

Other two key parameters that affected the quality of coating of roll-to-roll process are gravure roll speed and film line speed. Generally, the most comment setting of ratio between gravure roll speed and film line speed is 1.0. To study the effect of gravure roll speed, the furnace temperature was controlled at 60°C and film line speed was set at 1 m/min. The gravure roll speed was varied at 8 rpm, 16 rpm and 24 rpm which represents to 0.5 m/min, 1.0 m/min and 1.5 m/min, respectively (diameter of gravure roll = 20 mm). As can be seen in Fig. 3-7d, 3-7b, and 3-7e, phase separation of PS/PVP can be clearly achieved for both gravure roll speed of 16 rpm and 24 rpm showing quite similar frozen morphology of PS domains. Intriguingly, some of asymmetry PS domains can be seen at the gravure roll speed of 8 rpm as can be seen in Fig. 3-7d (gravure roll speed 50% of film line speed). Two assumptions are expected to reasonably explain these results. First, since the film line speed was notably higher than the gravure roll speed in this condition, air entrainment in the form of evenly spaced lines of fine bubbles which always developed in the machine direction may nestle the formation of spherical PS domains [7]. Second, the instability coating behavior according to the unmatching between the speed of film line and gravure roll causing the uneven and thin coating film which is likely to provide irregular shape of PS domains.

Then, the effect of film line speed was studied by varying film line speed at 0.5 m/min, 1.0 m/min, and 1.5 m/min. Control parameters were gravure roll speed and furnace temperature at 16 rpm and 60°C, respectively. As can be seen in Fig. 3-7f, 3-7b and 3-7g, all conditions provide similar circle in shape of PS domain. However, ribbing instabilities (coating flows with evenly spaced uniform down-web lines undulating the surface of the coating) can be seen by naked eyes on the coated film when the

film line speed decreased to 0.5 m/min which is the evidence of inappropriate coating condition (See in Fig. 3-8).

Finally, the effect of roll speed by keeping speed ratio at 1.0 on phase separation morphology was studied. All conditions show clearly phase separation with circle PS domains distributed evenly throughout the coated PVA film sample. Diameter of PS domains was 474 ± 182 nm, 687 ± 155 nm, and 1,253 ± 668 nm for film line speed/gravure roll speed of 0.5 m/min/8 rpm, 1.0 m/min/16 rpm and 1.5 m/min/24 rpm, respectively (Fig. 3-7h, 3-7b, and 3-7i). The increasing of PS domain diameter is expected to be the result of the thicker of coating film at faster roll speed condition [15, 16]. As explained by our proposed model in previous study [13], thicker fluid film resulted the thicker bicontinuous PS domains and after the evolution of phase separation from bicontinuous morphology to be more circle aiming to reduce surface tension, thicker bicontinuous domains is supposed to provide larger diameter of PS domains.

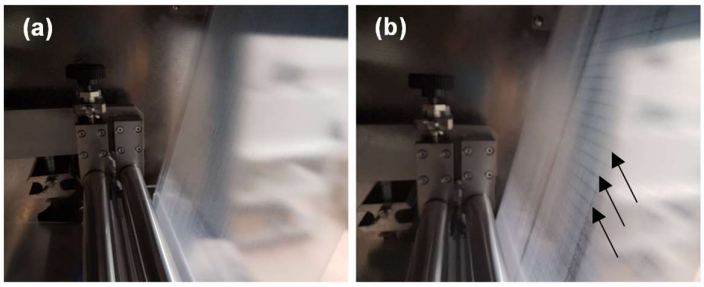

Fig. 3-8 The images of coated film (a) normal quality coated film surface; (b) ribbing instabilities (ribbing lines were indicated by arrows) at film line speed of 0.5 m/min and gravure roll speed of 16 rpm with furnace temperature of 60ºC (permitted reuse reproduction for doctor thesis from the publisher, cited and partially modified from ref. 14).

According to the results mentioned above, the optimum conditions to operate roll-to-roll machine for achieving clearly phase separation are at furnace temperature of 60ºC with the film line speed of 1.0 or 1.5 m/min and the gravure roll speed of 16 rpm or 24 rpm. Moreover, the results also show that PS domain diameter increases from ~500 nm to ~1,300 nm when the roll speed increased (film line and gravure roll speed by keeping ration as 1.0) from 0.5 m/min/8 rpm to 1.5 m/min/24 rpm,

respectively. To further study the effect of blend ratio and a total concentration of PS/PVP polymer mixture, furnace temperature at 60°C with film line speed of 1.0 m/min and the gravure roll speed of 16 rpm was used as a control parameter of roll-to-roll operating condition.

3-4-2 Morphology of PS domains before collection

The phase separation mechanisms of PS/PVP on PVA film via roll-to-roll process are complicated by the presence of the coating substrate versus the PS/PVP mixture and PS/PVP mixture versus air interfaces [11]. During the coating process and thin film formation, the solvent start to evaporate causing the rapid increase of polymer concentration and the frozen structure will be obtained.

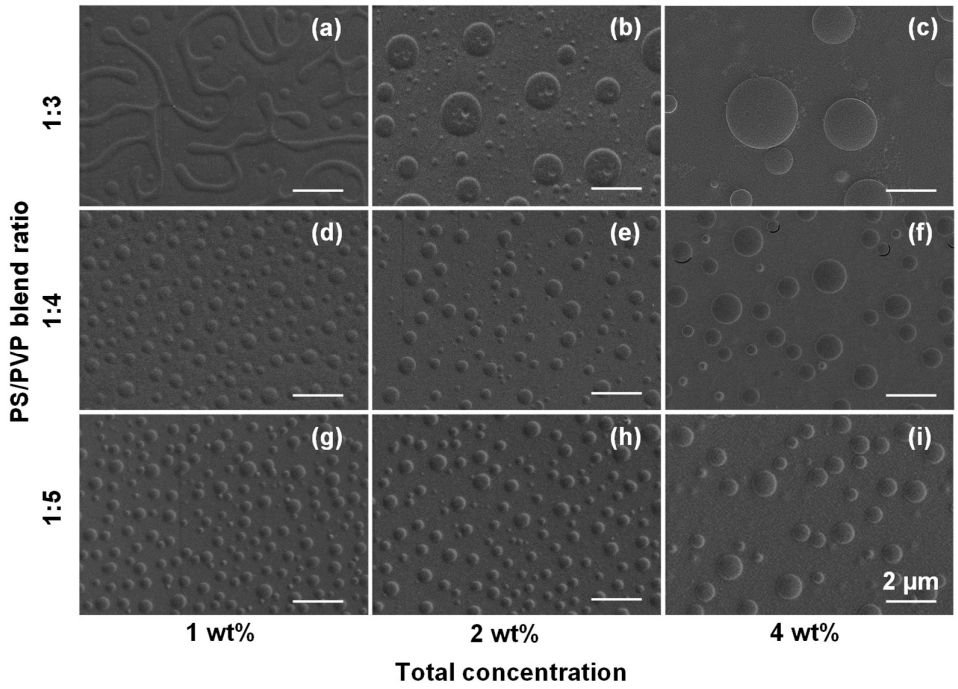

Fig. 3-9 SEM images of PS/PVP blend phase separation on the PVA film with blend ratio of 1:3 at total concentrations of 1 wt%, 2 wt%, and 4 wt% (a–c); blend ratio of 1:4 and total concentrations of 1 wt%, 2 wt%, and 4 wt% (d–f); blend ratio of 1:5 at total concentrations of 1 wt%, 2 wt%, and 4 wt% (g–i). All images shared the same scale bar of 2 µm as shown in Fig. 3-9i (permitted reuse reproduction for doctor thesis from the publisher, cited and partially modified from ref. 14).

In this study, frozen structure of polymer blend of PS/PVP system can be seen in Fig. 3-9. Island-like phase of PS domains surrounded by ocean-like of PVP on a PVA film were apparently observed at all conditions excluding that at a total concentration of 1 wt% with blend ratio of 1:3 (Fig. 3-9a). As explained in a simple model for the phase separation mechanism proposed in our previous study [13], the amount of minor component in this condition was sufficient to stable a bicontinuous morphology generated by spinodal decomposition when the system moving to two phase region. In other conditions, the concentration difference between the minor and the major component favors the formation of dispersed PS domains. Most PS domains were circular in shape and dispersed throughout the whole PVP matrix regardless of the location in both the width and length directions. This could be used to overcome the limitation of spin-coating which tend to provide elongated PS domains increasing with the radial distance from the center of the coating substrate from the same PS/PVP mixture [17]. We believe that the roll-to roll coating process ultimately eliminates the effect of centrifugal flow, which can provide a more homogenous phase separation morphology.

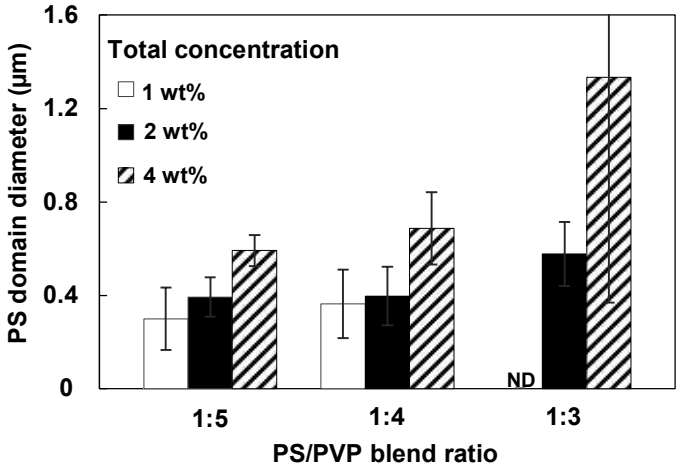

Fig. 3-10 Diameter of PS domains on the PVA film. Opened, closed, and striped columns show the coating conditions of each PS/PVP blend ratio by varying total concentrations from 1 to 2, and 4 wt%, respectively (permitted reuse reproduction for doctor thesis from the publisher, cited and partially modified from ref. 14).

The average diameter of the PS domains was from three samples which were individually prepared (N = 3, and at least 50 discs were chosen for each measurement). As shown in Fig. 3-10, the

average diameter varied in the range of 300 nm to about 1,335 nm at blends ratio of 1:5, 1:4 and 1:3, respectively. For a particular blend ratio, it is reasonable to expect that the size of dispersed PS domains increases with the PS fraction in the PS/PVP blend [18, 19]. For example, the diameter of PS domains slightly increased from 592 ± 66 nm to 687 ± 155 nm when changing the blend ratio from 1:5 to 1:4, at a total concentration of 4 wt%, whereas PS domains from a 1:3 blend ratio was obviously larger (1,335 ± 966 nm). Also, when changing the blend ratio from 1:5 to 1:3, the diameter of PS domains becomes less uniform, as indicated by a larger error bar being shown in Fig. 3-8. This could be rationally assumed that a thicker bicontinuous morphology could occur during the initial state of phase separation mechanism at higher total polymer concentration. By this reason when the thicker bicontinuous morphology breaks into irregular shape during phase separation process, less uniform PS domains were expected to form comparing with thinner bicontinuous morphology obtained at lower concentration.

3-4-3 Composition and morphology of PS discs after collection

Composition, diameter and thickness of PS discs

After repeatedly centrifugation and washing with water, PVP and PVA film as the major component and coating substrate were removed. The composition of these PS discs after washing process at a total concentration of 4% with a blend ratio of 1:4 was investigated by FTIR as can be seen in Fig. 3-11d. Spectra of obtained PS discs were compared with spectra of pure PS, PVA and PVP, respectively (Fig. 3-11a–11c). The absorbance peaks are located in a wide range of spectrum scale. The first peak at around 3,590–3,650 cm^{-1} is for OH stretching which is the strong evidence of the presence of PVA. The second peak is for aromatic C–H stretching at 3,000 cm^{-1} occurred due to the present of PS. The present PS is reconfirmed by the peak at 1,500 cm^{-1} which is aromatic C–C stretching. The other two peaks that are located at 1,700 and 1,290 cm^{-1} indicates C=O bond stretching vibration and C–N stretching, respectively. These two peaks are contributed by the existed of PVP in a sample. Finally, the small peak of C–O stretching at 1,050–1,150 cm^{-1} is reconfirmed the presence of PVA. According to these results, it could be concluded that obtained PS discs after washing process are PS-rich particles (PS discs that still included small amount of PVP and PVA) which are herein referred as PS discs in this paper. The precipitated PS discs in water were obtained after the centrifugation process. The whole

process is operated in water, without any use of organic solvent, desiccation or re-suspension, and the PS discs are directly collected in a one-pot manner. This result verifies the principle of our method very well.

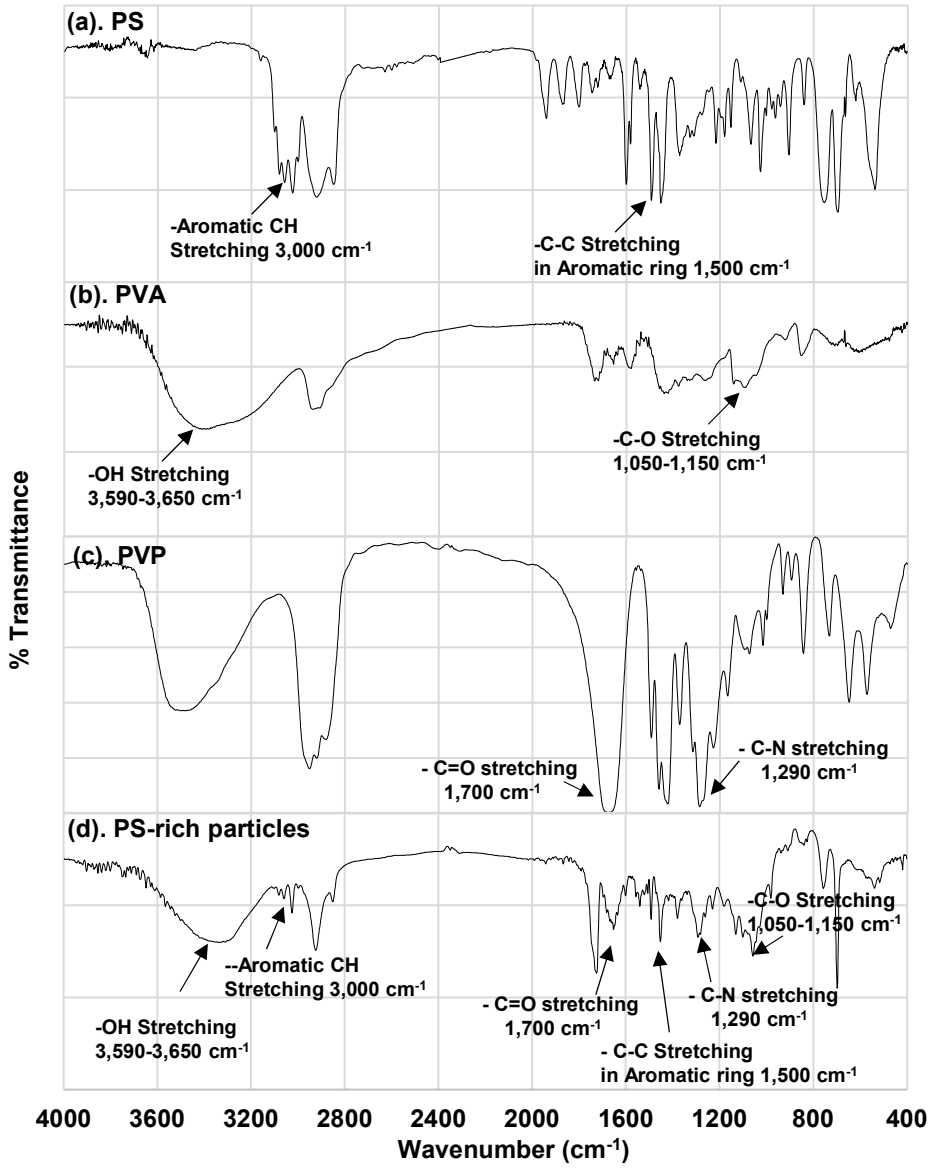

Fig. 3-11 FTIR-spectra of (a) pure PS, (b) pure PVA, (c) pure PVP, and (d) PS discs prepared at a total concentration of 4 wt% with a blend ratio of 1:4 (permitted reuse reproduction for doctor thesis from the publisher, cited and partially modified from ref. 14).

Apparently, the amount of collected PS discs is solely decided by the area of the PVA substrate. Here, a high concentration of PS discs collected PS discs from 3 pieces of 4×4 cm^2 substrates (48 cm^2),

and found a high concentration of PS discs. For example, in the case of 1:3 at a total concentration of 2 wt%, ~10^7 particles of PS discs in a final volume of 1 ml were obtained. Accordingly, the density of discs on the substrate film is ~2×10^5 particles/cm^2 (number of particles/areas = ~10^7 particles / 48 cm^2). Based on the film line speed of at 1 m/min, film area that can be coated in one minute is equal to 2,000 cm^2 (long × width; 100 × 20 cm^2) which equals to the production rate of ~4×10^8 particles/min (number of particles/areas × coated area in one minute).

Among number of proposed methods for polymer discs fabrication, the information of particle production rate (particles/time) is quite limited since they mainly focus on the effect of operating condition on particle morphology. Film stretching method reported the total production number of 10^8 to 10^{12} particles. This number corresponds to the production rate of ~9×10^4–9×10^8 particles/min based on the total fabrication time of ~1,115 min [20]. However, this method is two steps fabrication; starts with the spherical particle fabrication and follows by film stretching, which is burdensome. Automated stepper lithography reported the production rate at ~2.5×10^8 particles/min [21]. However, this method requires high technology with the sophisticated device, such as electron beam lithography and stepper, which is expected to have a skilled worker to operate which is unlikely to be an ideal case for an economical point of view. To the best of our knowledge, this is the first reported method to fabricate polymer micro/nano-discs at such a continuous large scale, which should make it possible and competitive with alternative methods to upscale to industrial quantities in future.

To understand more about the effect of blend ratio and total concentration on the morphology of PS discs, SEM images of PS discs under various fabrication conditions were detailed quantitative analyzed. In our collection process, a filter membrane with a pore size of 100 nm was used to screen out particles which have a diameter less than 100 nm. These small particles are undesired since their shape is closer to spherical. Moreover, their proportion among all the PS particles is limited (~2% for a blend ratio of 1:3 at a total concentration of 4%). We found that most of PS particles regardless of the fabrication condition were disc-like in shape while the particle size varied at each condition. Representative SEM images of the PS discs obtained are shown in Fig. 3-12a–12d.

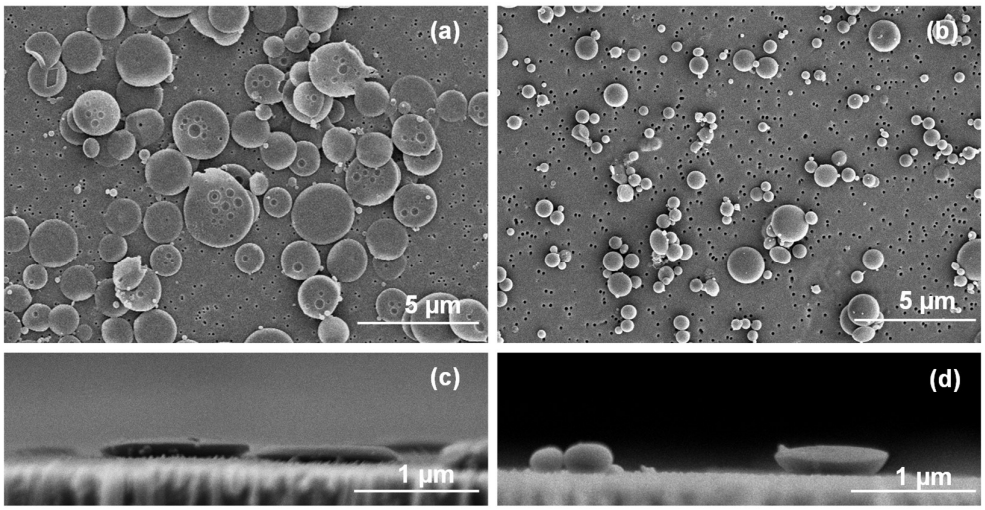

Fig. 3-12 SEM images of PS discs; (a) Top view and (c) cross-sectional view images of PS discs with a PS/PVP blend ratio of 1:3 at a total concentration of 2 wt%; (b) top view (d) cross-sectional view for a PS/PVP blend ratio of 1:5 at a total concentration of 4 wt%, respectively (permitted reuse reproduction for doctor thesis from the publisher, cited and partially modified from ref. 14).

Flatter PS discs were observed at a blend ratio of 1:3 at a total concentration of 2 wt%. Here, thinner coating layer can be expected at this lower total concentration, which acts like a dimensional confinement (see Fig. 3-12a and 3-12c for top-view and cross-sectional view, respectively). It should be noted here that there are craters on PS discs in this condition which is expected to be a frozen structure of small PVP domains in another bigger PS domains left from the rapid quenching during solvent evaporation process. This phenomenon is expected to induce by the dimensional confinement (thin liquid film thickness) at this low total concentration combined with the high portion of minor component in the mixture. At a blend ratio of 1:5 at a total concentration of 4 wt%, PS discs was seen to be more hemispherical in shape, driven mainly by surface tension since a thicker coating film layer was achieved at this high total concentration. (see Fig. 3-12b and 3-12d for top-view and cross-sectional view, respectively).

The average diameter of the PS discs was measured as shown in Fig. 3-13. The result shows that the average diameter of PS discs increases with the increasing of the total polymer concentration or by the changing of blend ratio from 1:5 to 1:3. For example, PS discs diameter increases from 426 ±

25 nm to 513 ± 14 nm when the total concentration increased from 1% to 4% in the case of a 1:5 blend ratio. If we consider the data for a total concentration of 4 wt%, the discs size significantly increases from 513 ± 14 nm to 862 ± 149 nm when changing of blend ratio from 1:5 to 1:3. It can be implied that the increasing of the total concentration or changing the blend ratio to 1:3 encourage the formation of larger PS discs, which can be explained by the following reasoning. In a spin-coating process, the evolution time of phase separation morphology is strongly determined by the solvent evaporation rate, which is related to the rotation speed [17], [18], [22]. In the case of a roll-to-roll coating, the solvent evaporation process becomes much more straightforward and the evaporation rate can be deemed as constant. When the composition of the polymer blend system enters a two-phase region in the phase diagram, the evaluation time for phase coarsening is the same regardless of the initial total concentration. Hence, the final phase separation morphology mainly depends on the thickness of liquid film at the point that the phase separation is triggered. In the case of low total concentration, growth of dispersed domains limit by the dimensional confinement of the thin liquid film, leading to the formation of smaller PS domains. Moreover, it is also reasonable to expect a larger size of PS discs at a blend system with a larger fraction of minor component (such as a blend ratio of 1:3 in PS/PVP), because the fluctuations in polymer concentration become much more marked.

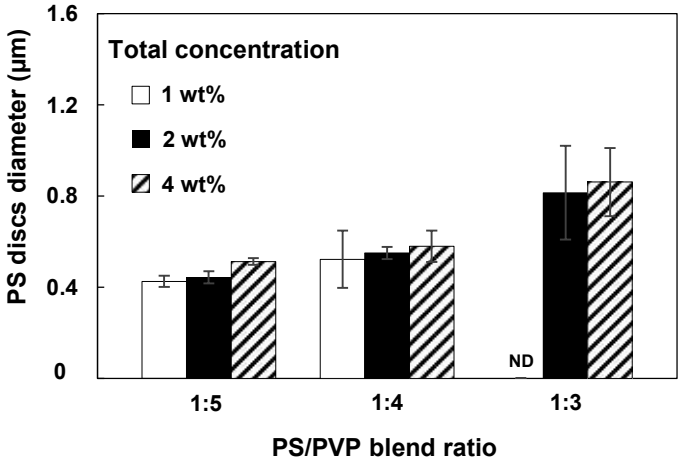

Fig. 3-13 Diameter of PS discs at each PS/PVP blend ratio when varying the total concentration from 1 wt% to 4 wt% (permitted reuse reproduction for doctor thesis from the publisher, cited and partially modified from ref. 14).

As mentioned previously, the thickness of PS discs is related to the thickness of liquid film present during the roll-to-roll coating. Here, the thickness of the obtained PS discs was measured, as shown in Fig. 3-14.

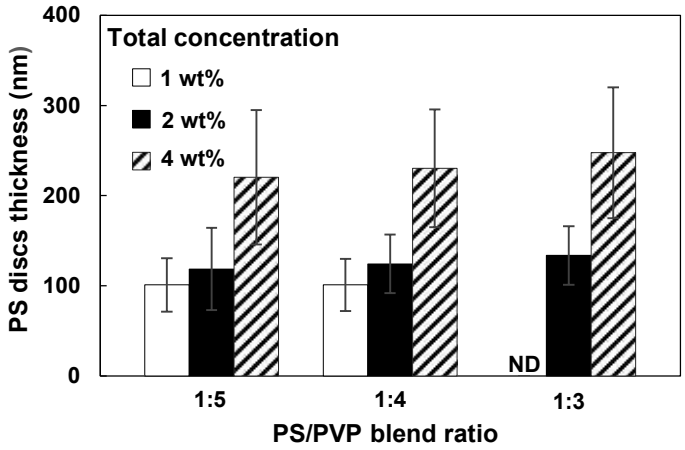

Fig. 3-14 Thickness of PS discs at each PS/PVP blend ratio when varying the total concentration from 1 wt% to 4 wt% (permitted reuse reproduction for doctor thesis from the publisher, cited and partially modified from ref. 14).

At the total polymer concentration of 1 wt%, the average thickness of PS discs at both blend ratios of 1:4 and 1:5 is about the same at around 100 nm. This number slightly increases with the increasing of the total concentration from 1 wt% to 2 wt% to be ~120 nm at all blend ratios. Then, it increases significantly up to ~230 nm at the total concentration of 4 wt% for all blend ratios. According to these results, it can be assumed that the blend ratio has minor influence on the thickness of PS discs, which is strongly dependent on the total polymer concentration which is related to the viscosity of the coating solution. This corresponds well with the result of the film thickness which varies by the feed solution viscosity. It was demonstrated that increasing viscosity of the feed solution can improve the emptying behavior (the ability to transferred fluid out of gravure roller cells onto the coating substrate). Hence, the thickness of coating film increases with the increasing of viscosity [5-7].

Therefore, it could be reasonably concluded that the growing of PS discs effects by increasing the total concentration and the fraction of minor component. Also, the effect of the blend ratio on the average diameter is stronger than that of the total concentration, while the thickness of the PS discs is

mainly controlled by the total concentration. Accordingly, this method shows potential to fabricate sub-micron scale discs, whose size can be controlled by varying the fabrication conditions.

Aspect ratio of PS discs

The shape of micro/nano-discs can be described by their aspect ratio, i.e., the ratio between the diameter and the thickness of a particle. Here, Fig. 3-15 shows the illustrations of PS discs from all the fabrication conditions with their calculated aspect ratio, using the actual average diameter and thickness.

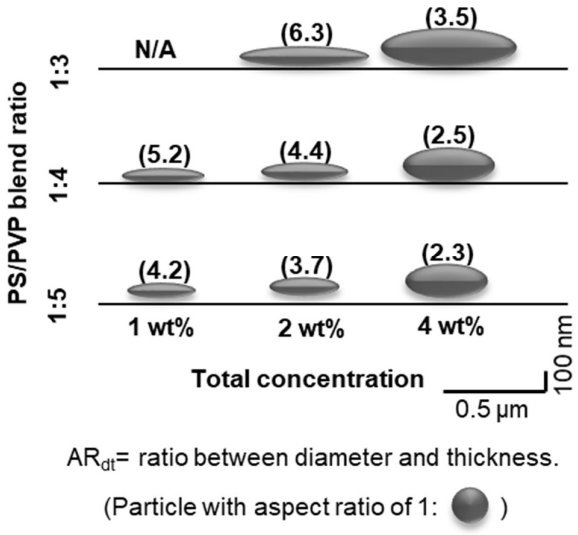

Fig. 3-15 Illustrations of PS discs at each PS/PVP blend ratio obtained by varying the total concentration from 1 wt% to 4 wt%. The aspect ratio is shown in parentheses (permitted reuse reproduction for doctor thesis from the publisher, cited and partially modified from ref. 14).

For the effect of blend ratio, the lowest AR_{dt} were obtained at the blend ratio of 1:5 at all total concentrations. The changing of blend ratio from 1:5 to 1:3 leads to an increase of both disc diameter and thickness. However, the increase of diameter is faster than that of thickness, which is reflected an increase in AR_{dt}. For the effect of total concentration, AR_{dt} were 5.2 and 4.2 at different blend ratios and a total concentration of 1 wt%. This number decreased with an increase of total concentration to 2 wt% to be 4.4 and 3.7. At the total concentration of 2 wt%, AR_{dt} was the highest at about 6.3 for a blend ratio of 1:3 as mentioned previously and can be clearly seen in the Fig. 3-12a top-view and Fig. 3-12c cross-sectional view, respectively. The decreasing of AR_{dt} at all blend ratios were observed when the

total concentration increases from 2 wt% to 4 wt% to be 3.5, 2.5 and 2.3 at blend ratios of 1:3, 1:4 and 1:5, respectively. We concluded that increasing the total polymer concentration leads to an increase of both disc diameter and thickness, but the increase in thickness is faster than that in diameter resulting in lower AR_{dt}.

Versatility of the process with other polymers

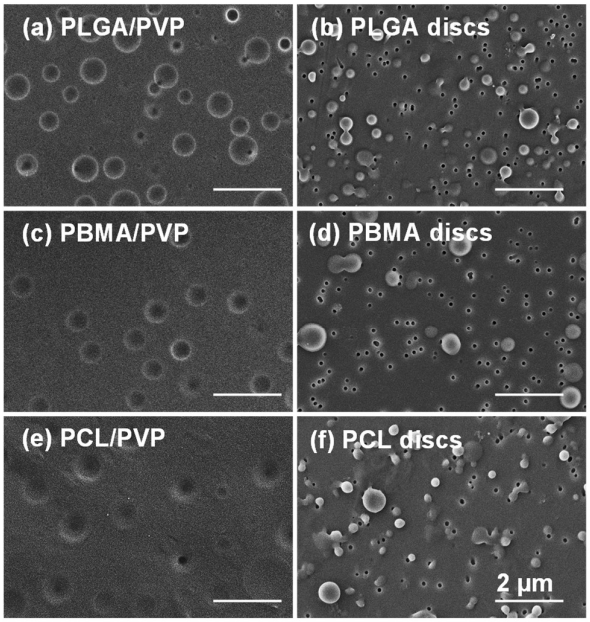

Fig. 3-16 SEM images of phase separation of PLGA, PBMA and PCL with PVP (a, c and e) and PLGA, PBMA and PCL discs (b, d and f) with a blend ratio of 1:4 at a total concentration of 4 wt%. All images share the same scale bar of 2 μm as shown in Fig. 3-16f (permitted reuse reproduction for doctor thesis from the publisher, cited and partially modified from ref. 14).

Since this proposed method employs polymer phase separation as a self-assembly process to fabricate polymer micro/nano-discs, it is expected that any other polymer blends which have apparent phase separation morphology could be applied to this method. Therefore, polymer mixtures of PLGA, PBMA and PCL with PVP at a total concentration of 4 wt% and blend ratio of 1:4 were prepared and studied to test this assumption. As can be seen in Fig. 3-16, similar to the case of PS/PVP, PLGA, PBMA, and PCL also provided apparent phase separation morphology as the minor component among the PVP matrix. Most of these polymer domains were circular in shape and dispersed homogenously

throughout the film. We were able to obtain PLGA, PBMA, and PCL discs by the same process used for the collection of PS discs, and they could be observed on a filter membrane.

3-5 Summary

With the combination of polymer blend phase separation and a roll-to-roll coating process, a new method to fabricate large amounts of polymer micro/nano-discs in a one-pot manner. By this method, the limitation of discontinuous fabrication as well as the complicated collection process required in conventional methods can be transcended. PS/PVP blend coated on a PVA substrate film was performed as a case study. PS discs could be collected by repeatedly washing with water in a one-pot manner since both major component (PVP) and coating substrate can be easily dissolved in water. The PS particles obtained were confirmed to be disc-like in shape with an average diameter varying from ~400 nm to ~800 nm while the thickness varied in the range from ~100 nm to ~250 nm. The size and aspect ratio of the obtained discs can be adjusted in a controlled manner by adjusting the fabrication conditions, such as the blend ratio and the total polymer concentration. By decreasing the total concentration with increasing the fraction of the minor component in the polymer blend, particles with a more disc-like shape (higher aspect ratio) could be achieved. However, decreasing of the total concentration combined with a higher fraction of the minor component may cause the occurrence of a bicontinuous phase morphology. We also succeeded to fabricate micro/nano-discs with other polymers, such as PLGA, PBMA and PCL, to demonstrate the universality of this method.

Since PVA substrate film used for the roll-to-roll coating in this study has a good extensibility and heat resistance, there is a high potential to combine this method with a stretching method for fabrication of polymer particles with further peculiar shapes. Although this work is still at an early stage, we anticipate the development of a large-scale, continuous fabrication method for polymer micro/nano-discs which would be of practical value in a wide range of applications such as drug delivery, medical imaging, surface coatings, etc.

References

[1] J. Park, K. Shin, C. Lee, Roll-to-roll coating technology and its applications: a review, Int J Precis Eng Man 17 (2016) 1–14.

[2] R. Abbel, Y. Galagan, P. Groen, Roll-to-roll fabrication of solution processed electronics, Adv. Eng. Mater 20 (2018) 1701190.

[3] D. Vak, H. Weerasinghe, J. Ramamurthy, J. Subbiah, M. Brown, D. J. Jones, Reverse gravure coating for roll-to-roll production of organic photovoltaics, Sol. Energy Mater Sol. 149 (2016) 154–161.

[4] S. J. Weinstein, K. J. Ruschak, Dip coating on a planar non-vertical substrate in the limit of negligible surface tension, Chem. Eng. Sci. 56 (2001) 4957–4969.

[5] N. Kapur, R. Hewson, P. A. Sleigh, J. L. Summers, H. M. Thompson, S. J. Abbott, A Review of gravure coating systems. Convertech & e-Print 5 (2012) 56–60.

[6] G. L. Booth, Coating Equipment and Processes Lockwood, Publishing Company: NY, 1970.

[7] H. Benkreira, O. Cohu, Direct forward gravure coating on unsupported web, Chem. Eng. Sci 53 (1998) 1223–1231.

[8] R. Søndergaard, M. Hösel, D. Angmo, T. T. L.-Olsen, F. C. Krebs, Roll-to-roll fabrication of polymer solar cells, Mater. Today 15 (2012) 36–49.

[9] I. C. Henderson, N. Clarke, Two-step phase separation in polymer blends, Macromolecules 37 (2004) 1952–1959.

[10] K. F. Chasib, B. M. Kadhim, Prediction of the behavior for polymer blends using thermodynamic model, Recent Adv Petrochem Sci 6 (2018) 555699.

[11] M. Geoghegan, G. Krausch, Wetting at polymer surfaces and interfaces, Prog. Polym. Sci. 28 (2003) 261–302.

[12] X. Sun, H. Li, S. Yan, I. Lieberwirth, Pattern formation and morphology in the course of drying a droplet of a ternary polymer solution, J. Appl. Polym. Sci 129 (2013) 1784–1792.

[13] H. Zhang, S. Takeoka, Morphological evolution within spin-cast ultrathin polymer blend films clarified by a freestanding method, Macromolecules 45 (2012) 4315–4321.

[14] W. Tuntanatewin, K. Tani, K. Ishikura, H. Zhang, Y. Okamura, One-pot fabrication of polymer micro/nano-discs via phase separation and a roll-to-roll coating process, Colloids Surf. A 586 (2020) 124274.

[15] S. A. Mauger, K. C. Neyerlin, A. C. Yang-Neyerlin, K. L. More, M. Ulsh, Gravure coating for roll-to-roll manufacturing of proton-exchange-membrane fuel cell catalyst layers, 165, J. Electrochem. Soc (2018) 1012–1018.

[16] N. Kapur, A parametric study of direct gravure coating, Chem. Eng. Sci 58 (2003) 2875–2882.

[17] S. Walheim, M. Böltau, J. Mlynek, G. Krausch, U. Steiner, Structure formation via polymer demixing in spin-cast films, Macromolecules 30 (1997) 4995–5003.

[18] L. Xue, J. Zhang, Y. Han, Phase separation induced ordered patterns in thin polymer blend films, Prog. Polym. Sci. 37 (2012) 564–594.

[19] R. Foudazi, S. Qavi, I. Masalova, A. Y. Malkin, Physical chemistry of highly concentrated emulsions, Adv. Colloid Interface Sci 220 (2015) 78–91.

[20] J.A. Champion, Y.K. Katare, S. Mitragotri, Making polymeric micro- and nanoparticles of complex shapes, Proc. Natl. Acad. Sci. U.S.A. 104 (2007) 11901–11904.

[21] C.J. Hernandez, T.G. Mason, Colloidal alphabet soup: monodisperse dispersions of shape-designed lithoparticles, J. Phys. Chem. C 111 (2007) 4477–4480.

[22] J.S. Gutmann, P. Müller-Buschbaum, M. Stamm, Complex pattern formation by phase separation of polymer blends in thin films, Faraday Discuss. 112 (1999) 285–297.

Chapter 4
Elongated polymer micro/nano discs and their surface adhesiveness

4-1 Background

As mentioned previously, polymer micro/nano particles tend to form to be sphere to obtain the minimum surface energy and, and thus sphere is considered as the simplest shape of particle to be fabricated. However, non-spherical polymer particles have been focused in these past several years driven by their unique and fascinating properties, even though the fabrication methods are more complicated (1-9). A group of non-spherical particles such as rod or ellipsoid theoretically have a larger contact surface area than spherical particles. Among them, disc micro/nano particles with high aspect ratio (the ratio between the major and minor axis of particle domain) are expected to provide outstanding adhesion efficiency since this geometry with one flat surface allows the particles to be close-fitting to the surface of the target sites (10). The adhesion efficiency is one of the most essential properties especially of polymer particles in drug delivery application. For example, to execute its diagnostic or therapeutic mission efficiently, the polymer particles have to firmly adhere to the surface of the target sites (*e.g.*, blood vessel wall or tumor) [(8)]. In addition, these high aspect ratio particles were less accessible to phagocyte by macrophages, specifically on their major axis, leading to a lower uptake by the liver and a longer circulation time in the blood [(11-13)]. These shape of particles, therefore, is expected to improve diagnostic sensitivity, therapeutic ability and enhance the efficiency in the field of injectable carriers in the drug delivery system. A variety of methods have been developed to fabricate high aspect ratio of non-spherical particles such as stretching polymer spheres embedded in PVA cast film [(14)], using the simple oil-in-water emulsion solvent evaporation technique [(15)], coating of silica on hematite spindle cores [(16)], utilizing imprint lithographic techniques called PRINT [(17)], using a sol-gel approach with a surfactant/co-structure direct agent (CSDA) mixture as a template [(18)], electrospinning of swollen nanoparticles [(19)], and using microfluidic device [(20)].

Stretching of polymer spheres embedded in a film matrix is one of the well-known methods because of their simplicity. However, drying of film casting which required long time causing difficulty to implement this process in a large scale [(14, 21)]. Some methods such as PRINT process were reported to be able to precisely fabricate the specific shape of particles including high aspect ratio of non-spherical particles. However, it is still expensive to set up the process and required a skilled worker to

operate which is unlikely to be an alternative method for large scale production [17, 20]. As mentioned in the last chapter, we have proposed the one-pot method to fabricate discs in a continuous manner by utilizing the roll-to-roll machine with polymer phase separation [22]. PVA film using as a coating substrate has excellent extendibility with a good heat resistance. Therefore, there is a high likelihood of combining roll-to-roll with polymer phase separation method with a film stretching to fabricate of polymer particles with further peculiar shapes.

4-2 Purpose

In this chapter, we propose a facile method to fabricate elongated micro/nano discs with larger contact surface area to target surfaces, based on our previously proposed method combining with PVA film stretching. The polymer mixture of biodegradable PLGA and PVP was used as a model as a minor and major component, respectively. Phase separation induced by the solvent evaporation during the roll-to-roll coating process created PLGA domains on PVA film. Then, PLGA domains formed on PVA film were stretched by a customized uniaxial stretcher. The effect of stretching temperature and percentage of film elongation on the shape of PLGA particles were studied. Finally, the surface adhesiveness of elongated PLGA discs was compared with three distinct shapes, namely control discs, spheres and elongated spheres by water-dropping test.

4-3 Material and methods

4-3-1 Materials

PLGA (L/G: 50:50; IV: 0.6 dL/g, M_w: 35,000; Polysciences, PA, USA) was used as a minor component for roll-to-roll coating and for fabrication spheres via SPG membrane emulsification, which is one of the well-known techniques to fabricate uniform spheres [23, 24]. PVP (M_w: 40,000; Sigma-Aldrich, MO, USA) was used as a major component for roll-to-roll coating by having chloroform (FUJIFILM Wako Pure Chemical Corporation, Osaka, Japan) as a cosolvent. All chemicals were used without further purification. PVA film (S-type, commercial called Hi-Selon) was used as the roll-to-roll coating substrate, purchased from Nippon Gohsei, Tokyo, Japan. This film can be completely

dissolved in water even at a low temperature and resist to most of organic solvents and chemicals. The width of the PVA film is 20 cm with the film thickness of ~60 μm. For fabrication of elongated spherical particles, PVA cast film were made from PVA (M_w: 30,000–70,000; Sigma-Aldrich), added with glycerol (FUJIFILM Wako Pure Chemical Corporation) as a plasticizer. PLL (Peptide Institute, Osaka, Japan) was coated glass substrate for PLGA particle morphology study, while a green fluorescence dye 3,3'-Dioctadecyloxacarbocyanine Perchlorate (DiOC18) (M_w: 881.72; Thermo Fisher Scientific, MA, USA) was used as a tracer in surface adhesiveness study.

4-3-2 Experimental design and data analysis

The optimal condition to fabricate elongated micro/nano discs with larger contact surface area was achieved by evaluation the effect of percent elongation and stretching temperature on the morphology of PLGA domains of PLGA/PVP on PVA film were examined. The length of major axis (x) and minor axis (y) as well as the aspect ratio (the ratio between the length of major and minor axis, x/y) were determined by image analysis using ImageJ software (NIH), from three samples which were individually prepared ($N = 3$, and at least 40 domains were chosen per each measurement). Values were given as mean ± standard deviation (SD).

Then, the optimal condition was used to fabricate the elongated discs. The morphology of elongated disc after collection process was determined. Similar to the PLGA domains, the length of major axis and minor axis, the aspect ratio, and the thickness of PLGA elongated discs were obtained from three samples which were individually prepared ($N = 3$, and at least 40 discs were chosen per each measurement). Values were given as mean ± SD. Finally, the surface adhesiveness of PLGA elongated discs was examined, comparing with discs before stretching, spheres and elongated spheres by using the water-dropping test. The particle remaining percentage after water-dropping was used as a parameter to compare the adhesiveness property of each particle shape. Values were obtained from three individually prepared samples ($N = 3$) and given as mean ± SD.

The fabrication methods of each particle shape, the determination methods of PLGA domains and particle morphology and the evaluation method of adhesiveness by water-dropping test will be discussed more in details in the next section.

4-3-3 Methods

Fabrication of PLGA discs via phase separation and roll-to-roll coating process

The process of coating a polymer mixture on a PVA film to fabricate PLGA domains was similar to method mentioned in Chapter 3 as shown in Fig. 4-1a. In summary, solutions of a mixture of PLGA and PVP as a minor and major component, respectively, were prepared in chloroform at the blend ratio of 1:4 (w/w) with the total polymer concentration at 4 wt%. The mixture solution was stirred overnight to obtain complete dissolution and was then coated on a PVA film using a roll-to-roll coating machine (reverse gravure coating, μCoater 350, Yasui Seiki, Kanagawa, Japan). The film line speed (also called web speed) was set at 1.0 m/min with micro gravure roll speed at 16 rpm, and a furnace temperature of 60°C. All of these preparation processes were conducted at room temperature (25°C) and normal humidity in a clean environment. Coated PVA film samples were cut into five 4×4 cm^2 pieces, put in 40 mL of distilled water and kept overnight. The dissolved solutions were then centrifuged five times at 21,500*g*, 4°C, for 15 min (Himac CT15RE, Hitachi, Tokyo, Japan).

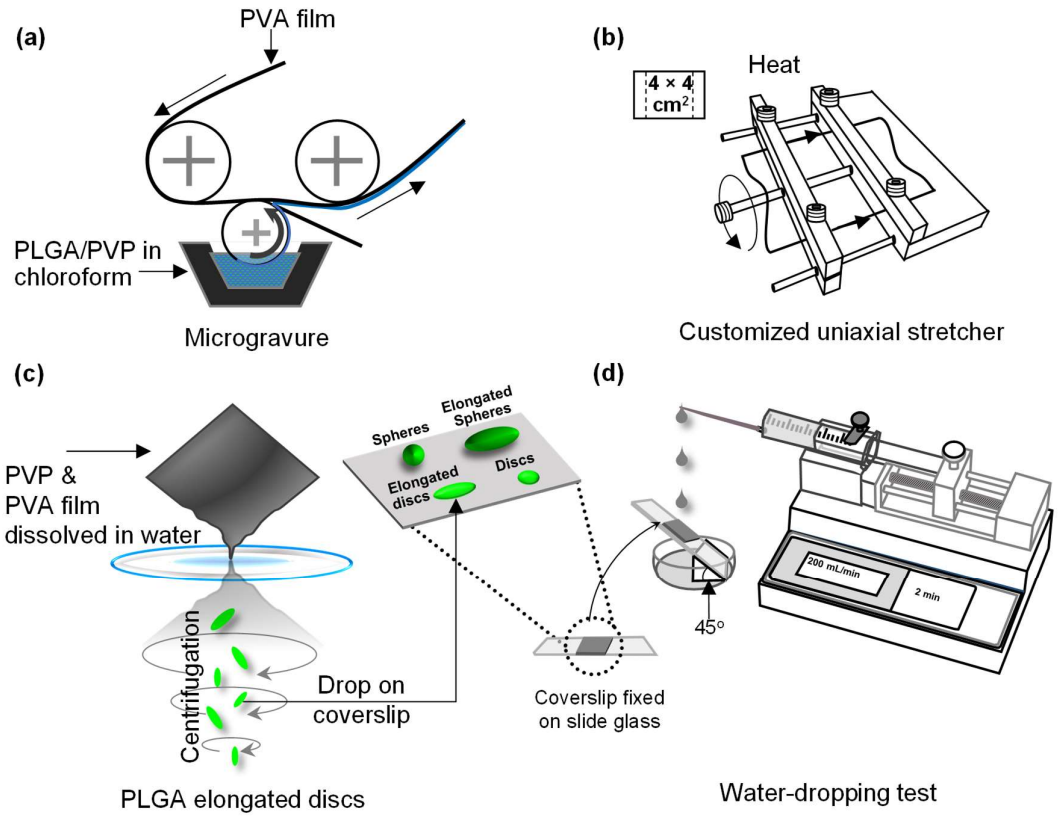

Fig. 4-1 Schematic diagram of a facile method to fabricate elongated discs and their adhesiveness evaluation. (a) continuous coating process via roll-to-roll coating machine; (b) film stretching method by customized uniaxial stretcher; (c) one-pot collection process; and (d) water-dropping test for adhesiveness evaluation (permitted reuse reproduction for doctor thesis from the publisher, cited and partially modified from ref. 25).

Fabrication of PLGA spheres by SPG emulsification method

Schematic diagram of the SPG emulsification method is shown in Fig. 4-2. The disperse phase was a solution of PLGA in chloroform at the concentration of 10 mg/mL for 10 mL, while a solution of PVA in water at the concentration of 10 mg/mL for 190 mL was a continuous phase. Disperse phase was pressed by nitrogen gas (N_2) at 40 kPa through the SPG membrane with the pores of 1 μm. The droplets formed into the continuous phase which is stirred by magnetic stirred at 400 rpm. PLGA

spheres were then obtained by water washing/centrifugation for three times at 2,380*g*, 4°C, for 10 min (LX-120, TOMY, Tokyo, Japan).

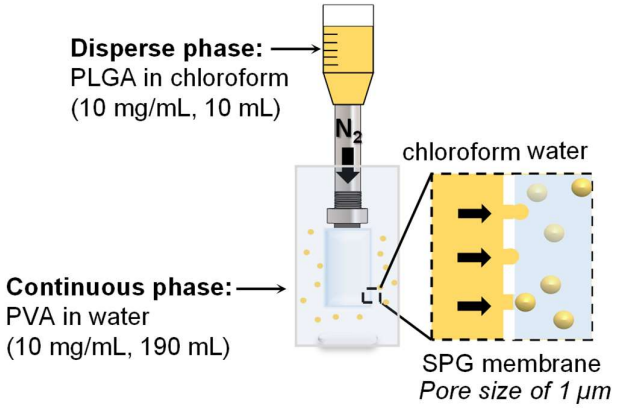

Fig. 4-2 Schematic diagram of SPG emulsification method for fabrication of PLGA spheres (permitted reuse reproduction for doctor thesis from the publisher, cited and partially modified from ref. 25).

Fabrication of PLGA elongated spheres and elongated discs

For elongated spheres, a previous reported of film stretching method was used by embedding PLGA spheres in PVA cast film [14, 21]. Initially, PVA solution at the concentration of 10% (w/v) was prepared at 85°C. Glycerol was added into this PVA solution to obtain the final concentration of 2% (w/v) for plasticizing and reducing the glass transition temperature (T_g) of the film. 1 mL of PLGA spheres at the concentration of ~10^9 particles/mL were added to 15 mL of this mixture. This mixture was casted and dried on 12 × 12 cm^2 flat surface to thicknesses of ~70 μm overnight.

The same film stretching method was used for fabrication of both PLGA elongated spheres and elongated discs. Embedded PVA cast film for elongated spheres and coated PVA film for elongated discs were typically cut into pieces of 4 cm × 6 cm. For stretching, the film was mounted to the customized uniaxial stretcher at 1 cm from the edge of the longer side to obtain the stretching area of 4 × 4 cm^2 (Fig. 4-1b). The uniaxial stretcher comprised two aluminum blocks mounted on a screw. The elongation percentage can be adjusted by screwing which will turn separates the blocks (Fig. 4-3).

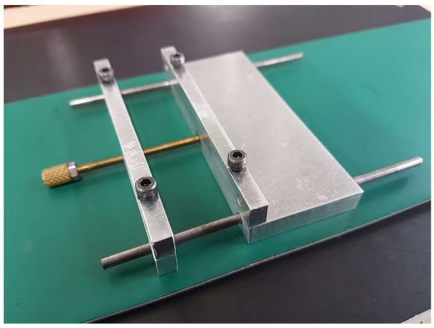

Fig. 4-3 The photo of the customized uniaxial stretcher (permitted reuse reproduction for doctor thesis from the publisher, cited and partially modified from ref. 25).

To study the effect of film stretching on PLGA domains, PVA film were stretched at 200%, 400% and 600% elongation, respectively, while embedded PVA cast film and coated PVA film fabricate were stretched at 600% elongation to fabricate elongated spheres and elongated discs for adhesiveness evaluation. All stretching processes were performed at a rate of 0.3–0.5 mm/s. In cases of heat-stretching, the film was conditioned in the oven (EO-600B ETTAS, Osaka, Japan) at a setting temperature for 5 min just before stretching. The samples were further kept in the oven for 1 min before cooling down at room temperature for 3 min. In the control case, the stretching tests were examined at room temperature (25°C) and normal humidity in a clean environment. The one-pot collection process using for PLGA discs mentioned in previous section was used to obtain the elongated spheres and elongated discs (Fig. 4-1c). After stretching, the mounting part of the film sample was cut off, put in 40 mL of distilled water, and kept overnight. The dissolved solutions were then centrifuged five times at 21,500*g*, 4°C, for 15 min.

Morphology of PLGA domains and particles

To investigate the phase separation morphology of PLGA/PVP on a PVA film and PLGA domains, the film samples were cut and observed by a field emission scanning electron microscope (FE-SEM, Hitachi S-4800, Hitachi, Tokyo, Japan) at an accelerating voltage of 3.0 kV. The length of major axis, minor axis, and the aspect ratio of PLGA domains were examined by FE-SEM image analysis. The repetition number of experiment and the method of data presentation were previously described.

To obtain the number of the PLGA particles obtained after collection, 1 mL of the centrifuged samples were counted under a microscope (20×, Eclipse TS100, Nikon Corporation, Tokyo, Japan) using a hemacytometer (SLGC A113, Sunleadglass, Saitama, Japan). Centrifuged samples were dropped on coverslips which were coated by PLL at the concentration of 0.1% (w/v) for 2 hr. Then, the samples were kept in refrigerator at 4ºC for 2 hr before washing by water, dried in a desiccator and observed by FE-SEM for investigation the morphology of PLGA particles on top-view. The sample was also investigated for side view. The samples were dropped on a 0.1 μm inorganic filter membrane (Whatman Anodisc, GE Healthcare Life Sciences, Maidstone, UK), dried in desiccator and examined by FE-SEM. All of the SEM samples were pre-treated by sputter-coating with platinum prior to investigation (4 mA, 60 s). The average of major and minor axis of PLGA particles after collection was obtained from the top view images and the thickness of the PLGA particles was from the side view images. The repetition number of experiment and the method of data presentation were previously described.

Adhesiveness evaluation by water-dropping test

DiOC18, green fluorescence using as a tracer, was added into the polymer mixture of PLGA/PVP for roll-to-roll and the disperse phase solution of PLGA for SPG emulsification at the final concentration of 0.1% (w/v), respectively, for evaluation the adhesiveness of each shape of the PLGA particles. These fluorescent-labelled discs and spheres were further used to fabricate fluorescent-labelled elongated discs and elongated spheres by using film stretching method as mentioned in previous section. PBS, important intracellular buffer (pH 7.4), was used to drop to the coverslip (18 × 18 mm^2) which was fixed on slide glass at a 45-degree angle to the floor. The flow rate was set at 50 mL/hr (low flow rate) and 200 mL/hr (high flow rate) by using syringe pump (SPS Syringe pump, AS ONE, Osaka, Japan). The distance from tip of the needle to the coverslip was set at about 8 cm for all the experiments (Fig. 4-1d). PLGA particles of 40 μL with the concentration of ~10^7 particles/mL were dropped on these coverslips and kept in refrigerator at 4ºC for 2 hr. The occupied areas by fluorescent-labelled particles on the coverslip before water-dropping were examined by fluorescence microscope (40×, Eclipse Ts2R-FL, Nikon Corporation) and measured by ImageJ software. The fluorescent

microscope stage was fixed to remain unchanged, and the occupied areas after water-dropping at the same position were re-examined. The particle remaining percentages after water-dropping were calculated from the comparison with occupied areas before water-dropping. The repetition number of experiment and the method of data presentation were previously described.

4-4 Results and discussion

4-4-1 Elongation of PLGA domains induced by film stretching

In the case of no stretching as shown in Fig. 4-4a, frozen structure of phase-separated PLGA domains from a PLGA/PVP blend on PVA film was look like island surrounded by the ocean. This were apparently observed at total concentration of 4 wt% with blend ratio of 1:4 (w/w). A simple model of the phase separation mechanism proposed in our previous study can be used to explain the formation of this island-liked domains among the matrix. Briefly, the concentration fluctuation between two phases, which induces by the solvent evaporation during coating process, leads to the formation a bicontinuous morphology. The irregular shapes were initially formed and develop to be spherical domains in the PVP matrix in order to reduce surface energy during phase separation process [(22)]. The results showed that PLGA domains dispersed throughout the whole PVP matrix regardless of the location in both wide and length directions. As shown in Fig. 4-4b, the average length of major axis (x) of PLGA domains was 714 ± 109 nm without film stretching. The average AR_{xy} (ratio of the length of major and minor axis) of these PLGA domains was 1.00 ± 0.04 which represents circular in shape, namely the length of major and minor axis is the same ($x \approx y$).

By varying percentage of elongation, the average length of major axis (x) of PLGA domains was 699 ± 44 nm at 200% elongation with AR_{xy} of 1.00 ± 0.02. This was unchanged from the sample without stretching in both size and shape (a difference less than 3%). The average length of major axis (x) still remain about the same when the PVA films were further stretched, representing 625 ± 60 nm and 659 ± 64 nm at 400% and 600% elongation, respectively. Correspondingly, AR_{xy} of PLGA domains at 400% and 600% elongation was 1.01 ± 0.01 and 0.99 ± 0.00, respectively, showing circular in shape. From these results, it can be concluded that the shape and size of PLGA domains were not affected by PVA film stretching even up to 600% elongation at room temperature.

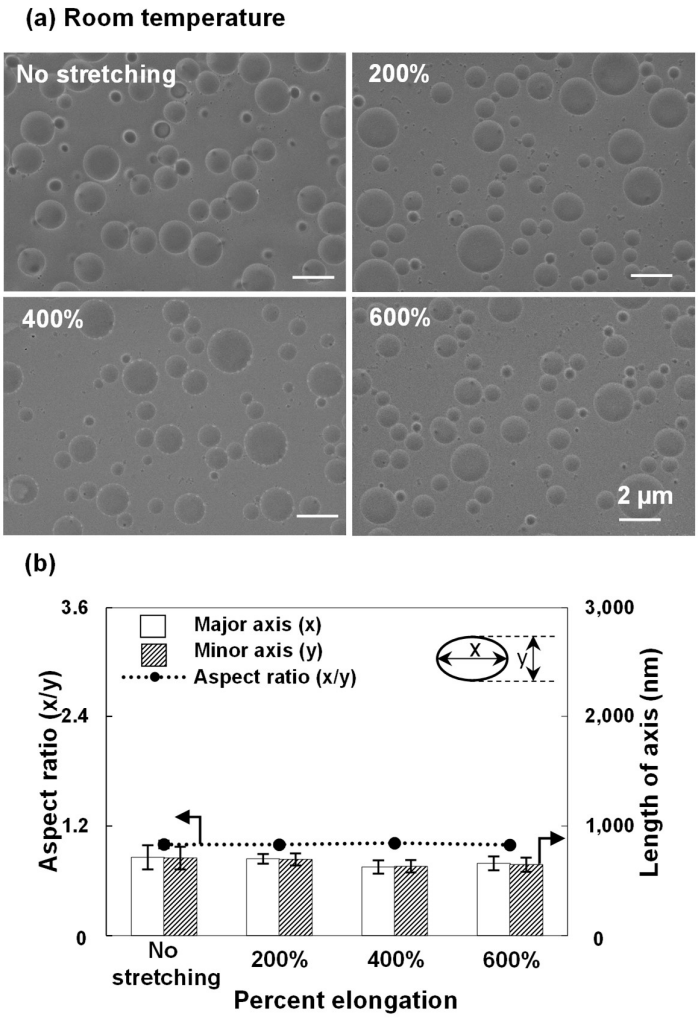

Fig. 4-4 At room temperature, (a) SEM images of PLGA domains stretched, and (b) the correlation between percent elongation and the length of major and minor axis as well as AR_{xy} (permitted reuse reproduction for doctor thesis from the publisher, cited and partially modified from ref. 25).

Correspondingly, AR_{xy} of PLGA domains at 400% and 600% elongation was about 1, showing circular in shape (1.01 ± 0.01 and 0.99 ± 0.00, respectively). From these results, it can be concluded that the shape and size of PLGA domains were not affected by PVA film stretching even up to 600% elongation at room temperature. This can be explained by the nature of PLGA and PVP at room temperature. Since T_g of PLGA and PVP were about 48°C [(26)] and 160°C [(27)], respectively, both minor and major components at room temperature are in frozen state where the polymers tend to be hard and brittle [(28)]. Therefore, it could be concluded that both minor and major components will not much affect

the shape of PLGA domains by stretching PVA film at room temperature since it is lower than T_g of as can be seen in Fig. 2b. These results agree well with the stretching of PVA cast film embedded by PS particles [22] and polymer blend thin film of dispersed PS domains in polyurethane (PU) matrix [29] at lower temperature than their T_g, where shape of PS particles and PS domains are remained unchanged after stretching. However, voids formation around domains during stretching which is one of the deformation mechanisms was not observed in the case of PLGA/PVP blend. This could be explained by the difference of micromechanical deformation process between rigid and soft filler. In the case of rigid filler such as PS, a stress builds up inside particles which leaded to the debonding at the filler and matrix interface. And the forming of voids, in the case of poor adhesion between filler and matrix, could be observed. Whereas, the particle cracking could be expected when the filler and matrix shows high adhesion [29-31]. On the other hand, the crazing in polymer matrix is expected to be the deformation mechanism when the minor component has less stiffness than the matrix. This explanation is supported by the enlarged SEM images showing the cracking of PS domains at 600% elongation at room temperature (see Fig. 4-5a and 4-5a′)., whereas there is no cracking in PLGA domains at the same elongation percentage (see Fig. 4-5b and 4-5b′) (permitted reuse reproduction for doctor thesis from the publisher, cited and partially modified from ref. 25).

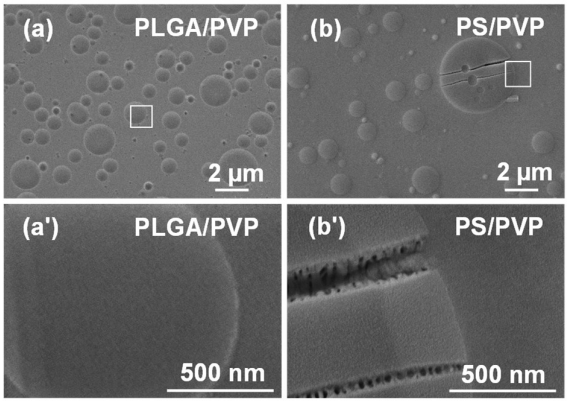

Fig. 4-5 Phase separation at room temperature with 600% elongation. (a) PLGA/PVP phase separation; (a') enlarged image of PLGA/PVP phase separation at the edge of PLGA domain; (b) PS/PVP phase separation; and (b') enlarged image of PS/PVP phase separation at the edge of PS domain at the same total concertation of 4 % and blend ratio 1:4 (w/w).

However, PLGA domains can be elongated by film stretching when samples were heated at 80 °C as can be seen in Fig. 4-6a. This temperature is considerably higher than T_g of PLGA, the PLGA domains were softened and AR_{xy} increased from 0.99 ± 0.04 with non-stretching to 1.13 ± 0.06 at 200% elongation. The shape of PLGA domains were prolonged in the stretching direction. The results showed that AR_{xy} of PLGA domains increased up to 1.37 ± 0.07 and 2.01 ± 0.06 at 400% and 600% elongation, respectively. As can be seen in Fig. 4-6b, the increasing of AR_{xy} was from the increasing of major axis length (x) aligned with the stretching direction; from non-stretching at 708 ± 80 nm to 1,397 ± 219 nm at 600% elongation, while the minor axis length (y) remained about unchanged around 700 nm.

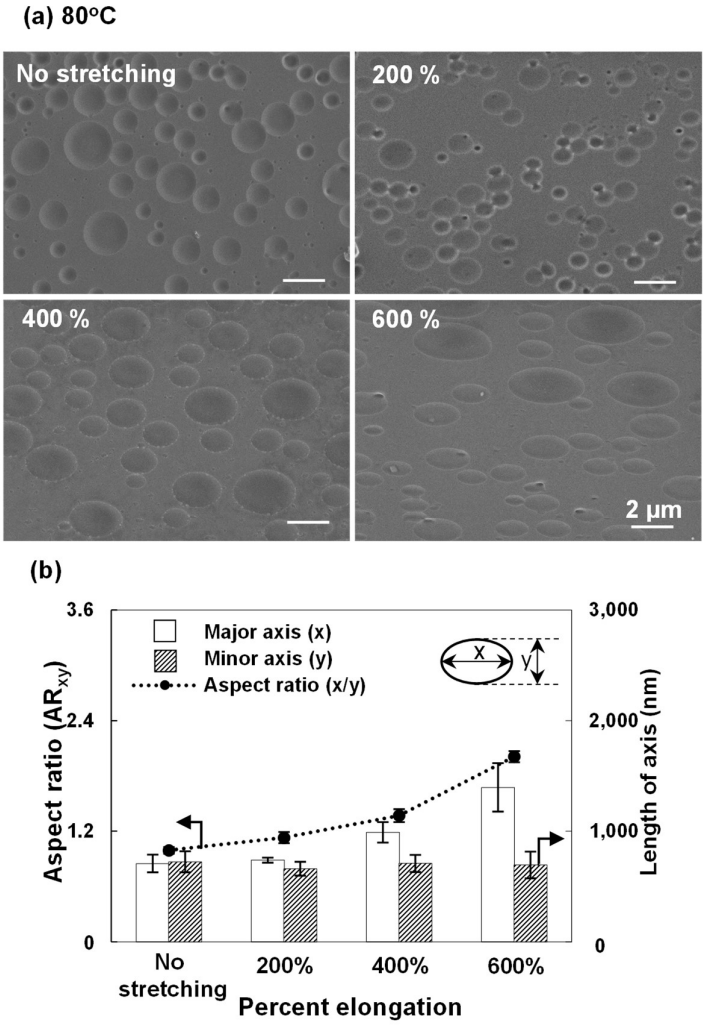

Fig. 4-6 At 80°C, (a) SEM images of PLGA domains stretched, and (b) the correlation between percent elongation and the length of major and minor axis as well as AR_{xy} (permitted reuse reproduction for doctor thesis from the publisher, cited and partially modified from ref. 25).

Furthermore, the effect of film stretching at 600% elongation on PLGA domain shape changing was studied by varying stretching temperature. As can be expected, softened PLGA domains by the increasing of temperature were observed according to the fact that the rigidness of a polymer decreases as the temperature increases. As can be seen in Fig.4-7a, the elongation of PLGA domains showed when film samples were stretched at a higher temperature. At 60°C, AR_{xy} of PLGA domains was 1.43 ± 0.03. This aspect ratio can increase up to 1.88 ± 0.02 and 2.01 ± 0.06 when film samples were stretched at 70°C and 80°C, respectively. The highest AR_{xy} of PLGA domains at 2.95 ± 0.09 was achieved when the temperature increased up to 90°C.

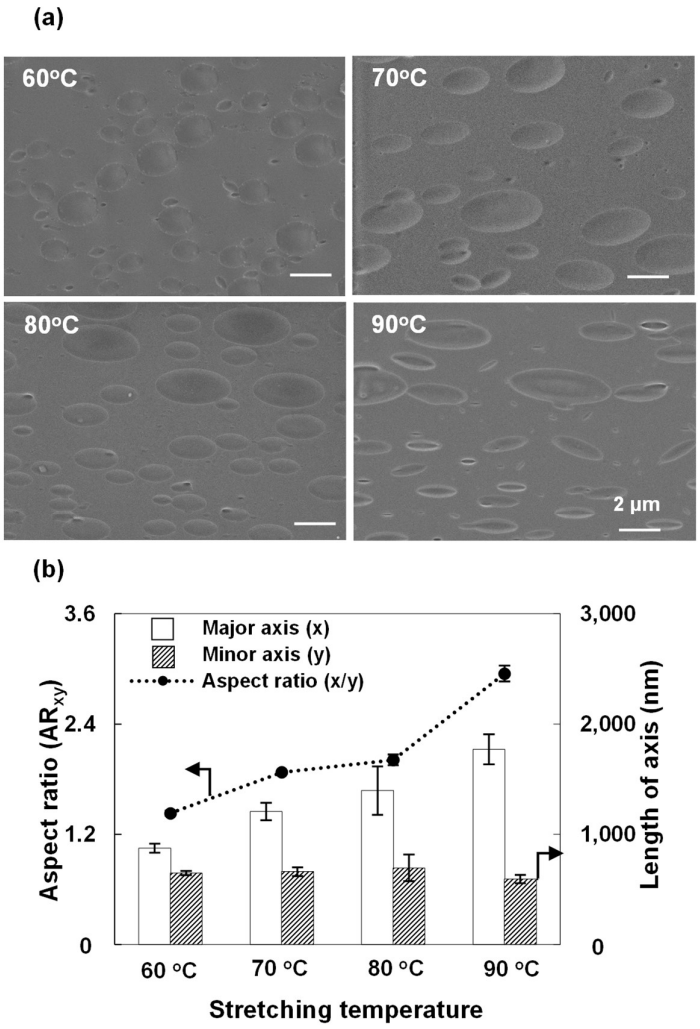

Fig. 4-7 (a) SEM images of PLGA domains at 600% elongation by varying stretching temperature at 60°C, 70°C, 80°C, and 90°C, respectively; and (b) the correlation between stretching temperature and the length of major and minor axis as well as AR_{xy} (permitted reuse reproduction for doctor thesis from the publisher, cited and partially modified from ref. 25).

Preliminary, it could be summarized that AR_{xy} of elongated discs can be controlled by the temperature. All of PLGA domains was elongated in the stretching direction showing ellipse domains in shape. Similar to the results mentioned in previous section, the increasing of AR_{xy} of PLGA domains when the increasing of temperature was mainly from the increasing of major axis length which aligned with the stretching direction (Fig. 4-7b). The major axis increased from ~660 nm of non-stretching at room temperature to ~1,800 nm with 600% elongation at 90°C, while the minor axis length was remained around 650 nm at all the temperatures.

4-4-2 PLGA elongated discs after collection process and other shapes of PLGA particles

Both of PVP matrix domain and PVA film, which are water soluble were removed after the centrifugation process to obtain PLGA elongated discs. Since there are no organic solvents consumed in this collection process, it is considered as an environmentally friendly. The number of elongated discs directly associated with the area of coated PVA film samples. With 5 pieces of 4×4 cm^2 substrates (original area before stretching), the concentration of the PLGA elongated discs from collection process at 80°C with 600% elongation in a final volume of 1 mL was ~10^8 particles. This concentration was about the same with the non-stretching sample as a control PLGA discs. This implies that the stretching process did not cause the losing of PLGA particles at this condition. In contrast, the concentration of the PLGA elongated discs at 90°C was only about ~10^3 particles/mL, which is obviously lower than the concentration of the control PLGA discs.

PLGA discs and elongated discs after the collection process are shown in Fig. 4-8a and 4-8a', as well as Fig. 4-8b and 4-8b' for top view and side view, respectively. The average diameter of discs before stretching was 681 ± 113 nm with AR_{xy} about 1, representing the circle in shape. Both axis lengths (*x* and *y*) are almost the same with PLGA domains before the collection of non-stretching films. For PLGA elongated discs after the collection process, the average length of major and minor axis was 1,396 ± 86 nm and 609 ± 56 nm, respectively, which equals to AR_{xy} of 2.3 ± 0.1. The length of the major and minor axis of these discs are in the same range as the length of elongated PLGA domains prior to collection. The thickness of elongated discs decreased from the thickness of non-stretching discs (from 102 ± 27 nm to 148 ± 33 nm). This decrease effected by the decreasing of cross-sectional

area of the coated PVA film during stretching process known as Poisson effect [32]. In addition, it should be noted here that both discs and elongated discs have a flat surface on one side. These could be the great advantage enhancing the ability to adhere to the surface of the target sites when using as drug carrier since the particles have more contact surface area. For comparison, two additional distinct shapes of particles namely PLGA spheres (Fig. 4-8c and 4-8c' for top view and side view) and elongated PLGA spheres by embedded film stretching process (Fig. 4-8d and 4-8d' for top view and side view) were fabricated.

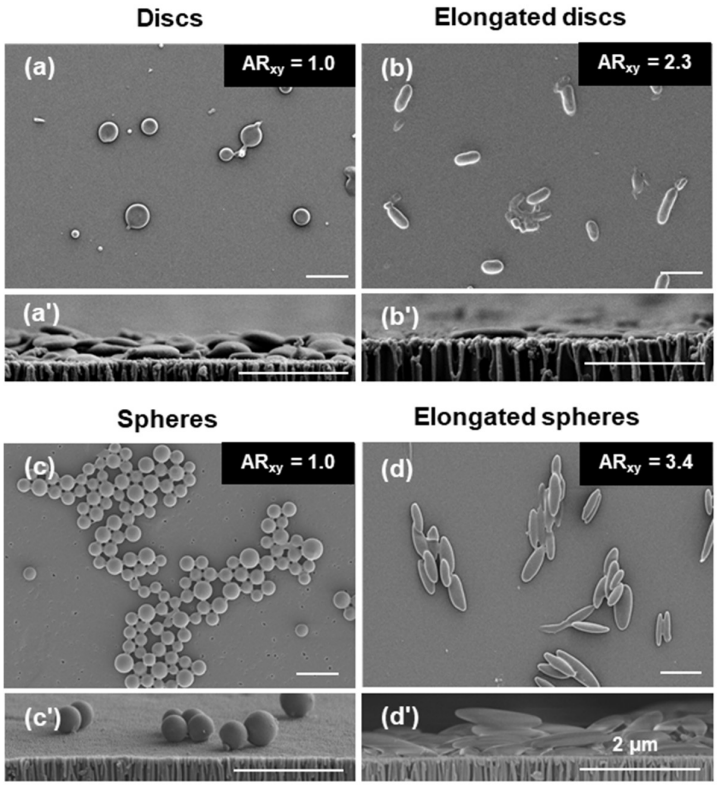

Fig. 4-8 PLGA particles after collection process. (a–d) top view images and (a'–d') side view images of discs, elongated discs, spheres and elongated spheres, respectively (permitted reuse reproduction for doctor thesis from the publisher, cited and partially modified from ref. 25).

PLGA spheres represent the general shape of polymer micro/nano particles, while elongated spheres represent elongated particles with high AR_{xy}. The average diameter of PLGA spheres was 929 ± 148 nm. The average length of major and minor axis of elongated spheres was 2,402 ± 590 nm and 708 ± 134 nm, respectively (see Table 4-1).

Table 4-1. Size and shape of each PLGA particles with surface area and estimated contact surface area.

Parameter	Unit	Discs	Elongated discs	Spherical	Elongated spherical
Major axis (x)	nm	681	1,396	929	2,402
Minor axis (y)	nm	-	609	-	708
Thickness (t)	nm	148	104	934	397
Surface area	nm^2	1.05×10^6	1.66×10^6	2.71×10^6	1.25×10^7
Estimated contact surface area	nm^2	3.64×10^5	6.68×10^5	N.A.*	1.31×10^5**

* The contact surface between spheres and the plate is practically a point by assuming the particle to be perfect rigid sphere [33].

** Assumed elongated spheres to be perfect ellipsoid in shape. The 2D of elongated spheres was plotted by using ellipse equation to estimate the length of contact surface area. Assumed the particle to be perfect rigid and contact surface area is referred to the area on the particle surface in a close distance of $h_o \sim 10$ nm from the substate [9].

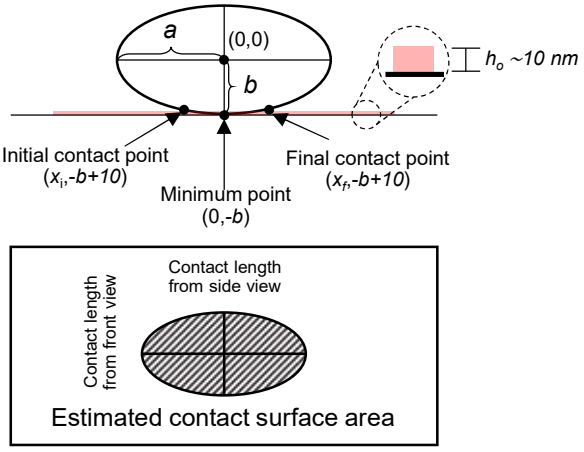

Fig. 4-9 Illustrations figure showing the calculation of estimated contact surface area of elongated discs (permitted reuse reproduction for doctor thesis from the publisher, cited and partially modified from ref. 25).

Both spheres and elongated spheres have larger total surface area than elongated discs about ~1.6 times and ~7.5 times, respectively. However, the estimated contact surface areas of spheres (ball-like shape) and elongate spheres (rugby ball-like shape) are very limited since there is no flat surface area as can be found in discs and elongated discs (see Fig. 4-9). The adhesiveness comparison of these

four distinct shapes of PLGA particles namely discs, elongated discs, spheres and elongated spheres will be discussed in the next section.

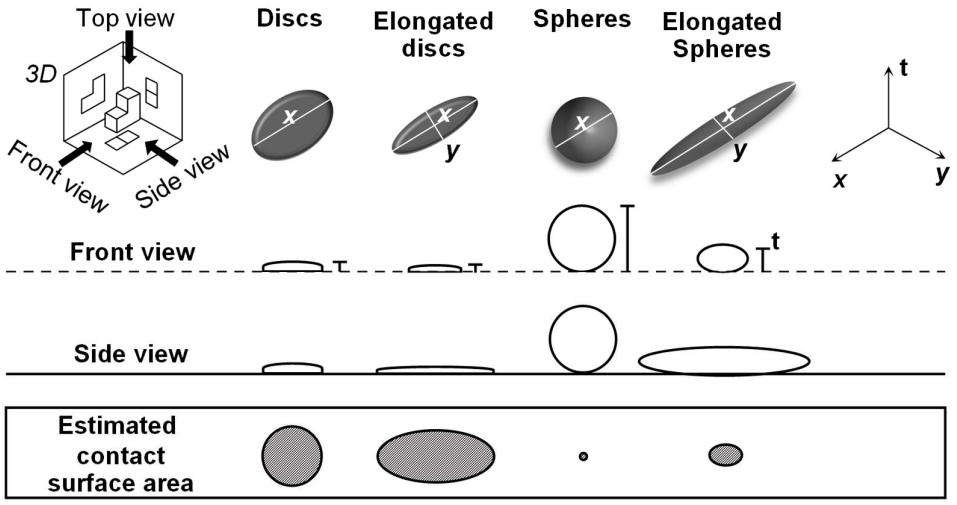

Fig. 4-10 Illustrations 3D figures of PLGA particles in different shapes with estimated surface area (permitted reuse reproduction for doctor thesis from the publisher, cited and partially modified from ref. 25).

4-4-3 Surface adhesiveness of PLGA elongated discs by water-dropping test

The adhesiveness of PLGA particles in different shapes was evaluated by water-dropping test, using coverslips as the model surface of the target sites. All of PLGA particles labelled with a green fluorescence dye (DiOC18), were dropped on a coverslip and attached on the substrate by physically adsorption. Under fluorescent microscope, all of PLGA particles in different shapes attached thoroughly on the coverslips before the dropping test (see Fig. 4-11a, b, c and, d for 50 mL/hr and a‴, b‴, c‴ and, d‴ for 200 mL/hr). The occupied areas by PLGA particles on coverslips were measured by ImageJ software and the remaining percentage of particles after the water-dropping was calculated from the occupied area before the dropping test at the same position. Assuming PLGA particles are applied as a drug carrier into the body, physiological PBS buffer [34] were used to represent the force to detach particles from coverslips in this water-dropping.

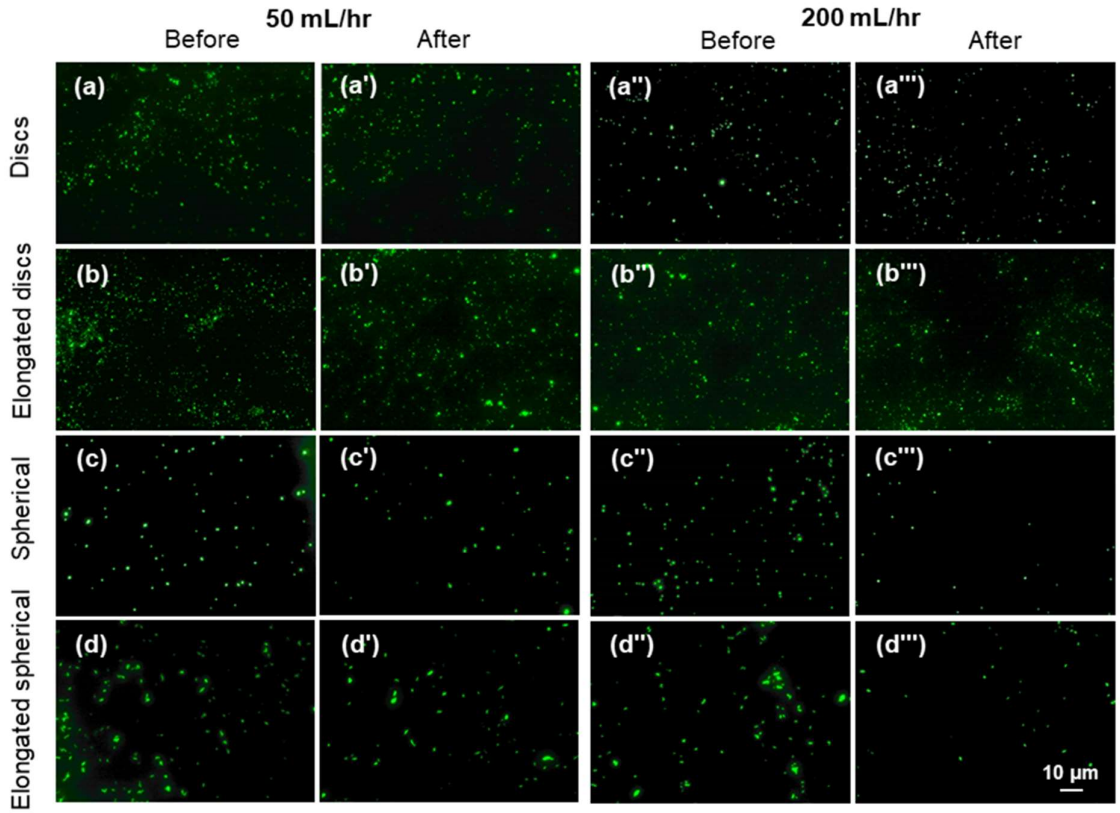

Fig. 4-11 Fluorescent microscopic images at the same position before (a, b, c and, d) and after (a′, b′, c′ and, d′) water-dropping test at 50 mL/hr and at 200 mL/hr before (a″, b″, c″ and, d″) and after water-dropping test (a‴, b‴, c‴ and, d‴) of discs, elongated discs, spheres, and elongated spheres, respectively (permitted reuse reproduction for doctor thesis from the publisher, cited and partially modified from ref. 25).

After water-dropping, it is obviously seen that a certain number of particles were detached from the substrates at both dropping flow rates. The remaining percentage of PLGA particles in different shapes based on the occupied areas of particles after water-dropping were shown in Fig. 4-12. At low flow rate (50 mL/hr), elongated disc particles showed the highest remaining percentage representing about 70.1 ± 6.0%, while the disc particles showed about 45.5 ± 2.3% after water-dropping. The remaining percentage of other two shapes namely spheres and elongated spheres were 19.3 ± 5.9% and 31.5 ± 3.0%, respectively. The same trend was repeatedly observed at a high flow rate (200 mL/hr). The elongated disc particle represents the highest remaining percentage at 50.7 ± 1.3% followed by disc

particles at 35.4 ± 3.3%, while spherical and elongated spherical particles are still the two which have the lowest the remaining percentage at 8.1 ± 2.6% and 23.0 ± 6.1%, respectively.

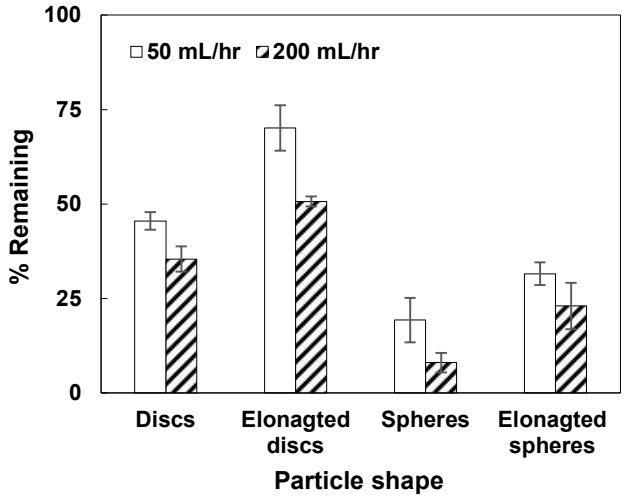

Fig. 4-12 The comparison of percent remaining after water-dropping of each shape at 50 mL/hr (opened columns) and at 200 mL/hr (striped columns) (permitted reuse reproduction for doctor thesis from the publisher, cited and partially modified from ref. 25).

Even though, elongated discs have less total surface area (1.66×10^6 nm^2) than spheres before elongation (2.71×10^6 nm^2) (see Table 4-1). After water-dropping, elongated discs can achieve the remaining percentage of *ca*. 51% and 43% higher than that observed in spheres at low and high flow rates, respectively. In the same manner, elongated discs also showed higher remaining percentage than elongated spheres (higher *ca*. 39% and 28% at low and high flow rates, respectively), which has a surface area even about 7.5 times larger than the elongated discs. This indicates that the total surface area is not the key parameter that controls the adhesiveness of PLGA particles. On the other hand, it is reasonable to assume that the contact surface area is directly associated with the adhesion strength of particles to the surface of the substrate. Illustrations of different shapes of PLGA particles showed that elongated discs may have the largest contact surface area in comparison to control discs, spheres and elongated spheres. (see Fig. 4-10). This explained the improving of adhesiveness comparing between control discs and elongated discs where the remaining percentage increased from *ca*. 46% to *ca*. 71% at low flow rate and from *ca*. 35% to be *ca*. 51% at high flow rate, when the contact surface area increased from 3.64×10^5 nm^2 to 6.68×10^5 nm^2. Moreover, it also explained that control spheres and

elongated spheres have low adhesiveness because of the limited contact surface area. These results agree well with the recent theoretical and computational studies which indicated that non-spherical particles may have higher margination and adhesion probability at the wall due to a larger contact surface area [9], [35].

4-5 Summary

We propose a facile method combining phase separation and a roll-to-roll coating process with a stretching method to fabricate elongated polymer micro/nano discs with higher aspect ratio and larger contact surface area by having PLGA/PVP as a model. The result showed that aspect ratios of PLGA domains can be controlled by stretching temperature and elongation percentage. The aspect ratio of the elongated discs can be increase up to 2.3, at 600% elongation and 80 ºC. Accordingly, the estimated contact surface area increased about 1.8 times from controlled discs (non-stretching). These elongated discs showed the best adhesiveness over discs, spheres, and elongated spheres by water-dropping test. In addition, the result shows that the adhesiveness of PLGA particles is strongly related with contact surface area. It worth noting that this improving of adhesiveness by this proposed method could enhance the drug carrier efficiency by fully utilizing the ability to delivery drug to the targets. In addition, there is also high potential to apply this proposed method with a wide range of polymers only if apparent phase separation morphology with PVP could be obtained, which will broaden the usage of elongated polymer micro/nano discs in a wide range of applications especially in drug delivery.

References

[1] B. Yu, H. Cong, Q. Peng, C. Gu, X. Xu, C. Tian, F. Zhai, Current status and future developments in preparation and application of nonspherical polymer particles, Adv. Colloid Interface Sci. 256 (2018) 126–151.

[2] J. Chen, N. Clay, H. Kong, Non-spherical particles for targeted drug delivery, Chem. Eng. Sci. 125 (2015) 20–24.

[3] L.K. Koegel, T. Vernon, R.L. Koegel, B.L. Koegel, A.W. Paullin, Particle shape: a new design parameter for micro- and nanoscale drug delivery carriers, J Control Release. 121 (2007) 3–9.

[4] A.B. Jindal, The effect of particle shape on cellular interaction and drug delivery applications of micro- and nanoparticles, Int. J. Pharm. 532 (2007) 450–465.

[5] S. Venkataraman, J.L. Hedrick, Z.Y. Ong, C. Yang, P.L.R. Ee, P.T. Hammond, Y.Y. Tanf, The effects of polymeric nanostructure shape on drug delivery, Adv. Drug Deliv. Rev. 63 (2011) 1228–1246.

[6] A. Banerjee, J. Qi, R. Gogoi, J. Wong, S. Mitragotri, Role of nanoparticle size, shape and surface chemistry in oral drug delivery, J. Control. Release 238 (2016) 176–185.

[7] X. Zhu, C. Vo, M. Taylor1, B.R. Smith, Non-spherical micro- and nanoparticles in nanomedicine, Mater. Horizons 6 (2019) 1094–1121.

[8] P. Decuzzi, M. Ferrari, The adhesive strength of non-spherical particles mediated by specific interactions, Biomaterials 27 (2006) 5307–5314.

[9] M. Cooley, A. Sarode, M. Hoore, D. A. Fedosov, S. Mitragotri, S. A. Gupta, Influence of particle size and shape on their margination and wall-adhesion: Implications in drug delivery vehicle design across nano-to-micro scale, Nanoscale 2018, 10, 15350–15364.

[10] H. Zhang, M. Fujii, Y. Okamura, L. Zhang, S. Takeoka, Massive fabrication of polymer microdiscs by phase separation and freestanding process, ACS Appl. Mater. Interfaces 8 (2016) 16296−16302.

[11] S. Muro, C. Garnacho, J. A. Champion, J. Leferovich, C. Gajewski, E. H. Schuchman, S. Mitragotri, V. R. Muzykantov, Control of endothelial targeting and intracellular delivery of therapeutic enzymes by modulating the size and shape of ICAM-1-targeted carriers, Mol. Ther. 16 (2008)1450–1458.

[12] J. W. Yoo, S. Mitragotri, Polymer particles that switch shape in response to a stimulus, Proc. Natl. Acad. Sci. U.S.A. 107 (2010) 11205–11210.

[13] J. A. Champion, S. Mitragotri, Role of target geometry in phagocytosis, Proc. Natl. Acad. Sci. U.S.A. 2006, 103, 4930–4934.

[14] C. C. Ho, A. Keller, A, J. A. Odell, R. H. Ottewill, Preparation of monodisperse ellipsoidal polystyrene particles, Colloid Polym. Sci. 271 (1993) 469−1479.

[15] M. J. Heslinga, E. M. Mastria, O. J. Eniola-Adefeso, Fabrication of biodegradable spheroidal microparticles for drug delivery applications, Control. Release 138 (2009) 235–242.

[16] T. Ding, Z. Liu, K. Song, C. H. Tung, Synthesis of monodisperse ellipsoids with tunable aspect ratios, Colloids Surf. A 336 (2009) 29–34.

[17] S. E. A. Gratton, P. A. Ropp, P. D. Pohlhaus, J. C. Luft, V. J. Madden, M. E. Napier, J. M. DeSimone, The effect of particle design on cellular internalization pathways, Proc. Natl. Acad. Sci. U.S.A. 105 (2008) 11613–11618.

[18] H. Meng, S. Yang, Z. Li, T. Xia, J. Chen, Z. Ji, H. Zhang, X. Wang, S. Lin, C. Huang, Z. H. Zhou, J. I. Zink, A. E. Nel, Aspect ratio determines the quantity of mesoporous silica nanoparticle uptake by a small GTPase-dependent macropinocytosis mechanism, ACS Nano 5 (2011) 4434–4447.

[19] C. Herrmann, A. Turshatov, D. Crespy, Fabrication of Polymer Ellipsoids by the electrospinning of swollen nanoparticles, ACS Macro Lett. 1 (2012) 907–909.

[20] S. Xu, Z. Nie, M. Seo, P. Lewis, E. Kumacheva, H. A. Stone, P. Garstecki, D. B. Weibel, I. Gitlin, G. M. Whitesides, Generation of monodisperse particles by using microfluidics: Control over size, shape, and composition, Angew. Chem. Int. Ed. 44 (2005) 724–728.

[21] J. A. Champion, Y. K. Katare, S. Mitragotri, Making polymeric micro- and nanoparticles of complex shapes, Proc. Natl. Acad. Sci. U.S.A. 104 (2007) 11901–11904.

[22] W. Tuntanatewin, K. Tani, K. Ishikura, H. Zhang, Y. Okamura, One-pot fabrication of polymer micro/nano-discs via phase separation and a roll-to-roll coating process, Colloids Surf. A 586 (2020) 124274.

[23] S. Omi, A. Matsuda, K. Imamura, M. Nagai, G. H. Ma, Synthesis of monodisperse polymeric microspheres including polyimide prepolymer by using SPG emulsification technique, Colloids Surf. A 153 (1999) 373–381.

[24] F. Qi, J. Wu, T. Yang, G. Ma, Z. Su, Mechanistic studies for monodisperse exenatide-loaded PLGA microspheres prepared by different methods based on SPG membrane emulsification, Acta Biomater. 10 (2014) 4247–4256.

[25] W. Tuntanatewin, P. Mekwatanakarn, H. Zhang, Y. Okamura, Facile fabrication of elongated polymer micro/nano discs and their surface adhesiveness, J Appl Polym Sci. (2020) e49798.

[26] L. Mu, S. S. Feng, A novel controlled release formulation for the anticancer drug paclitaxel (Taxol®): PLGA nanoparticles containing vitamin E TPGSJ, Control. Release 86 (2003) 86, 33–48.

[27] M. M. Knopp, N. E. Olesen, P. Holm, P. Langguth, R. Holm, T. J. Rades, Influence of Polymer Molecular Weight on Drug–Polymer Solubility: A Comparison between Experimentally determined solubility in PVP and prediction derived from solubility in monomer, Pharm. Sci. 104 (2015) 2905–2912.

[28] K. Balani, V. Verma, A. Agarwal, R. Narayan, Biosurfaces: A Materials Science and Engineering Perspective, K. Balani, V. Verma, A. Agarwal, R. Narayan, Eds.; Wiley: NY, Chapter A1 (2015) 329–344.

[29] H. Zhang, D. Sakagami, W. Huang, H. Kimura, Y. Okamura, Measurement and modelling of tensile moduli of polymer blend thin films with phase separated structures, Polymer 190 (2020) 122233.

[30] G. M. Kim, G. H. Michler, Micromechanical deformation processes in toughened and particle-filled semicrystalline polymers: Part 1. characterization of deformation processes in dependence on phase morphology, Polymer 39 (1998) 5689−5697.

[31] G. M. Kim, G. H. Michler, Micromechanical deformation processes in toughened and particle-filled semicrystalline polymers: Part 2. Model representation for micromechanical deformation processes, Polymer 39 (1998) 5699−5703.

[32] S. Dogru, B. Aksoy, H. Bayraktar, B. E. Alaca, Poisson's ratio of PDMS thin films, Polym. Test 69 (2018) 375–384.

[33] J. M. Thredgold, S. K. Lucas, P. G. Howlett, On the contact of a rigid sphere and a thin plate, Math Comput Model 43 (2006) 119–131.

[34] C. Svensén, P. Rodhe, In Pharmacology and Physiology for Anesthesia, H. C. Hemmings, T. D. Egan, Eds.; W.B. Elsevier: MA, Chapter 33 (2013) 574–592.

[35] M. Xiong, Y. Bao, X. Yang, Y. Zhu, J. Wang, Delivery of antibiotics with polymeric particles, Adv. Drug Deliv. Rev. 78 (2014) 63–76.

Chapter 5
Conclusions and future prospects

5-1 Conclusions

In this research, we successfully established the facile method for fabrication of polymer micro/nano discs and elongated polymer micro/nano discs with higher aspect ratio. By this purposed method, the continuous fabrication process of discs can be achieved with the collection/washing process in one-pot manner. In addition, since the adhesiveness properties of particles is directly associated with the contact surface area, elongated polymer micro/nano discs will enhance the drug carrier efficiency by fully utilizing the ability to delivery drug to the targets. There is also high potential to utilize this proposed method with a wide range of polymers only if apparent phase separation morphology with PVP could be obtained.

Chapter 1 presented the introduction, which explained the fabrication methods of polymer particles which can be classified in to two groups namely; the fabrication method that derives directly from monomer and the one that is from preformed polymer. The applications of polymer micro/nano particles and discs were also described. Thereafter, the limitation of current processes for fabrication discs were stated which leads to the motivation of this study.

Chapter 2, we successfully propose a facile method to fabricate polymer discs by hot-press process combined with a sacrificial matrix technique. This method can be utilized different kinds of polymer microspheres with a wide range of size to fabricate polymer discs. These polymer discs enhanced interfacial adhesion compared to that of the microspheres, owing to their larger contact surface area in geometry. This is expected to improve their performances in both particle-based targeted drug delivery and latex turbidimetric immunoassay.

Chapter 3, we successfully propose a new method to fabricate large amounts of polymer micro/nano-discs in a one-pot manner with the combination of polymer blend phase separation and a roll-to-roll coating process. Since both major component (PVP) and coating substrate can be easily dissolved in water, discs could be collected by repeatedly washing with water in a one-pot manner. The size and aspect ratio of the obtained discs can be adjusted in a controlled manner by adjusting the fabrication conditions, such as the blend ratio and the total polymer concentration. We also succeeded

to fabricate micro/nano-discs with other polymers, such as PLGA, PBMA and PCL, to demonstrate the universality of this method.

Chapter 4, we successfully propose method to fabricate elongated polymer micro/nano discs with higher aspect ratio and larger contact surface area. This method combining phase separation and a roll-to-roll coating process with a stretching method. The aspect ratio of the elongated discs can be increase up to 2.3, at 600% elongation and 80ºC. Accordingly, the estimated contact surface area increased about 1.8 times from controlled discs (non-stretching). These elongated discs showed the best adhesiveness over discs, spheres, and elongated spheres by water-dropping test which is corresponding well with the contact surface area. In addition, there is high possibility to apply this process with a wide range of polymers only if apparent phase separation morphology with PVP could be obtained.

Although this work is still at an early stage, we anticipate the development of a large-scale, continuous fabrication method for polymer micro/nano-discs and elongated polymer micro/nano discs with higher aspect ratio which would be of practical value in a wide range of applications such as drug delivery, medical imaging, surface coatings, etc. Specifically, the improving of adhesiveness by this proposed method is expected to enhance the drug carrier efficiency by fully utilizing the ability to delivery drug to the targets.

5-2 Future prospects

Many studies and experiments have been left for the future due to the limitation of time which is worth noting here. Even though, some polymer disc and elongated disc properties have been examined namely the adhesiveness test by the airflow using microchamber in Chapter 2 and the adhesiveness test by water-dropping in Chapter 4, the additional experiments to expose more on the properties of these particles would be the advantage for further development for end use application.

Even through, the adhesiveness is the crucial properties, enhancing the ability to delivery drug to the target site. It should be noted here that the excellent adhesiveness may turn to the drawback if the particles adhere to the undesired place, such as blood vessel, instead of the target site. Accordingly, further study of particle surface modification to control the specific adhesion position when using particles as drug carrier would be completed the picture of the development. There have a number of studies have addressed the specific localization of nanoparticles in cells [(1)], for example the relationship between the surface functionality of AuNPs and their accumulation in organs [(2)], the aid of targeting agents for cell-specific delivery such as SK-BR-3 cells, a breast cancer cell line, overexpresses the Herceptin receptor HER-2 [(3, 4)].

Furthermore, as mentioned prior, drug delivery system (DDS) is the key application of polymer particles. One of the crucial information is the flow pattern, the migration, and the retention mechanism of polymer particles in blood vessel. Therefore, the additional experiments to simulate the flow of polymer particles in micron channel (the well-known simulated model for blood vessel) will provide more understanding about the flow behavior of difference shape of particles. In our research group, flow behavior of micro/nano particles in the flow channel of microfluidic devices (see Fig. 5-1) has been previously studied. This microdevice was made by polydimethylsiloxane (PDMS) which is the most widely used material in microfluidic device fabrication [(5)]. The flow behavior as well as flow distribution of fluorescent particles was investigated by a confocal laser microscope (see Fig. 5-2).

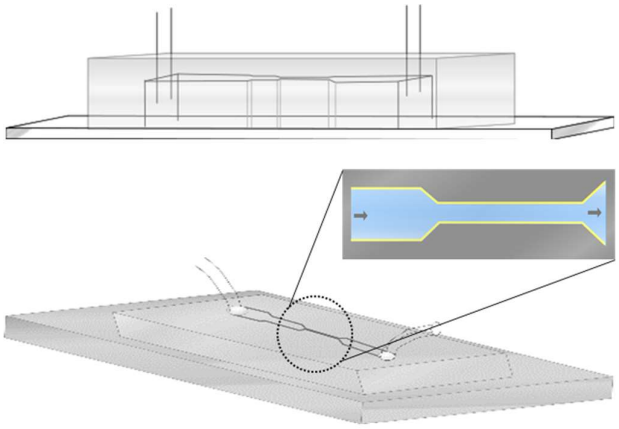

Fig. 5-1 PDMS microfluidic device with design of microchannel used in our previous study.

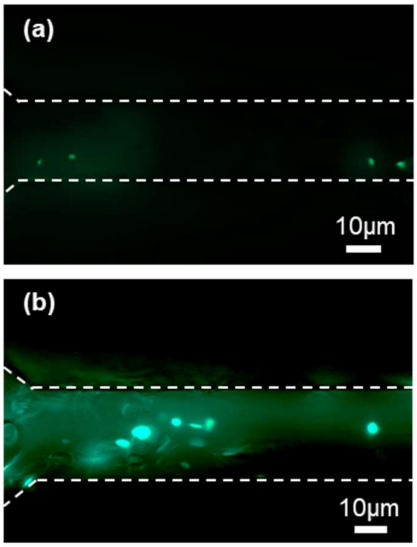

Fig. 5-2 The sample picture of the flow behavior of fluorescent PLGA discs in the microchannel of PDMS microfluidic device.

By the using of microfluidic device, more information about flow behavior, flow distribution and attachment and/or detachment from the micro channel wall of polymer particles etc., will be understood. In addition, the effect of particle morphology such as shape, diameter, thickness, and aspect ratio on these parameters will be able to evaluate. This information will maximize the efficiently of utilizing polymer particles as a drug carrier.

As reported in Chapter 2, the cluster of intermolecular formed by the cross-linkages of ε-amino groups of lysine residue in protein BSA coated on particle with GA could observed. This is worthy to look in deep more in their special structure and their bonding mechanism. This may lead to the new type of material that may provide special properties such as the isotropic property.

Another absorbing experiment is the using of polymer particles in the end application. Preliminary work has been tested and discussed as reported in Chapter 2 about the using of BSA-coated PS particles as aggregation assay comparing between discs and sphere. However, it would be a worthwhile contribution if it will be further studied in more details. Accordingly, further studied will complete the picture of using polymer particles as the aggregation assay such as, the using other polymer particles like PLGA, the effect of aspect ratio of polymer particles, the concentration of both BSA and GA, reaction time on the aggregation efficiency. The fluorescent particles couple with the fluorescent microscopy is expected to be used to clearly show the aggregation behavior of mixture.

Another interesting prospect is the ability to use these polymer particles as a drug carrier. Previously in our research group, the using of PLLA discs via hot pressing process as a Meropenem (MEPM) carriers for pulmonary administration has been intensely studied and provided very positive results. Accordingly, polymer discs from our proposed continuous fabrication method as mentioned in Chapter 3 could be the tool to scale up for the industrial scale. Thus, the performance of these polymer discs as a MEPM carriers for pulmonary administration have to be reconfirmed and investigated. Moreover, the using of the elongated discs with different aspect ratio fabricated from our proposed method as mentioned in Chapter 4, as a MEPM carriers for pulmonary administration will be very interesting. The adsorption amounts, release percentage, administration ability of polymer discs and elongated discs will be very useful to maximized the unitality of these polymer particles as a drug carrier

With these future works, the efficiency of these particles could be maximized. Plus, it is expected to be used in a wide range of applications to overcome the limitation of conventional problem where the present methods could not serve the needs properly.

References

[1] K. Kobayashi1, J. Wei, R. Iida, K. Ijiro, K. Niikura, Surface engineering of nanoparticles for therapeutic applications, Polymer Journal 46, (2014) 460–468.

[2] S. T. Kim, K. Saha, C. Kim, V. M. Rotello, The role of surface functionality in determining nanoparticle cytotoxicity. Acc. Chem. Res. 46, (2013) 681–691.

[3]. J.-O. You, P. Guo, D. T. Auguste, A drug-delivery vehicle combining the targeting and thermal ablation of HER2þ breast-cancer cells with triggered drug release. Angew. Chem. Int. Ed. 52, (2013) 4141–4146.

[4]. J. Baselga, L. Norton, J. Albanell, Y. -M. Kim, J. Mendelsohn, Recombinant humanized anti-HER2 antibody (Herceptin) enhances the antitumor activity of paclitaxel and doxorubicin against HER2/neu overexpressing human breast cancer xenografts. Cancer Res. 58, (1998) 2825–2831.

[5] J. Frienda, L. Yeo, Fabrication of microfluidic devices using polydimethylsiloxane, Biomicrofluidics 4, (2010) 026502.

Appendix

Appendix A
Morphology evaluation of polymer domains and particles by ImageJ

How to use ImageJ to evaluate morphology of polymer domains and particles

ImageJ is an open source image processing program designed for scientific multidimensional images. This program is useful for getting information from image. There are a number of different ways to evaluate particle diameter. As an example, the method how to determine diameter of PS discs as mentioned in Chapter 3 will be shown as followed.

First, open selected SEM image in ImageJ (see Fig. A1-a). Then, we have to create the scale bar as a reference distance for calculation based on the scale bar showed in SEM image. To create scale bar, select the straight-line tool and draw a line on the image of a specific length, in this case 10 μm by using the scale bar on the SEM image as a guide (see Fig. A1-b). Then, go to the *analyze tab* and select the *set scale* menu item where the set scale box will pop-up. Fill all the parameters namely the known length of your line (in this case is 10 μm), the pixel aspect ratio (should be 1.0) and change the distance units to be μm. Check the box "Global" if would like to use this setting for all the pictures or keep it blank if would like to use different scale setting for each picture. Finally, click the ok button showing in the left bottom of this set scale box to complete the setting.

To measure the diameter of PS discs, draw a line from the edge of discs from the left to the right by press and hold shift key during drawing the line to obtain a perfect strait line at zero-degree angle (parallel with the scale bar). To label each particle, go to the *analyze tab* and select the set measurements menu item where the set measurements box will pop-up. Select add to overlay box to and click ok box in the bottom left of the box complete the setting. Plus, you can customize measurement parameters in this set measurements menu such as decimal numbers, standard deviation, and mean etc., by checking each parameter showing in this measurement's menu box. After drawing the line, you can press and hold Ctrl key and click "M" key. The measured particles will be labelled with number (see Fig. A1-c) and the diameter length will be shown in the result pop-up box. The particle diameter can be continuously measured with the same process as mentioned here and the number will be run continuously from previous number. In the case of wrong measurement, the specific number of particles can be selected from the result pop-up box (selected data will turn black) and the delete can easily achieve by right-clicking and selecting cut menu.

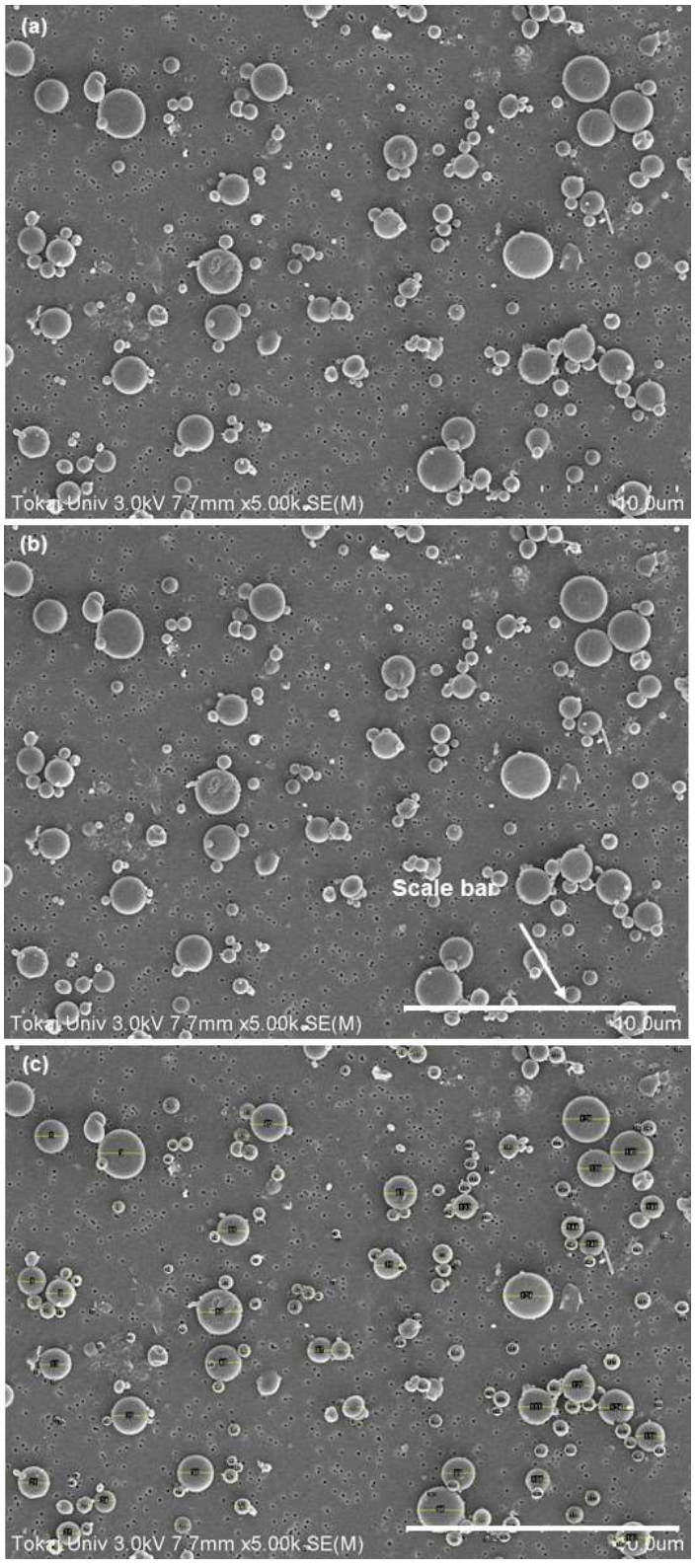

Fig. A1 SEM images of PS discs at the blend ratio of 1:4 at total concentration of 4% (a) before measurement (b) with scale bar and (c) the diameter line across each particle.

The result as well as the picture with labelled number can be exported easily by going to file and save as menu showing on the top of result box and ImageJ tools box, respectively, which can be used for further evaluation. This mentioned process was also used to evaluate diameter of polymer particles, diameter of polymer domains, as well as the thickness of particles.

Appendix B
Measurement of the occupied areas in water-dropping test by ImageJ

How to use ImageJ to evaluate the particle occupied areas in water-dropping test by ImageJ

As mentioned in chapter 4, the particle occupied areas in water-dropping test was used to investigate the adhesiveness of each shape of particles. Accordingly, the example of how to measure occupied areas of PLGA sphere will be shown as followed. Similar to the method using to measure diameter of polymer particles, the method to measure occupied area begins with the opening selected fluorescent image in ImageJ (see Fig. B1-a). The picture has to be converted from RGB color to be 8-bit for further evaluation (see Fig. B1-b) by go to the *image* tab and select the type menu. Then, the picture was converted to be black and white by go to the *image* tab, then in adjust menu and select threshold menu. All of the occupied area by fluorescent particles was then converted to be black by adjusting threshold percentage as can be seen in Fig. B1-c. Finally, go to the *analyze* tab, then selected analyze particle menu, the analyze particle box will be pop-up accordingly. In this the analyze particle box, selected "Outlines" in the drop item of show, and selected box of display results, clear results, and summarize. Finally, select "ok" in the bottom left to complete the process. The outline of particle as can be seen in Fig. B1.d will pop-up with the area number as a summary for further calculation.

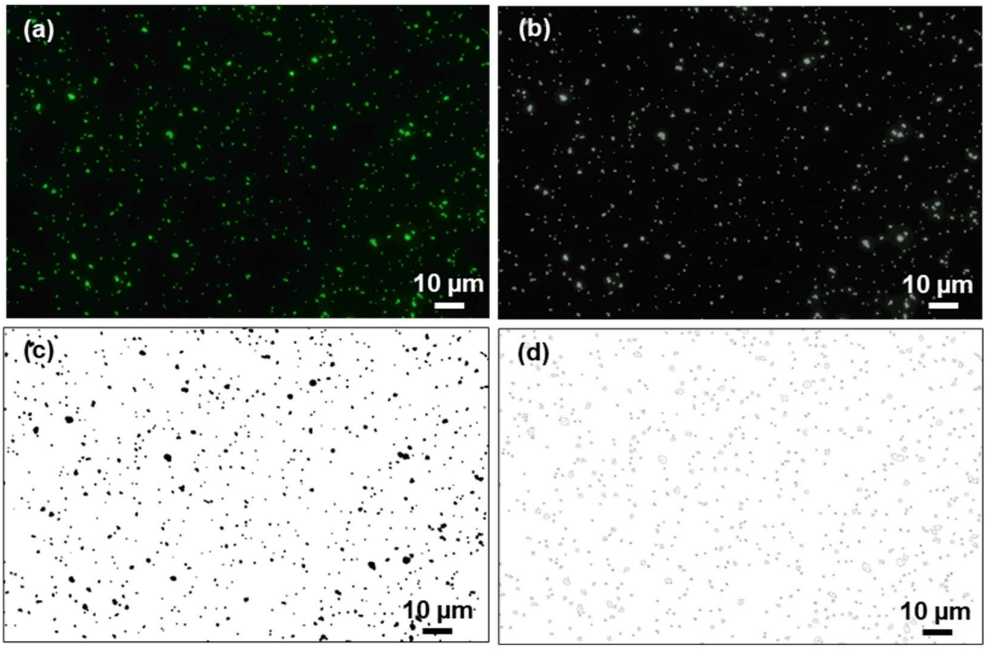

Fig. B1 Fluorescent images of PS sphere (a) before measurement (b) after convert to image to be 8 bits (c) after covert occupied area to be black, and (d) the occupied area with outline after analyzing.

Appendix C
The estimated contact surface area of elongated spheres

How to calculate the estimated contact surface area of elongated spheres

As mentioned in Table 4-1, the estimated contact surface area of elongated spheres was shown as 1.31×10^5 nm^2. The calculation of this estimated contact surface area begins with the assumption of that elongated spheres is perfect ellipsoid in shape. Then, the ellipse which is the 2D of elongated spheres was plotted by using ellipse equation to estimate the length of contact surface area from both front view and side view (see Fig. C1).

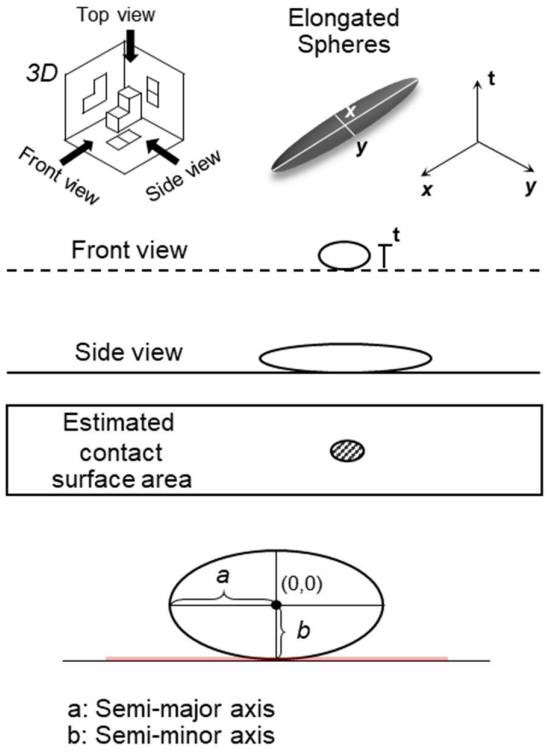

Fig. C1 The model of elongated spheres with the 2D projection picture from both front view and side view (permitted reuse reproduction for doctor thesis from the publisher, cited and partially modified from ref. 25).

The semi-minor axis (b) of ellipse shape from 2D projection picture from both front view and side view is the same which is the thickness of elongated sphere divided by two (b = 198.5 nm). While, the semi-major axis of ellipse shape from 2D projection picture is major axis (x) and minor axis (y) of elongated spheres for front view and side view, respectively. Next, we assumed the particle to be perfect rigid and contact surface area is referred to the area on the particle surface in a close distance of $h_o \sim$ 10 nm from the substate [(2)]. According to the standard ellipse equation as shown in Fig. C2, the estimated

contact surface area of elongated sphere can be achieved by the calculation of the length of contact line from front view and side view of elongated sphere. From front view, the contact point when y = -b+10 and -b+10, which is the initial and final contact point, respectively, is x = -110.94 and 110.94. On the other hand, the contact point is x = -376.39 and 376.9. Accordingly, the estimated contact surface area of elongate sphere will be the area of ellipse with the major axis of 752.78 nm (2×376.39) and with the minor axis of 221.89 nm (2×110.94) which is equal to 1.31×10^5 nm^2.

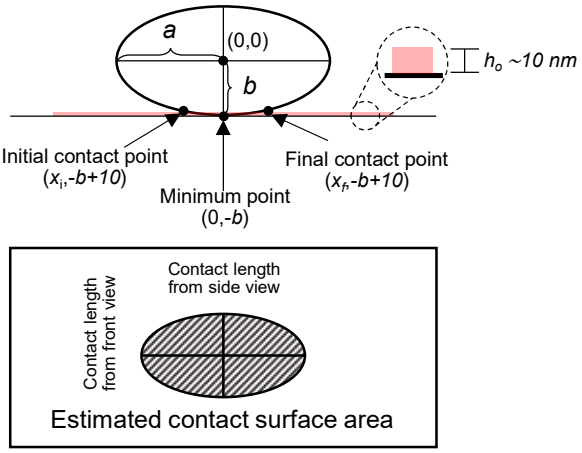

$$x = \sqrt{a^2 \times (1 - \frac{y^2}{b^2})}$$

Fig. C2 Model of contact surface area of elongated spheres with the 2D projection picture with standard ellipse equation (permitted reuse reproduction for doctor thesis from the publisher, cited and partially modified from ref. 25).

Reference

[1] W. Tuntanatewin, P. Mekwatanakarn, H. Zhang, Y. Okamura, Facile fabrication of elongated polymer micro/nano discs and their surface adhesiveness, J Appl Polym Sci. (2020) e49798.

[2] M. Cooley, A. Sarode, M. Hoore, D. A. Fedosov, S. Mitragotri, S. A. Gupta, Influence of particle size and shape on their margination and wall-adhesion: Implications in drug delivery vehicle design across nano-to-micro scale, Nanoscale 2018, 10, 15350–15364.

LIST OF ACHIEVEMENT

1. [Original paper] W. Tuntanatewin, K. Tani, K. Ishikura, H. Zhang, and Y. Okamura, "One-pot fabrication of polymer micro / nano-discs via phase separation and a roll-to-roll coating process," Colloids Surfaces A 586, 124274 (2020).
2. [Original paper] W. Tuntanatewin, P. Mekwatanakarn, H. Zhang, Y. Okamura, Facile fabrication of elongated polymer micro/nano discs and their surface adhesiveness, J Appl Polym Sci. (2020) e49798.
3. [Original paper] H. Zhang, W. Tuntanatewin, K. Ishikura, D. Sogabe, K. Sugawara, A. Tokui, A. Nakagawa, Y. Okamura, Polymer discs with high interfacial adhesion fabricated from hot-pressing of microspheres, ACS Appl. Polym. Mater. 2 (2020) 3355−3364.
4. [Domestic conference] W. Tuntanatewin, H. Zhang and Y. Okamura. "Fabrication of hemiellipsoidal micro/nano particles by stretching method via phase separation and a roll-to-roll coating process". The 12th meeting in Tokai University Micro/Nano Enlightenment (Tμne12) (2020.02.27, Shonan Campus, Tokai University).
5. [Domestic conference] W. Tuntanatewin, H. Zhang and Y. Okamura. "Fabrication of polymer micro/nano-discs with various aspect ratio controlled by stretching method via polymer phase separation". 高分子学会関東支部第 2 回神奈川地区講演会 (2019.6.28, 東海大学湘南校舎).
6. [International conference] W. Tuntanatewin, H. Zhang and Y. Okamura. "Fabrication of polymer micro/nano-discs with various aspect ratio controlled by stretching method via polymer phase separation". Okinawa Colloids 2019 (2019.11.06, Okinawa).
7. [International conference] W. Tuntanatewin, H. Zhang and Y. Okamura. "One-Pot Fabrication of Polymer Micro/Nano-Discs via Polymer Phase Separation". The 28th Annual Meeting of MRS-J (2018.12.19, Kitakyushu).

ACKNOWLEDGEMENT

My deep gratitude goes first to my thesis advisor, Professor Yosuke Okamura, who always patiently and kindly guided me through my graduate education. His enthusiasm in guiding and formulating question and methodology keep me constantly engaged with my research. His insightful feedback and comment pushed me to sharpen my thinking and brought my work to a higher level.

My appreciation also extends to Dr. Hong Zhang. His mentoring and encouragement have been especially valuable, and his expertise with kind suggestion contributed the crucial part of this dissertation. Without his always support and encouragement, this success would not have been possible.

I would like to show my gratitude to my dissertation committee: Professor Osamu Kanie (department of applied biochemistry), Professor Michio Iwaoka (department of chemistry), Professor Rio Kita (Micro/Nano Technology Center) and Professor Hiroshi Kimura (department of mechanical engineering) for generously offering their time, support, guidance and good will throughout the preparation and review of document and presentation.

I would also like to thank all the research staffs of Tokai University for their valuable guidance throughout my experiment for using each equipment. They provided me with tools that I needed to find the right direction and successfully complete my dissertation.

I am indebted to all Okamura's laboratory member who were always so helpful in numerous ways. With their generosity make my time at Tokai University enjoyable and memorable. Special thanks to Pinyo for all your assistances both in and outside laboratory and all of Thai's students (Peem, Four, K.Kung, Tan and Pao) for all your support. Also, thanks for particle team (Yoshida, Nakashima, Ishikura, Tani, Tokui, Tanahashi, Ichi, Sugawara) for your kind assistance and teaching me all the things. I always feel warm to be a part of Okamura's laboratory member.

I gratefully acknowledge the funding received towards my PhD from Japan International Cooperation Agency (JICA). Without funding from JICA, my dream to pursue the PhD in Japan would not be possible. I also would like to thanks all of staffs at international education center especially Terao san who work in collaboration with JICA to provide all the support seamlessly.

I would like to say a heartfelt thank you to family for always believing in me and encouraging me to follow my dreams. And finally, to my wife, Araya, who has been by my side throughout this PhD and has always supported all of my decisions. I would not have had the courage to embark on this journey in the first place without your encouragement. I consider myself the lucky person to have you with me.